Check for updates

Author Manuscript

Development of Electrolytes under Lean Condition in Lithium-Sulfur Batteries

Jianjun Chen[#], *Yuqing Fu*[#], *Juchen Guo*[*]

Jianjun Chen, Prof. Juchen Guo
Department of Chemical and Environmental Engineering, University of California, Riverside, California 92521, United States
*Email: juguo@ucr.edu

Yuqing Fu
Department of Chemistry, University of California, Riverside, California 92521, United States

[#]These authors contributed equally to the work

Keywords: Lithium-sulfur batteries; Lean electrolyte; Solvation; Kinetics; Polysulfides

Abstract

Lithium-sulfur (Li-S) batteries stand out as one of the promising candidates for next-generation electrochemical energy storage technologies. A key requirement to realize high-specific-energy Li-S batteries is to implement low amount of electrolyte, often characterized by the electrolyte/sulfur (E/S) ratio. Low E/S ratio aggravates the known challenges for Li-S batteries and introduces new one originated from the high concentration of polysulfides in limited electrolyte reservoir. In this review, the connections between the fundamental properties of electrolytes and the electrochemical/chemical reactions in Li-S batteries under lean electrolyte condition are elucidated. The emphasis is on how the solvating properties of the electrolyte affect the fate of polysulfides. Built upon the mechanistic analysis, different strategies to design lean electrolytes to improve the overall process of Li-S reactions and Li anode protection are discussed.

1. Introduction

Lithium-ion batteries (LIBs) have dominated the high-energy rechargeable battery market since their commercialization in early 90s.[1] However, the graphite anode and transition metal oxide cathodes become the bottleneck of further increasing the energy density of LIBs.[2] Lithium-sulfur (Li-S)

This is the author manuscript accepted for publication and has undergone full peer review but has not been through the copyediting, typesetting, pagination and proofreading process, which may lead to differences between this version and the Version of Record. Please cite this article as doi: 10.1002/adma.202401263.

This article is protected by copyright. All rights reserved.

batteries are considered a promising alternative due to their high specific capacity, low electrochemical potential of Li, and the abundance and high capacity of sulfur.[3] Despite the high theoretical value of 2600 Wh kg^{-1}, the realistic specific energy of Li-S batteries is much lower and dictated by a parameter named electrolyte/sulfur (E/S) mass ratio.[4] **Figures 1a** and **1b** display the mass percentage of cell components under two E/S ratios (1 and 5) in a 2-Ah Li-S pouch cell with practical parameters including 1000 mAh g^{-1} specific capacity of sulfur, 6 mg_s cm^{-2} sulfur loading, 64% sulfur content in cathode, N/P ratio of 1.3 (*i.e.*, 30% Li excess), and 6-µm Cu and 12-µm Al current collectors.[5] It is clear that the electrolyte can easily take up the majority of the total cell mass with high E/S ratio. The relationship between E/S ratio and specific energy of Li-S batteries is illustrated in **Figure 1c** based on the same cell parameters. To achieve specific energy higher than 500 Wh kg^{-1}, E/S mass ratio at approximately 3 must be implemented. Even with cell parameters superior to those used in Figure 1, it is undoubtfully that low E/S ratio is the key to achieve high-energy Li-S batteries.

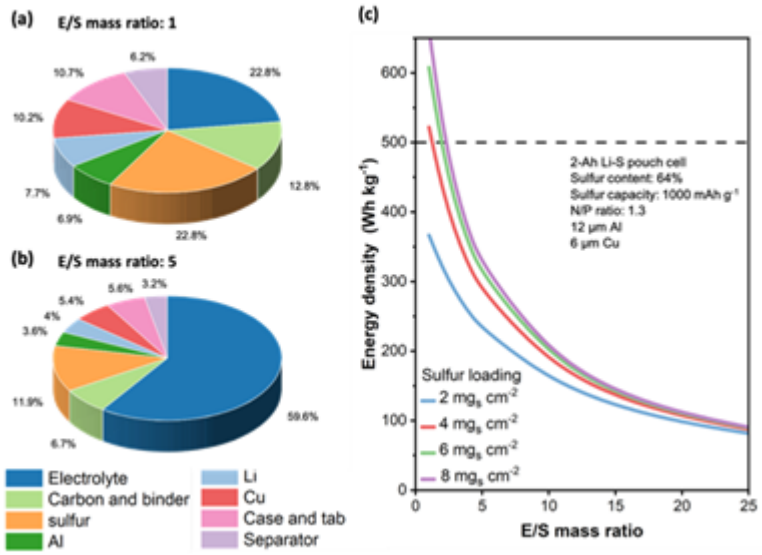

Figure 1. The significance of E/S ratio to Li-S batteries. Mass percentage of cell components in a 2-Ah Li-S pouch cell with E/S mass ratio at (a) 1 and (b) 5. (c) Specific energy of a 2-Ah Li-S pouch cell as a function of E/S ratio with different sulfur loadings.

Low E/S ratio, *i.e.*, lean electrolyte condition, induces complex Li-S electrochemical processes distinctly different from what we learn from the flooded electrolyte condition. A fundamental requirement for Li-S electrolytes is the ability to dissolve the intermediate species of Li-S reaction, *i.e.*, lithium polysulfides (LiPSs). The properties related to polysulfides dissolution including saturation concentration, rate of dissolution, and affinity to the electrode all play important roles in the Li-S electrochemical reaction process. Based on the solubility of polysulfides, Li-S electrolytes can be categorized as fully solvating (high solubility), weakly solvating (low solubility), and non-solvating electrolyte (very low solubility), which result in solid-liquid-solid, solid-transient liquid-solid, and solid-solid sulfur reduction process, respectively.[6] The most common Li-S electrolytes are based on

This article is protected by copyright. All rights reserved.

Author Manuscript

15214095, 2024, 29, Downloaded from https://advanced.onlinelibrary.wiley.com/doi/10.1002/adma.202401263 by Office Of Scientific And Technical Information, Wiley Online Library on [19/08/2025]. See the Terms and Conditions (https://onlinelibrary.wiley.com/terms-and-conditions) on Wiley Online Library for rules of use; OA articles are governed by the applicable Creative Commons License

an ether solvent composed of 1,2-dimethoxyethane (DME) and 1,3-dioxolane (DOL), which have high solubility of polysulfides. It is conventionally accepted that sulfur undergoes a solid-liquid-solid reduction process in DME/DOL electrolytes described by Reactions 1 to 7.[7] The elemental sulfur (with S_8 molecular unit) is first reduced to soluble S_8^{2-} anions coordinating to Li^+ cations in the electrolyte. As the reaction proceeds, a multistep chain-shortening process takes place, where S_8^{2-} is reduced to short chain polysulfides S_4^{2-} (Reactions 2 to 4). These steps attribute to the first plateau in the discharge voltage profile delivering a quarter of the theoretical capacity (418 mAh g^{-1}). The second voltage plateau is attributed to the continuous reduction of S_4^{2-} to insoluble Li_2S_2/Li_2S in a liquid-solid conversion process (Reactions 5 and 6). The final step is the solid-state conversion of insoluble Li_2S_2 to Li_2S (Reaction 7). The total conversion from S_4^{2-} to Li_2S offers a capacity of 1254 mAh g_s^{-1}.

$$S_8 + 2e^- \rightarrow S_8^{2-} \quad \text{(Reaction 1)}$$

$$3S_8^{2-} + 2e^- \rightarrow 4S_6^{2-} \quad \text{(Reaction 2)}$$

$$S_8^{2-} + 2e^- \rightarrow 2S_4^{2-} \quad \text{(Reaction 3)}$$

$$2S_6^{2-} + 2e^- \rightarrow 3S_4^{2-} \quad \text{(Reaction 4)}$$

$$S_4^{2-} + 4Li^+ + 2e^- \rightarrow 2Li_2S_2 \quad \text{(Reaction 5)}$$

$$S_4^{2-} + 8Li^+ + 6e^- \rightarrow 4Li_2S \quad \text{(Reaction 6)}$$

$$Li_2S_2 + 2Li^+ + 2e^- \rightarrow 2Li_2S \quad \text{(Reaction 7)}$$

Polysulfides at various steps co-exist in the real electrolyte with different solubility, concentration, and affinity to the electrode. As a result, the so-called solid-liquid-solid conversion is ambiguous. Instead of connecting the sulfur conversion process to macroscopic properties such as polysulfide solubility and concentration, it is necessary to clarify the process from a microscopic view. The dissolution of high-order polysulfide (*i.e.*, S_8^{2-}) is a solvation process determined by the solvating strength of Li^+ cation and the solvents. The affinity of S_8^{2-} to the electrode directly effects sulfur conversion since only S_8^{2-} anions adsorbed on the electrode can participate in charge transfer. The dissolution of S_8^{2-} can affect the overall reduction through mass transfer: When the dissolution rate of S_8^{2-} is lower than the rate of elemental S_8 reduction, dissolution of S_8^{2-} becomes the rate-limiting step of the entire sulfur reduction process. This is the scenario could be found in weakly solvating electrolytes. Therefore, fast dissolution of S_8^{2-} is preferred from the perspective of elemental sulfur reduction. However, when the dissolution rate of S_8^{2-} is also higher than the rate of S_8^{2-} reduction, S_8^{2-} will be accumulated in the electrolyte and diffuse out the vicinity of cathode causing parasitic reactions with Li anode. This scenario could be found in fully solvating electrolytes. Overall, to achieve high sulfur capacity and minimize LiPS-related side reactions requires a balanced S_8^{2-} dissolution rate in concert with sulfur reduction and S_8^{2-} adsorption on electrode and reduction. It is worth noting that S_8^{2-} anions are reduced to low-order polysulfides with lower solubility (stronger coordination between Li^+ cation and the polysulfide anion), which leads to the generation of Li_2S

This article is protected by copyright. All rights reserved.

Author Manuscript

15214095, 2024, 29, Downloaded from https://advanced.onlinelibrary.wiley.com/doi/10.1002/adma.202401263 by Office Of Scientific And Technical Information, Wiley Online Library on [19/08/2025]. See the Terms and Conditions (https://onlinelibrary.wiley.com/terms-and-conditions) on Wiley Online Library for rules of use; OA articles are governed by the applicable Creative Commons License

through disproportionation of the lower order LiPSs. Continuous accumulating Li_2S hinders electrochemical reduction of all sulfur: this is the reason full capacity is rarely achieved. The requirement of low E/S ratio further imposes restraint on all the processes in sulfur reduction. In this review, we focus on connecting the electrolyte properties to the Li-S behaviors under lean electrolyte condition and the electrolyte-design strategies based on tuning polysulfide solvation properties, redox mediator, and homogeneous catalysis to improve the kinetics of electrochemical reduction of sulfur.

2. Fundamental of Li-S electrolytes

Electrolyte concentration, dielectric constant (ε) or Gutmann donor number (DN) of solvents, and coordinating ability of anions determine the solvation behavior in the Li-S electrolyte. The Li^+ solvation has profound effects to the dissolution process and solubility of LiPSs during the electrochemical redox of sulfur as illustrated in **Figure 2**. Dielectric constant describes the electrostatic interactions between electric charges, thus effecting the polysulfide dissolution and ionic pair dissociation in electrolytes.[8] DN is a quantitative measurement of the nucleophilicity or Lewis basicity, thus often used in battery electrolytes to elucidate the ability of solvents or anions to interact with Lewis acidic Li^+ cations.[9] DN is a good measure to the Li^+ solvation energy except solvents effected by the chelate effect.[9-10] For instance, the DN of glymes follows the trend of G1 (DME) > G2 (diethylene glycol dimethyl ether) > G4 (tetraethylene glycol dimethyl ether) > G3 (triethylene glycol dimethyl ether) (**Table 1**), while the Li^+ solvation energy solvation energy follows the trend of G4 > G3 > G1 > G2.[11] Solvation structure of Li^+ is of great significance to the batteries performance because it is involved in the interphase formation.[12] In Li-S electrolytes, solvation plays an even more important role since the polysulfide anions participate Li^+ solvation thus the dissolution and solubility of polysulfide anions are closely related to their solvation structure, which depends on the dielectric constant, DN, and salt concentration.[13] solvents with high dielectric constant or DN are expected to have strong coordination with Li^+ that the linear carbonates with lower dielectric constant occupy the out layer of the solvation structure, while cyclic carbonates dominate the inner layer.[14] Anions with different DN also impact the solvation structure of Li^+. Introducing anions such as nitrate (NO_3^-) with high DN have been demonstrated to weaken the Li^+-solvent coordination, resulting in such anions enter the inner solvation layer.[15] In diluted electrolytes, the main solvation configuration is dominated by free solvents and solvent-separated ion pairs (SSIP), which is composed of 3 to 4 solvent molecules coordinating a Li^+ ion (Figure 2). By increasing the Li salt concentration, the anions start to enter the first solvation shell and the configuration starts to shift to contact ion pairs (CIP) or cation-anion aggregates (AGG). While general understanding of solvation structure has been established, advanced tools to quantitatively analyze the solvation structure and de-solvation process are needed to gain more insight.

This article is protected by copyright. All rights reserved.

Author Manuscript

15214095, 2024, 29, Downloaded from https://advanced.onlinelibrary.wiley.com/doi/10.1002/adma.202401263 by Office Of Scientific And Technical Information, Wiley Online Library on [19/08/2025]. See the Terms and Conditions (https://onlinelibrary.wiley.com/terms-and-conditions) on Wiley Online Library for rules of use; OA articles are governed by the applicable Creative Commons License

Author Manuscript

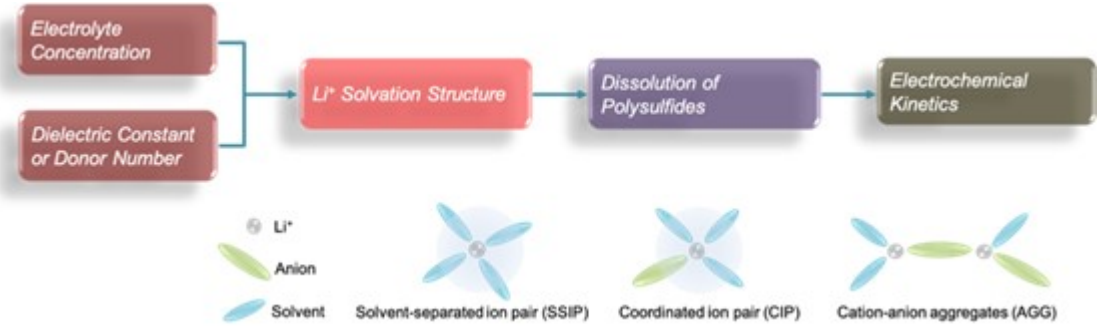

Figure 2. Correlation between the properties of electrolytes and the electrochemical reaction kinetics through Li^+ solvation and polysulfide anions dissolution. The lower panel shows the schematic illustration of solvation structures.

An ideal electrolyte should also exhibit following features: wide electrochemical window, wide temperature range, good chemical stability, low density, low flammability and high flash point to guarantee the safety,[16] and low cost. The known electrolytes barely satisfy all the requirements, thus it's necessary to elucidate the structure-property relationship of different solvents, salts and additives to provide a paradigm for the design of high-performance Li-S batteries.

2.1. Solvents

Carbonates have been demonstrated commercial success of LIBs due to the high electrochemical stability and ionic conductivity (Table 1).[17] However, the chemically incompatibility with polysulfide species limit its applicability in Li-S batteries. The carbon atom of the carbonate molecule acts as an electrophile which will be attacked by the nucleophilic polysulfides.[18] This nucleophilic reaction leads to the loss of active material and quick capacity fading. Sulfur confined within a microporous structure or covalently immobilized within a polymeric host is compatible with carbonate-based electrolytes,[19] but this type of Li-S chemistry is out of the scope of this review.

Table 1. Physiochemical properties of solvents used in Li-S batteries:[4c, 20]

Solvent	Viscosity [cP]	DN (Kcal mol^{-1})	Dielectric constant ε	Density (g cm^{-3})	Melting temperature (°C)	Boiling temperature (°C)
EC (ethylene carbonate)	1.9 (40 °C)	16.4	90.3 (40 °C)	1.32 (40 °C)	36.5	238
DEC (diethyl carbonate)	0.75	16	2.8	0.97	−43	126
DMC (dimethyl carbonate)	0.59	15.1	3.1	1.07	4.6	90
FEC (fluoroethylene carbonate)	3.33	*n.a.*	78.4	1.45	20	210
DME/G1 (1,2-dimethoxyethane)	0.46	20	7.2	0.86	-58	84.5
G2 (diethylene glycol dimethyl ether)	1.14	19.5	7.2	0.94	-64	162
G3 (triethylene glycol dimethyl ether)	2.5	14	7.5	0.99	-45	216
G4 (tetraethylene glycol dimethyl ether)	4.05	16.6	7.7	1	-30	275
DOL (1,3-dioxolane)	0.6	21.2	7.1	1.06	-97	76.5
THF (tetrahydrofuran)	0.67	20	11.5	1.66	-108	66

This article is protected by copyright. All rights reserved.

15214095, 2024, 29, Downloaded from https://advanced.onlinelibrary.wiley.com/doi/10.1002/adma.202401263 by Office Of Scientific And Technical Information, Wiley Online Library on [19/08/2025]. See the Terms and Conditions (https://onlinelibrary.wiley.com/terms-and-conditions) on Wiley Online Library for rules of use; OA articles are governed by the applicable Creative Commons License

BTFE (bis(2,2,2-trifluoroethyl)ether)	0.7	*n.a.*	4.4	1.4	25	63
TTE (hydrofluoroether)	1.43	1.9	6.2	1,53	-94	93
TMS/SL (sulfolane)	10.3 (30 °C)	14.8	43 (30 °C)	1.26 (30 °C)	28	287
DMSO (dimethyl sulfoxide)	1.99	29.8	46.5	1.09	18.5	189
AN (acetonitrile)	0.34	14.1	36	0.78	-48.8	81.5
TMP (trimethyl phosphate)	1.3	23	20.6	1.2	-47	197
TEP (triethyl phosphate)	1.6	23.4	13.1	1.07	-56.5	215
DMA (N,N-dimethylacetamide)	0.95	27.8	37.8	0.94	-20	165
DMF (N,N-dimethylformamide)	0.80	26.6	36.7	0.95	-61	153
TMU (1, 1, 3, 3-Tetramethylurea)	1.5	29.6	23.6	0.97	-1.2	176.5

Ethers are the most common solvents employed in Li-S batteries due to their great compatibility with Li and high solubility of polysulfides.[21] Linear ethers such as DME, G3 and G4 and cyclic ether such as DOL are the typical ether solvents used in Li-S batteries.[22] The solubilities of Li_2S_8 in some pure ether solvents and ether-based electrolytes are listed in **Table 2**.[23] The solubility in pure solvents indicates that solvent with higher dielectric constant renders higher Li_2S_8 solubility. For electrolytes, the solubility of Li_2S_8 decreases with increasing concentration of Li salt with anions with low DN such as bis(trifluoromethanesulfonyl)imide ($TFSI^-$); On the other hand, the solubility increases by adding Li salt with anions with high DN such as NO_3^- into 1 M LiTFSI solution in DOL/DME. This observation suggests that the connection between dissolution of polysulfides and Li^+ solvation is complex. It is worth noting that the cleavage of the cyclic structure of DOL during Li deposition can generate a stable SEI layer to protect Li anode.[24] On the other hand, the cyclic structure of DOL renders high viscosity, thus hindering efficient ion transport. Therefore, DOL has only been used as a co-solvent with linear ethers.[25] [26]

Table 2. Solubility of Li_2S_8 in different solvents or electrolytes used in Li-S batteries:

Solvents/electrolytes	Li_2S_8 solubility (M_s)	Solvents/electrolytes	Li_2S_8 solubility (M_s)
DMSO	~28[27]	DMF	~32[27]
DMA	~32[27]	DMI	~36[27]
THF	~10[28]	DME/DOL (1:1 by volume)	~5.92[28]
1 M LiTFSI in DOL/DME (1:1 by volume)	~4[29]	1 M LiTFSI and 0.2M $LiNO_3$ in DOL/DME	~6.6[30]
1.38 M LiTFSI in G3 (TFSI: G3 in 1:4 by molar)	~5.84[31]	1.13 M LiTFSI in G4 (TFSI: G4 in 1:4 by molar)	~6[31]
4.5 M LiTFSI in G4 (TFSI: G4 in 1:1 by molar)	~0.06[31]	4.8 M LiTFSI in DME (TFSI: DME in 1:1 by molar)	~0.2[10]
5.5 M LiTFSI in G3 (TFSI: G3 in 1:1 by molar)	~0.24[32]	4.7 M $LiNO_3$ in G3 (NO_3: G3 in 1:1 by molar)	~6[32]
1M LiTFSI in G4/HFE (1:4 by molar)	~0.01[31]	1.5 M LiTFSI in TMS/TTE (1:1 by molar)	~0.264[33]

Sulfones and sulfoxides are also potential solvents for Li-S batteries, featuring high dielectric constant, high thermal stability and low toxicity.[34] Due to the high dielectric constant and polysulfide compatibility, sulfones possess high solubility to polysulfides, which is beneficial to avoid polysulfides saturation under lean electrolyte condition.[28] But the high viscosity and poor Li anode stability result in degradations and poor rate capability in the sulfone-based Li-S cells. To alleviate the problem of high viscosity, ethyl methyl sulfone (EMS) with a lower viscosity is commonly used as a

This article is protected by copyright. All rights reserved.

Author Manuscript

15214095, 2024, 29, Downloaded from https://advanced.onlinelibrary.wiley.com/doi/10.1002/adma.202401263 by Office Of Scientific And Technical Information, Wiley Online Library on [19/08/2025]. See the Terms and Conditions (https://onlinelibrary.wiley.com/terms-and-conditions) on Wiley Online Library for rules of use; OA articles are governed by the applicable Creative Commons License

solvent[35] other than tetramethylene sulfone (TMS).[36] The Li-S battery study by Nazar et al. using EMS as the solvent delivered high capacities of sulfur at 1320 mAh g^{-1}.[37]

Fluorinated ethers have emerged as a new type of co-solvents in Li-S electrolytes: They enable the formation of LiF-rich SEI layer on Li to suppress dendrite growth and improve Li plating-stripping reversibility.[38] Fluorinated ethers also exhibits low polysulfide solubility due to their low DN attributed to the strong electronegativity and high steric hindrance of fluorine atoms.[39],[40] A typical example, 1,1,2,2-Tetrafluoroethyl-2,2,3,3-tetrafluoropropyl ether (TTE or HFE) was confirmed with a low solubility of higher-order polysulfides of ~3.2 mM with respect to sulfur.[41]

2.2. Lithium salts

Understanding the mechanism on how the anions of Li salts affecting the Li^+ solvation and sequentially the dissolution of polysulfides is crucial to design lean electrolyte for Li-S batteries. The dissolution of lithium salts is determined by the Li^+-solvent interactions.[42] Lithium salts with weakly coordinating (low DN) anions are the rational choices for Li-S electrolytes due to their ability to dissociate in aprotic solvents. Good ionic conductivity of a lithium salt is the result of a balance between dissociation and mobility.[43] Although lithium hexafluorophosphate ($LiPF_6$) stands out as the choice of salt for commercial LIBs, its inadequate solubility in ether based electrolytes and thermal stability limit its application in Li-S batteries.[44] LiTFSI is the most common salt used in the electrolytes due to its balanced features such as high solubility, high anion mobility, high chemical stability, good compatibility with polysulfides. While electrolyte based on lithium bis(fluorosulfonyl)imide (LiFSI) has better ionic conductivity and lower viscosity,[45] it may lead to decreased stability of Li-S batteries due to the breakage of the weak N-S bond in the FSI^- anion, which generates irreversible lithium sulfate ($LiSO_x$).[46] Lithium salts with high-DN anions that promote the dissolution of polysulfides are emerged as good candidates recently, and they will be discussed in high solvating electrolytes section.

2.3. Additives

Additives are chemicals added to Li-S electrolytes with low content to provide specific functionalities. Lithium nitrate ($LiNO_3$) is the most widely used additive to alleviate the parasitic reactions between the Li metal and polysulfides by forming a stable passivation SEI layer on Li.[47] The generation of a dense SEI layer by adding $LiNO_3$ is also beneficial for alleviating the shuttle phenomenon.[48] In addition, redox mediators are an important category of additives designed to improve the Li-S redox kinetics. Metallocene and polycyclic aromatic hydrocarbons have been demonstrated to enhance electron transfer between these redox mediator and the electrode.[49] Organopolysulfides and thiols are able to chemically react with polysulfides to improve the redox kinetic and alleviate the polysulfide accumulation.[50] The synergy between additives, solvents, and salts plays a key role in realizing high-performance Li-S batteries under lean electrolyte condition.

This article is protected by copyright. All rights reserved.

Author Manuscript

15214095, 2024, 29, Downloaded from https://advanced.onlinelibrary.wiley.com/doi/10.1002/adma.202401263 by Office Of Scientific And Technical Information, Wiley Online Library on [19/08/2025]. See the Terms and Conditions (https://onlinelibrary.wiley.com/terms-and-conditions) on Wiley Online Library for rules of use; OA articles are governed by the applicable Creative Commons License

2.4. Failure Mechanisms under Lean Electrolyte Condition

From the performance point of view, Li-S batteries under lean electrolyte condition fail to achieve high specific capacity of sulfur and/or high cycle stability comparing to the flooded cells. The underlying cause can be complex and multifaceted. For instance, fast dissolution of S_8^{2-} promotes in-depth reduction of elemental sulfur, but it also saturates the electrolyte with Li_2S_8 when the volume of electrolyte is low.[51] The electrochemical reduction of S_8^{2-} is sequentially hindered by the inferior mass transfer in the viscous electrolyte, and the Li_2S_8 reacts with Li anode. Massive and uncontrolled Li_2S deposition from both electrochemical and chemical reductions occurs leading to cathode passivation, anode passivation, and loss of active materials. In another scenario in Li-S electrolyte with low Li_2S_8 solubility, low solubility can very quickly saturate the electrolyte thus limiting the reduction of elemental sulfur, particularly when a relatively high current is drawn. In these two scenarios with distinctly different electrolytes, the Li-S battery can fail for the same apparent reasons of high discharge overpotential. Therefore, it is critical to fully understand the failure mechanism of Li-S batteries under lean electrolyte condition at molecular level.

Operando electrochemical impedance spectroscopy (EIS) combined with galvanostatic intermittent titration technique (GITT) and distribution of relaxation time analysis (DRTA) are developed to decouple the kinetic bottleneck during discharge process.[5, 52] In the lean electrolyte composed of 1 M LiTFSI in DOL/DME (volume ratio 1/3) and 5 wt.% $LiNO_3$, the accumulation of polysulfides in the electrolytes deteriorates the wettability towards cathodes and separators, contributing to the increased ohmic resistance of batteries.[53] Meanwhile, the viscosity of electrolytes significantly increases and the conductivity drops due to the rapid increase of polysulfides concentration, which reduces the charge transfer kinetics.[5, 53-54] In addition, the low-order polysulfides from reducing high-order ones disproportionate to insulating Li_2S and sulfur precipitates on the cathode, setting large diffusion barrier for charge transfer process. Therefore, the sluggish charge transfer kinetics[54] are identified as the general rate-limiting factor under lean condition for the typical Li-S electrolytes based on DOL/DME solvent. The sluggish reaction kinetics is affected by other complex interfacial processes in Li-S batteries.[55] The discharge intermediates of polysulfides generally have a poor affinity to the cathode surface that is usually composed of nonpolar carbon materials. Different low-order polysulfides in electrolyte can chemically react to generate Li_2S precipitate and high-order polysulfides, which may lead to inaccessible sulfur species in the liquid electrolyte thus irreversible loss of sulfur and capacity fading.[56]

The lean electrolyte condition also aggravates the failure of Li-S batteries by electrolyte consumption on the Li anode side.[53] The performance of pouch cells using 1 M LiTFSI in DOL/DME (volume ratio 1/3) and 5 wt.% $LiNO_3$ with an E/S mass ratio at 3 fades rapidly. After injecting electrolyte with an E/S mass ratio at 1 to the failed pouch cell, the discharge capacity was able to recover to 80% of

This article is protected by copyright. All rights reserved.

Author Manuscript

15214095, 2024, 29, Downloaded from https://advanced.onlinelibrary.wiley.com/doi/10.1002/adma.202401263 by Office Of Scientific And Technical Information, Wiley Online Library on [19/08/2025]. See the Terms and Conditions (https://onlinelibrary.wiley.com/terms-and-conditions) on Wiley Online Library for rules of use; OA articles are governed by the applicable Creative Commons License

the initial value with reduced polarization. The cycled cathodes from those failed cells still retain high specific capacity. In contrast, the cycled Li anode in the failed cell showed drastic volume expansion due to porous Li deposition and dead Li. High content of precipitated Li polysulfides was also discovered at the charged anode, indicating a severe shuttle phenomenon.

3. Electrolyte Design to Tune the Solubility of Polysulfides

3.1. Low-concentration electrolytes

Low concentration electrolytes are demonstrated to benefit the mass transport due to their ability to promote ion migration.[57] The low concentration also result in lower density (**Figure 3**a), which can slightly improve the specific energy at the same E/S volume ratio.[57b] The low-concentration electrolytes possess desirable properties such as low viscosity and excellent electrode wettability while maintaining acceptable ion conductivity (Figure 3b-d). But more importantly, the solvation of Li^+ cation in the low-concentration electrolyte do not favor dissolution of polysulfides.[57b, 58]

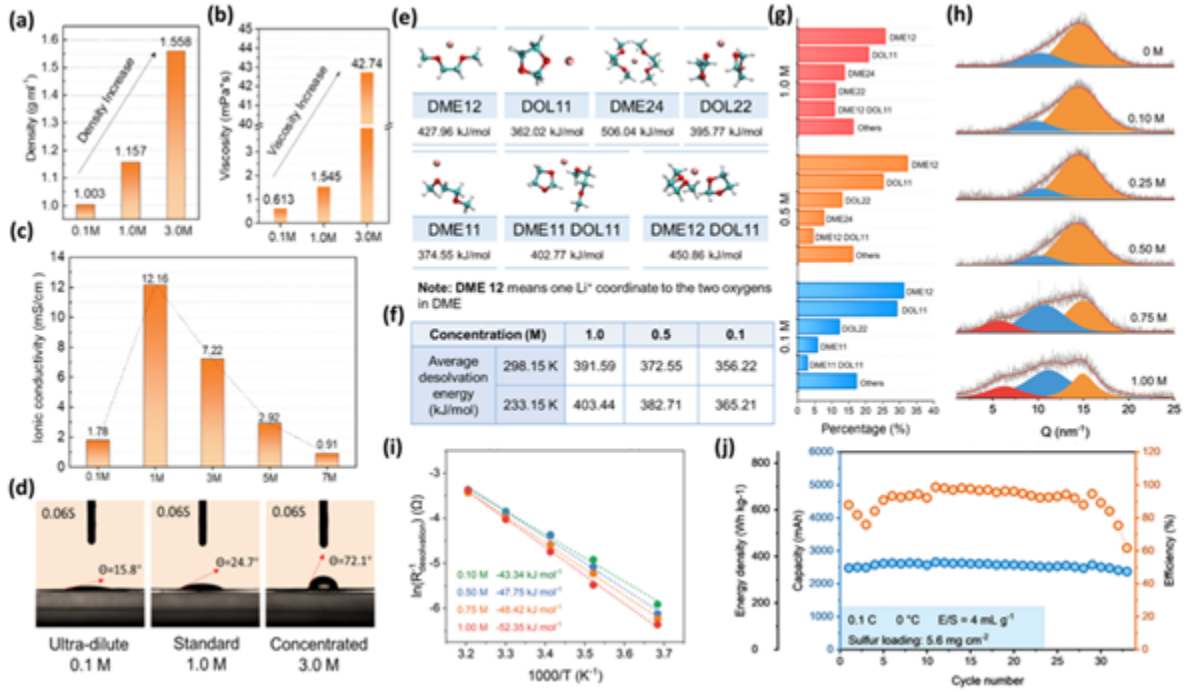

Figure 3. (a-d) Comparison studies of physical properties including (a) density, (b) viscosity, (c) ionic conductivity, and (d) wetting ability among electrolytes with different concentrations. The digital photographs of the different molarity electrolyte droplet contact angles on sulfur cathode, showing much less salt, lower density, lower viscosity and better wetting properties of a dilute (0.1 M) electrolyte. Reproduced with permission.[57b] Copyright 2020 American Chemical Society. (e) The main Li^+ solvation structures in three electrolytes; DME12 means one Li^+ coordinate with two oxygens in a DME molecule. (f) Average Li^+ de-solvation energy in different electrolytes at 298.15 K and 233.15 K. (g) The proportion of various Li^+ solvated structures in electrolytes with different LiTFSI concentrations. (h) Gaussian deconvolution of the experimental SAXS data of Li^+ solvation

This article is protected by copyright. All rights reserved.

Author Manuscript

15214095, 2024, 29, Downloaded from https://advanced.onlinelibrary.wiley.com/doi/10.1002/adma.202401263 by Office Of Scientific And Technical Information, Wiley Online Library on [19/08/2025]. See the Terms and Conditions (https://onlinelibrary.wiley.com/terms-and-conditions) on Wiley Online Library for rules of use; OA articles are governed by the applicable Creative Commons License

structure with different LiTFSI concentrations. (i) Activation energy of Li^+ de-solvation in different electrolytes. (j) The cycling performance of Li-S batteries with 0.5 M electrolyte under practical conditions and a low-temperature environment (0 °C). Reproduced with permission.[59] Copyright 2022, Wiley-VCH

Low concentration also results in low de-solvation energy of Li^+ solvation. In conventional DME/DOL-based electrolyte, DME serves as bidentate ligand that two oxygen atoms of DME bind with Li^+ cations (Figure 3e-g), while DOL and Li^+ cations form monodentate complex. Studies have shown a stronger interaction energy between Li^+ cations and DME than that with DOL,[59] indicating that Li^+ cations prefer to be solvated by DME. Such preference is more significant as the Li^+ concentration increases, which is consistent with their higher de-solvation energy (Figure 3f). By calculating the weighted averaged binding energy for all possible complexes, a positive correlation of binding energy with the LiTFSI concentration is found (Figure 3g), implying a lower de-solvation barrier for facile mass transfer at low concentration. Small-angle X-ray scattering (SAXS) was conducted to determinate the solvation environment of electrolytes with different concentrations (Figure 3h). The peaks at about 11 and 14 nm^{-1} can be ascribed to DOL and DME. While the new peak emerges around 6 nm^{-1}, which originates from the formation of cation-anion aggregates with more long-range interactions, when the LITFSI concentration is at 0.75 M and 1.0 M. The activation energy of de-solvation also decreases with decreasing concentration (Figure 3i). The benefit of low de-solvation energy from low-concentration electrolyte was demonstrated by an Ah-level pouch cell with sulfur loading of 5.6 mg cm^{-2} and E/S ratio of 4 mL g^{-1} at low temperature. The Li-S pouch cell was able to deliver a specific capacity of ~1000 mAh g^{-1} and maintained cycling for 30 cycles (Figure 3j).

3.2. Weakly solvating electrolytes

Weakly solvating electrolytes have been proposed for lean-electrolyte Li-S batteries.[6a] This concept is opposite to the conventional understanding of Li-S electrolytes: Instead of having adequate solubility of polysulfides, the weakly solvating electrolytes have very modest solubility so that it avoids high concentration of polysulfides in the electrolyte. However, if the rate of electrochemical reduction of sulfur is higher than the rate of dissolution of S_8^{2-} when a high current is drawn, the kinetics of sulfur reduction in weakly solvating electrolytes becomes S_8^{2-} dissolution control, which is in turn controlled by S_8^{2-} reduction. Therefore, rate performance and capacity of high-loading electrode in these electrolytes may be limited. The solubility of polysulfides is highly dependent on the solvents: polysulfide anions dissolve by coordination with Li^+ cations and becoming part of the Li^+ solvation structure by weakening the coordination from the solvent molecules.

This article is protected by copyright. All rights reserved.

Author Manuscript

15214095, 2024, 29, Downloaded from https://advanced.onlinelibrary.wiley.com/doi/10.1002/adma.202401263 by Office Of Scientific And Technical Information, Wiley Online Library on [19/08/2025]. See the Terms and Conditions (https://onlinelibrary.wiley.com/terms-and-conditions) on Wiley Online Library for rules of use; OA articles are governed by the applicable Creative Commons License

Reducing the Lewis basicity of solvents and weakening the interaction strength of lithium-solvents, are capable of preventing the dissolution of polysulfides (**Figure 4**a).[60] In such principle, the DN number and dielectric constant are used to select solvents with desired solubility of polysulfides. Reducing the proportion of Lewis basic sites such as O atoms, introducing the non-solvating alkyl units and steric hindrance groups to the solvent skeletons are demonstrated to reduce the Li^+-solvent coordination strength (Figure 4b).[61] Based on this strategy, the weakly solvating ether based electrolytes exhibited a significant superiority with good compatibility with Li metal and high oxidation resistance.[62] Introducing electron-withdrawing groups such as fluorine atoms can also reduce the Lewis basicity of solvents. Tuning the position of fluorinated groups and the degree of fluorination can regulate the polysulfide solubility of solvents. In consideration to the undesired high reactivity of α-fluorinated molecules to Li metal, other fluorinated sites are recommended although the fluorinated groups at α site can impose the highest electron-drawing effect.[63] Gao *et al.* explored a series of ethers with a range of polysulfides solubility by manipulating fluorine percentage and the position of fluorinated sites (Figure 4c).[64] As shown in Figures 4d and 4e, the solubility of polysulfides generally decreases with increasing number of F atoms in the ether molecule. The position of the O and F atoms also affects the solubility. For instance, fluorinated-1,2-diethoxyethane (F4DEE) and fluorinated-1,4-dimethoxybutane (F4DMB) are isomers, but F4DEE has a much higher Li_2S_6 solubility than F4DMB (140 mM_s versus 70 mM_s). Decreasing the solubility of polysulfides enables fast disproportionation of polysulfides at the interface, therefore, the reduction of sulfur goes through a "solid-transient liquid-solid" pathway. As displayed in Figure 4f, this reaction pathway is characterized with a single discharge plateau from electrolytes based on F3DEE and F4DEE, which have similar Li_2S_6 solubility of ~140 mM_s. The electrolytes with higher polysulfide solubility, based on non-fluorinated ethers, demonstrated the conventional two-plateau discharge profiles; on the other hand, the electrolytes with very lower polysulfide solubility, such as F4DMB and F5DEE, led to very low discharge capacity and large overpotential at room temperature. This observation clearly indicates that very low polysulfide solubility can easily induce the kinetic bottleneck to the reduction of elemental sulfur, which can be alleviated at higher temperature (Figure 4g). With an electrolyte based on F4DMB, which has mid-range polysulfide solubility, under lean electrolyte condition (E/S ratio of 5 $mL\ g_s^{-1}$) the Li-S battery achieved an average capacity of 787.3 mAh g^{-1} at 60 °C for 150 cycles (Figure 4h). It is worth noting that the sulfur loading in the demonstration was low as well as the C rate, and the high sulfur-loading performance was much worse. This is a strong indication electrolyte with low polysulfide solubility can induce kinetic limitation.

This article is protected by copyright. All rights reserved.

Author Manuscript

15214095, 2024, 29, Downloaded from https://advanced.onlinelibrary.wiley.com/doi/10.1002/adma.202401263 by Office Of Scientific And Technical Information, Wiley Online Library on [19/08/2025]. See the Terms and Conditions (https://onlinelibrary.wiley.com/terms-and-conditions) on Wiley Online Library for rules of use; OA articles are governed by the applicable Creative Commons License

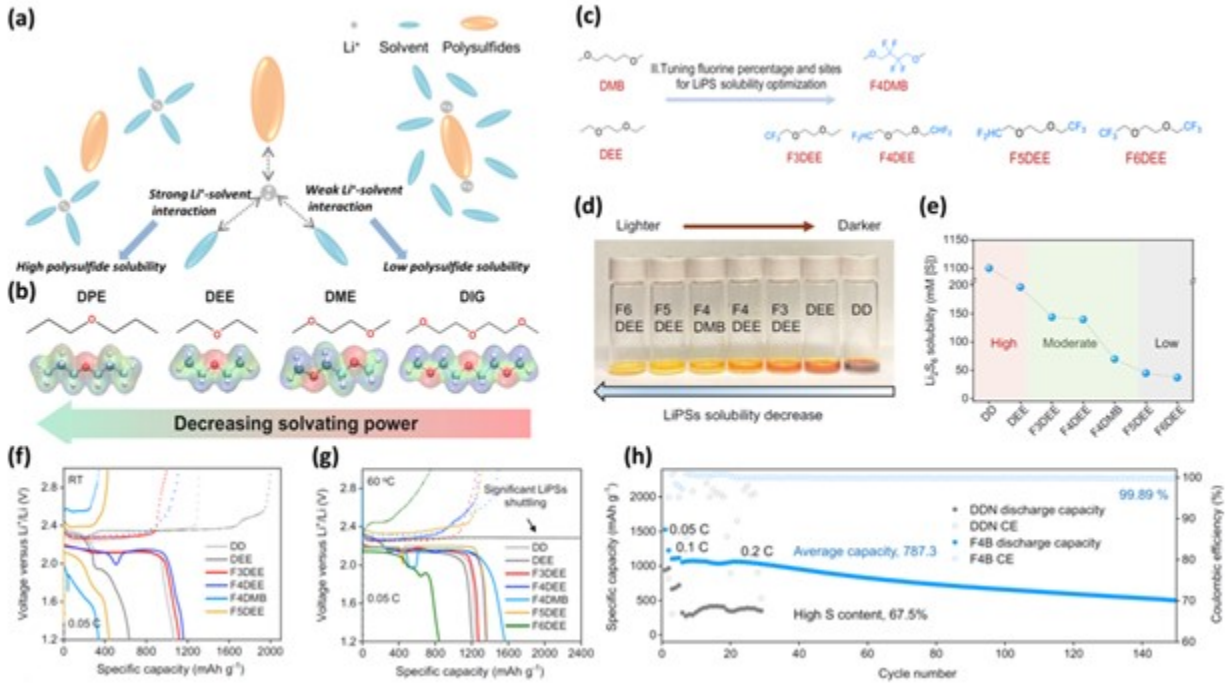

Figure 4. Manipulating the structure of solvents to decrease the solubility of polysulfides. (a) The stronger Li^+-solvent interaction compared to Li^+-polysulfide interaction prevents the dissolution of polysulfides. (b) The electrostatic potential (ESP) maps of the studied ether molecules. The red, green, and white spheres stand for the O, C, and H Atoms, respectively. Reproduced with permission.[61a] Copyright 2023 The Author(s), published by Springer Nature under the terms of the Creative Commons CC-BY 4.0 license. (c) The molecular structures of F6DEE, F5DEE, F4DMB, F4DEE, F3DEE, DEE, and DMB. (d) Photograph of 0.1 M Li_2S_6 (based on stoichiometric amounts of S_8 and Li_2S) in different electrolyte solvents. From left to right are F6DEE, F5DEE, F4DMB, F4DEE, F3DEE, DEE, and DD. All the solutions are saturated except for DD. (e) Polysulfide solubility of each solvent. The voltage profiles of Li-S cells using DD, DEE, and fluorinated ether electrolytes at 0.05 C at (f) room temperature and (g) 60 °C. (h) Cycle stability of Li-S cells with lean F4DMB electrolyte. The cell was operated at 0.05 C for the first two cycles and then at 0.1 C for three cycles, followed by continuous cycling at 0.2 C at 60 °C. Reproduced with permission.[64] Copyright 2023 The Author(s), published by United States National Academy of Sciences (United States) under the terms of the Creative Commons CC-BY 4.0 license.

Increasing the salt concentration can also drive the electrolyte into a weakly solvating regime that has lower polysulfide solubility (**Figure 5**a). Typical dilute electrolytes contain free solvents and solvent-separated ion pairs, the latter one is composed of 3 to 4 solvent molecules coordinate with a Li^+ ion. The high-concentration electrolytes contain no free solvent molecules, and the number of solvent molecules coordinated to a Li^+ cation is 1 to 2. The salt anions enter the solvation sheath to form contact ion pairs or cation-anion aggregates. Such coordination structure does not favor dissolution of

This article is protected by copyright. All rights reserved.

Author Manuscript

15214095, 2024, 29, Downloaded from https://advanced.onlinelibrary.wiley.com/doi/10.1002/adma.202401263 by Office Of Scientific And Technical Information, Wiley Online Library on [19/08/2025]. See the Terms and Conditions (https://onlinelibrary.wiley.com/terms-and-conditions) on Wiley Online Library for rules of use; OA articles are governed by the applicable Creative Commons License

polysulfides. For example, a high concentration solution of LiTFSI in G4 (approximately 4.5 M) is reported with a very low solubility of polysulfides of 60 mM_S.[65] An interesting observation is that in electrolytes based on LiTFSI and ethers, both very low concentration[57] and high concentration lead to decreased polysulfide solubility comparing to the typical concentration of 1 M. This indicates that the proportion of solvent and anion in the Li^+ solvation structure plays a crucial role to determine the solubility of polysulfide, but the correlation is not monotonic.

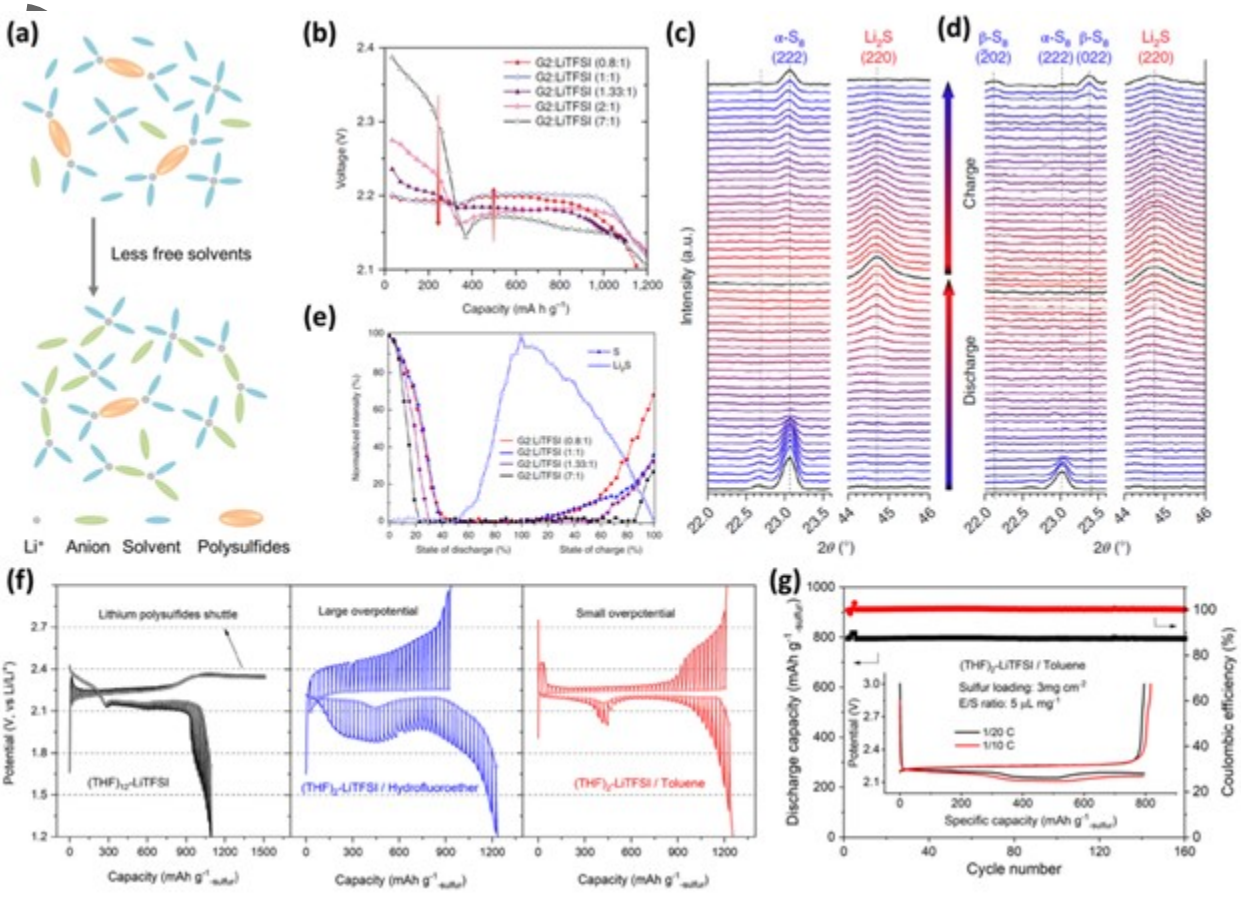

Figure 5. (a) Reducing free solvents to decrease the solubility of polysulfides. (b) The equilibrium voltages as a function of the SOD for different G2:LiTFSI electrolytes; the arrows indicate the descending G2:LiTFSI. (c, d) The operando XRD patterns of the sulfur cathodes in the G2:LiTFSI (1:1) (c) and (7:1) (d) electrolytes as a function of the status of discharge and charge. (e) The quantification of sulfur evolution on discharge and charge (consumption and re-formation) for different electrolytes, as normalized to the original amount of sulfur in the cathode. As a representative, Li_2S is also shown for the G2:LiTFSI (1:1). The relative amount of each phase is quantified by integrating its major peak. Reproduced with permission.[66] Copyright 2018, Nature Publishing Group. (f) The GITT voltage profiles (current pulse of C/20 for 20 min, followed by a relaxation time for 2 h) of Li-S cells in the three electrolytes, showing the dependence of quasi-equilibrium cell voltage on the electrolyte microstructure. The empty circles plot the cell voltage in a thermodynamic equilibrium. GITT, galvanostatic intermittent titration technique. (g) Cycling stability

This article is protected by copyright. All rights reserved.

Author Manuscript

15214095, 2024, 29, Downloaded from https://advanced.onlinelibrary.wiley.com/doi/10.1002/adma.202401263 by Office Of Scientific And Technical Information, Wiley Online Library on [19/08/2025]. See the Terms and Conditions (https://onlinelibrary.wiley.com/terms-and-conditions) on Wiley Online Library for rules of use; OA articles are governed by the applicable Creative Commons License

of cells under lean electrolyte and high sulfur loading conditions (3 mg cm_{sulfur}^{-2}, 55 °C, C/10, fixed discharge capacity of 800 mAh g^{-1}), and the inset shows the voltage profiles. Reproduced with permission.[67] Copyright 2023, Cell Press.

Nazar and coworkers studied the effect of LiTFSI concentration in G2 on the Li-S electrochemical reaction behaviors. It was discovered that decreasing the ratio between G2 and LiTFSI transformed the conventional solid-liquid-solid route of Li-S reaction to the solid-transient liquid-solid state conversion (Figure 5b).[66] The discharge curve exhibits a transition from the 'slope followed by plateau' and the 'single-slope' profile to a distinct 'equipotential bi-plateau' profile. *Operando* XRD characterization of sulfur was used to understand the conversion pathway. The dynamics of sulfur consumption is slower in electrolytes with a lower G2:LiTFSI ratio, and the reformation of sulfur after charge is mainly α-S_8 while β-S_8 is formed in electrolyte with G2:LiTFSI in 7:1 molar ratio (Figures 5c to 5e). In the electrolyte with low G2:LiTFSI ratio, the first plateau with lower potential is attributed to that the solid S_8 undergoes a two-phase reaction to form nominal Li_2S_4 (Reaction 8), which is kinetically enabled by a marginal solubility of polysulfides. The nominal Li_2S_4 subsequently is further reduced to Li_2S and Li_2S_3 (Reaction 9). The voltage slightly rises in this step, which is attributed by an unusual equilibrium of the cleavage of a divalent polysulfide into a monovalent radical (Reaction 10). Under lean electrolyte condition with a E/S ratio of 5 µl mg^{-1}, the cells using the electrolyte with the G2:LiTFSI ratio of 0.8:1 demonstrated a significantly improved capacity retention of 720 mA h g^{-1} over 100 cycles. However, similar to the Li-S cells with weakly solvating electrolytes using fluorinated ether F4DMB as solvent,[65] the sulfur areal loading in the demonstrated cell is relatively low at 2 mg cm^{-2}. This is another evidence that weakly solvating electrolytes can induce kinetic bottleneck due to their low polysulfide solubility.

$$S_8 + 4Li^+ + 4e^- \rightarrow 2Li_2S_4 \qquad \text{(Reaction 8)}$$

$$Li_2S_4 + 2Li^+ + 2e^- \rightarrow Li_2S_3 + Li_2S \qquad \text{(Reaction 9)}$$

$$4Li_2S_3 \rightarrow 4Li_2S + S_8 \qquad \text{(Reaction10)}$$

Due to the strong attraction between contact ion pairs and cation-anion aggregates introduced by high concentration of salt, it is challenging for such electrolyte to provide adequate ionic conductivity. The poor ionic conductivity and high viscosity of high-concentration electrolyte lead to large overpotential and consequent limited cycle life. Weakly solvating solvents with low viscosity and miscibility with base electrolytes, especially fluorinated ethers, have been widely employed as an ideal diluent to reduce viscosity and maintain the unique characteristics of the solvated electrolytes. Due to their low solvating characteristic, introduction of fluorinated ethers is able to further lower the solubility of polysulfides.[65] A high-concentration LiTFSI electrolyte in acetonitrile [$(ACN)_2$-LiTFSI] is reported

This article is protected by copyright. All rights reserved.

Author Manuscript

15214095, 2024, 29, Downloaded from https://advanced.onlinelibrary.wiley.com/doi/10.1002/adma.202401263 by Office Of Scientific And Technical Information, Wiley Online Library on [19/08/2025]. See the Terms and Conditions (https://onlinelibrary.wiley.com/terms-and-conditions) on Wiley Online Library for rules of use; OA articles are governed by the applicable Creative Commons License

with a high viscosity of 138 cP and ionic conductivity of 1.35 mS cm^{-1}. Adding 1,1,2,2-tetrauoroethyl 2,2,3,3-tetrauoropropyl ether (TTE) to $(ACN)_2$-LiTFSI with a volume ratio of 1:1 resulted in a much lower viscosity of 8.6 cP and higher ionic conductivity of 1.57 mS cm^{-1}.[68] The Li-S cells that incorporate the mixture of $(CAN)_2$-LiTFSI: TTE at 1:1 volume ratio displayed lower overpotential, higher reversible capacity and cyclability compared to Li-S cells using $(ACN)_2$-LiTFSI electrolyte. Liu *et al.* also demonstrated that aromatic solvents were ideal diluent with anti-solvating behavior and low viscosity.[67] Toluene, benzene, fluorobenzene, benzene-trifluoride and toluene/CS_2 are explored as diluents for high concentration ethereal electrolytes, and all those solvents is well miscible and maintain similar solvating characteristics. Benefiting from the lower viscosity of toluene (toluene: 0.58 cP, TTE: 1.43 cP), $(THF)_2$-LiTFSI/toluene electrolyte exhibits a lower viscosity of 4.27 cP than that of $(THF)_2$-LiTFSI/TTE (5.31 cP) at 35 °C. Those features of $(THF)_2$-LiTFSI/toluene electrolyte help to facilitate the sulfur redox kinetics with a much lower voltage hysteresis of ~100 mV, while a voltage hysteresis of about 360 mV is observed when using the $(THF)_2$-LiTFSI/TTE electrolyte (Figure 5f). The corresponding batteries were able to maintain 800 mAh g^{-1} for 160 cycles with sulfur areal of 3 mg cm^{-2} and E/S ratio at 5 mL g_s^{-1} at 55 °C (Figure 5g). Again, it is noticeable that this weakly solvating electrolyte only worked well with relative low sulfur loading at high temperature. The performance significantly deteriorated when a higher sulfur loading of 6.3 mg cm^{-2} was used.

3.3. Highly solvating electrolytes

High solvating electrolytes are a clear choice for good electrochemical kinetics because the high polysulfide solubility ensures the reduction of sulfur is controlled by its intrinsic kinetics.[69] Polysulfides alternate the sluggish solid-solid sulfur conversion to dissolution-assisted conversion processes, serving as intrinsic redox mediators.[70] Thus, boosting the solubility of polysulfides can in principle accelerate the overall kinetics. In the solid-liquid-solid conversion pathway, adequate polysulfide solubility is essential to avoid the undesired saturation and precipitation. High solvating solvents, characterized by DN or dielectric constant, are expected to enable high polysulfides solubility. The solvents with different DN and dielectric constant are summarized in Table 1. The solvents with high DN and dielectric constant such as dimethyl sulfoxide (DMSO), dimethylformamide (DMF), 1,3-dimethyl-2-imidazolidinone (DMI) and dimethylacetamide (DMA) are demonstrated to dissolve high content of Li_2S_8 up to 28-38 M_s (Table 2). DMI, DMA and DMSO are also able to dissolve more than 9 M_s Li_2S_6 (**Figure 6**a).[27] The much-improved solvation capacity is believed to promote sulfur utilization under lean electrolyte conditions.

In addition to the higher solubility of LiPSs, the Li cation complex exhibits soft Lewis acid characteristic in high DN electrolytes because the positive charge of the cation is shielded. Thus, the free radical $S_3^{\bullet-}$ as Lewis soft base is found to be stabilized in the high DN electrolytes.[71] The green color in DMI and DMSO solutions and the blue color in DMA solution indicate the presence of $S_3^{\bullet-}$

This article is protected by copyright. All rights reserved.

Author Manuscript

15214095, 2024, 29, Downloaded from https://advanced.onlinelibrary.wiley.com/doi/10.1002/adma.202401263 by Office Of Scientific And Technical Information, Wiley Online Library on [19/08/2025]. See the Terms and Conditions (https://onlinelibrary.wiley.com/terms-and-conditions) on Wiley Online Library for rules of use; OA articles are governed by the applicable Creative Commons License

(Figure 6a).[27] The operando X-ray absorption near edge structure spectroscopy (XANES) also supports the presence of $S_3^{\bullet-}$ during discharge in the Li-S cells with high DN electrolyte DMA (Figure 6b).[72] The $S_3^{\bullet-}$ exhibits a distinctive low-energy feature corresponding to the 1s-3p(π*) transition, which is detected at an energy level of 2468.5 eV. The presence of $S_3^{\bullet-}$ drives the liquid-solid-liquid reaction process with different redox behaviors. From CV curves, the high DN electrolytes based on DMSO exhibits two widely separately reduction peaks and three oxidation peaks in contrast to typical two close reduction peaks and one oxidation peak in DME/DOL electrolytes (Figure 6d, f).[73] The different redox characteristics indicate a varied reaction pathway, which was characterized with *operando* UV-vis spectroscopy. UV-vis spectra are known for detection of polysulfide dianions and radicals: peaks at 492 nm attributed to S_8^{2-}, 475 nm attributed to S_6^{2-}, 420 nm attributed to S_4^{2-}, 270 nm attributed to S_3^{2-}, and 617 nm attributed to $S_3^{\bullet-}$ free radical.[74] During the sulfur reduction process in medium solvating DME/DOL electrolytes, S_4^{2-} is found to be the dominant intermediate that participates the multistep chain-shortening process. While the stabilization of the $S_3^{\bullet-}$ can provide additional reaction conversion by providing the solvation-mediated radical pathway. In the first redox peak of about 2.7 V, S_8 is electrochemically reduced to S_8^{2-} anion (Reaction 1), which is further reduced to S_4^{2-} (Reaction 11). S_8^{2-} anions also disproportionate to S_6^{2-} anion and elemental sulfur (Reaction 12), and S_6^{2-} anion is capable to dissociate into $S_3^{\bullet-}$ radicals in high solvating electrolytes (Reaction 13).[72] The radical $S_3^{\bullet-}$ serves as a key redox mediator to promote the electrochemical reduction of S_4^{2-} (Reactions 14 to 17). However, further research under lean electrolytes found that the equilibrium of the dissociation of S_6^{2-} into $S_3^{\bullet-}$ shift toward S_6^{2-} at high concentration.[74] Gupta *et al.* demonstrated that the presence of radical $S_3^{\bullet-}$ inclined to diminish in DMSO and 1-methylimidazole (MeIm), while DMA still exhibited evident of $S_3^{\bullet-}$.[74]

$$S_8^{2-} + 2e^- \rightarrow 2S_4^{2-} \quad \text{(Reaction 11)}$$

$$S_8^{2-} \leftrightarrow S_6^{2-} + 1/4\, S_8 \quad \text{(Reaction 12)}$$

$$S_6^{2-} \leftrightarrow 2S_3^{\bullet-} \quad \text{(Reaction 13)}$$

$$S_3^{\bullet-} + 2e^- \rightarrow S_3^{2-} \quad \text{(Reaction 14)}$$

$$2S_3^{2-} + 2S_3^{\bullet-} \leftrightarrow 3S_4^{2-} \quad \text{(Reaction 15)}$$

$$S_4^{2-} + 1/4\, S_8 \leftrightarrow 2S_3^{\bullet-} \quad \text{(Reaction 16)}$$

$$S_4^{2-} + 8Li^+ + 6e^- \rightarrow 4Li_2S \quad \text{(Reaction 17)}$$

This article is protected by copyright. All rights reserved.

Author Manuscript

15214095, 2024, 29, Downloaded from https://advanced.onlinelibrary.wiley.com/doi/10.1002/adma.202401263 by Office Of Scientific And Technical Information, Wiley Online Library on [19/08/2025]. See the Terms and Conditions (https://onlinelibrary.wiley.com/terms-and-conditions) on Wiley Online Library for rules of use; OA articles are governed by the applicable Creative Commons License

Author Manuscript

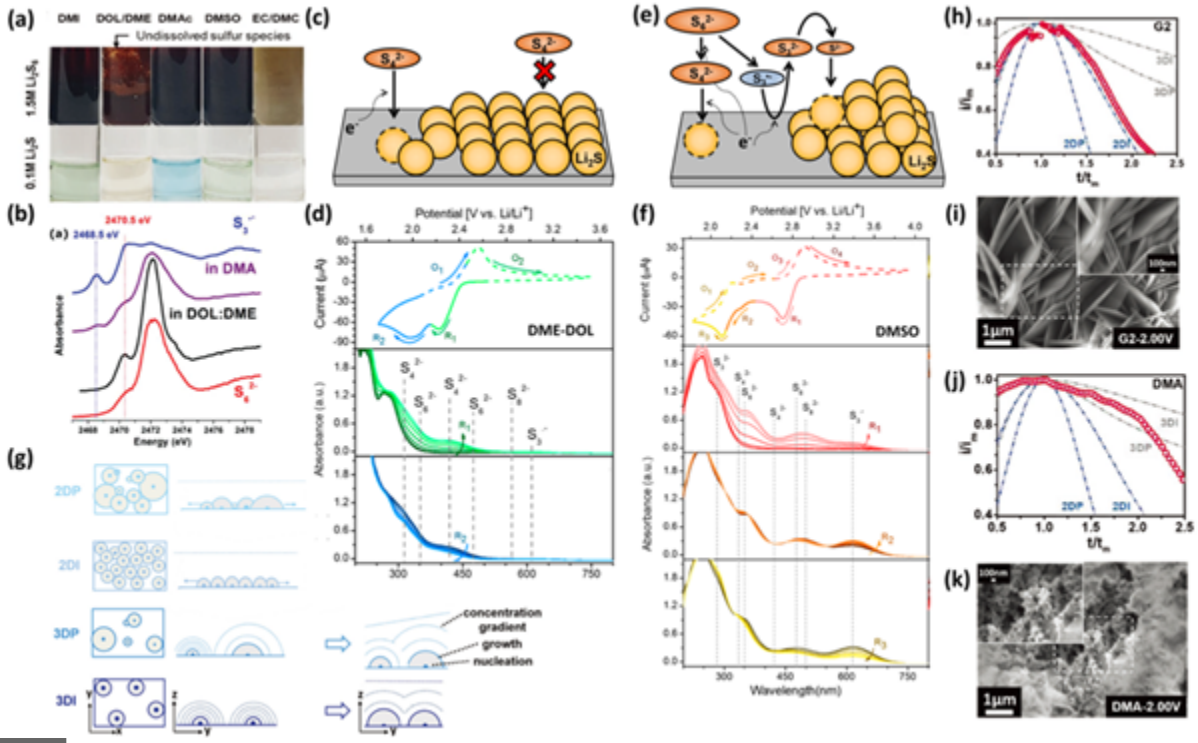

Figure 6. The high solvating electrolytes stabilize the free radical $S_3^{\bullet-}$ to improve the reaction kinetics. (a) Optical images of (top) 1.5 M Li_2S_6 in various solvents and (bottom) filtrate of 0.1M Li_2S in the same solvents. Reproduced with permission.[27] Copyright 2020, Wiley-VCH. (b) Sulfur K-edge XANES studies of experimental spectra collected during discharge (around 340 mAh g^{-1}) in Li-S cells using DMA or DOL:DME electrolytes compared with $S_3^{\bullet-}$ and S_6^{2-} reference materials. Reproduced with permission.[72] Copyright 2015, Wiley-VCH. (c) A schematic illustrating Li_2S nucleation in Li-S batteries with moderate solvating electrolytes. (d) CV of 2.0 mM S_8-1.0 M LiTFSI in DOL:DME (1:1), and operando UV-vis absorption spectra of each reaction steps (Color from dark to light with the arrow in each panel represents the changes over time. (e) A schematic illustrating Li_2S nucleation in Li-S batteries with high solvating electrolytes. (f) CV of 2.0 mM S_8-1.0 M LiTFSI in DMSO, and operando UV-vis spectra of each reaction step. (Color from dark to light with the arrow in each panel represents the changes over time; UV band attribution: S_8^{2-} at 492 nm, S_6^{2-} at 475 and 350 nm, S_4^{2-} at 420 and 325 nm, S_3^{2-} at 270 nm, $S_3^{\bullet-}$ at 617 nm. Reproduced with permission.[73] Copyright 2016, American Chemical Society. (g) Schematic illustration of 2DP/2DI (BFT models) and 3DP/3DI (SH models) (*x*-*y* is parallel to the substrate; *y*-*z* is vertical to the substrate). Chronoamperograms of Li_2S deposition in electrolyte based on G2 (h) and DMA (j) at 2.00 V versus Li^+/Li, and the corresponding dimensionless transient current-time relationship in comparison with theoretical 2D and 3D models. i_m: peak current; t_m: time needed to achieve the peak current. SEM images of final Li_2S deposits on carbon paper in G2 (i) and DMA (k). Reproduced with permission.[75] Copyright 2019, Wiley-VCH.

This article is protected by copyright. All rights reserved.

15214095, 2024, 29, Downloaded from https://advanced.onlinelibrary.wiley.com/doi/10.1002/adma.202401263 by Office Of Scientific And Technical Information, Wiley Online Library on [19/08/2025]. See the Terms and Conditions (https://onlinelibrary.wiley.com/terms-and-conditions) on Wiley Online Library for rules of use; OA articles are governed by the applicable Creative Commons License

In addition to the radical-assisted pathway, the high solvating electrolyte promote charges transfer and solvent-assisted phase transfer, alleviating the dependence of triple-phase boundaries for redox reactions (Figure 6c, e).[72, 76] To probe the effect of electrolyte properties on Li_2S deposition, Li *et al.* developed potentiostatic electrodeposition method to elucidate the Li_2S deposition behaviors.[75] The solvent-mediated Li_2S deposition is ascribed to the theoretical models of 2D instantaneous nucleation in the low-DN glyme-based electrolytes and 3D progressive nucleation in high-DN electrolytes (Figure 6g).[77] In glyme-based electrolytes with low DN such as G2, Li_2S inclines to precipitate once produced with a high nucleation rate and higher density of nuclei according to the 2D instantaneous nucleation (Figure 6h, i). In comparison, the high-DN electrolytes reduce the Li_2S nucleation rate, forming a sporadic distribution of nuclei with uneven size. high-DN electrolyte has higher solubility of lower order polysulfides, thus the Li_2S growth is mainly controlled by the mass transport of lower order polysulfides in the electrolytes, presenting a 3D progressive nucleation behavior (Figure 6j, k).

However, high-DN electrolytes show incompatibility with the Li anode, exacerbating the Li metal corrosion and electrolyte consumption. The high-DN solvents often exhibit high reactivity with Li metal and the inability of the formation of a durable and reliable SEI layer.[69, 74] This issue can be alleviated with DOL as so-solvent or $LiNO_3$ as additive.[27, 78] Baek *et al.* reported DMI as high-DN solvent and $LiNO_3$ as additive with reasonable compatibility with the Li anode for Li-S batteries.[27] The addition of $LiNO_3$ enables the cells work with 59.6% of its original capacity after 80 cycles under E/S ratio of 5 mL g_s^{-1}, while the sulfur loading is only 1 mg cm^{-2}. When using higher sulfur loading of 5 mg cm^{-2}, the Li-S batteries failed with shallow discharge behavior even increasing E/S ratio to 6 mL g_s^{-1}. Tetramethylurea (TMU) is also a high-DN solvent and more lithium-compatible than DMA and DMSO.[78] The large dipole moment of TMU affords strong solvation effect to stabilize $S_3^{\bullet-}$, the radical pathway improves the conversion efficiency to Li_2S with a high initial capacity of 1524 mAh g^{-1} at 0.05 C under E/S ratio of 3 mL g_s^{-1} in a pouch cell. However, even with the introduction of DOL and $LiNO_3$, the cycle stability was still limited with only about 7 cycles due to the electrolyte consumption under lean condition.

Solvent structure engineering represents a promising strategy to incorporate new desirable traits while retaining the features of the original solvent.[64] Pyridine (PN) possesses high DN of 33.1 kcal mol^{-1}, thus PN and its derivatives are expected to enable the radical pathway. Tuning the electron-donating nature of PN through introducing electronegative functional groups, such as fluorine is validated to address the high reactivity between PN and Li metal.[79] The 3-, and 4- fluoropyridine (3-FPN, and 4-FPN) still display high DNs of 29.7 kcal mol^{-1} and 30.3 kcal mol^{-1} and are able to stabilize $S_3^{\bullet-}$ radical (**Figures 7**a and 7b). 3-FPN demonstrates improved compatibility with Li metal with immersion test (Figure 7c). Benefiting from the derived LiF-rich SEI layer and stabilization of $S_3^{\bullet-}$, 3-FPN-based electrolytes enable the cell with 8.0 mg_s cm^{-2} sulfur loading and E/S ratio of 8 mL g_s^{-1} to deliver a high initial specific capacity of ~1322 mAh g^{-1} and stable cycling over 40 cycles.

This article is protected by copyright. All rights reserved.

Author Manuscript

15214095, 2024, 29, Downloaded from https://advanced.onlinelibrary.wiley.com/doi/10.1002/adma.202401263 by Office Of Scientific And Technical Information, Wiley Online Library on [19/08/2025]. See the Terms and Conditions (https://onlinelibrary.wiley.com/terms-and-conditions) on Wiley Online Library for rules of use; OA articles are governed by the applicable Creative Commons License

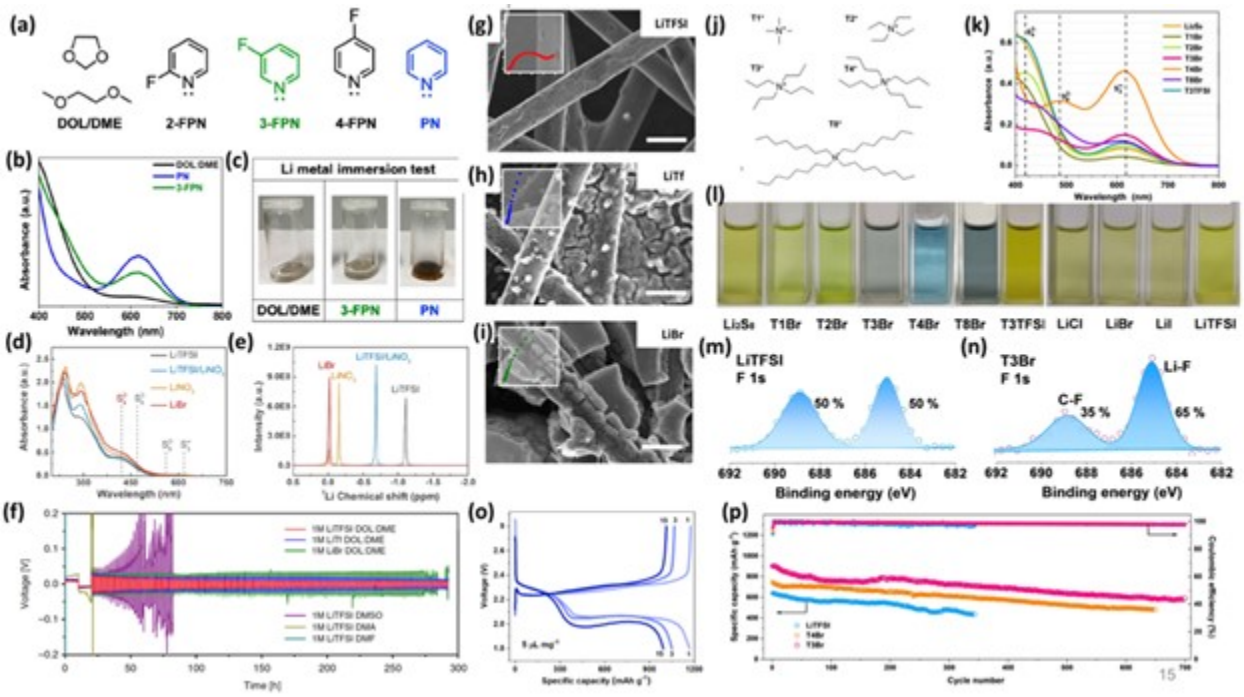

Figure 7. Strategies to address the issue of incompatibility between the high solvating electrolytes and Li metal. (a) Chemical structures of 1,3-dioxolane, dimethoxyethane (DOL/DME), pyridine (PN) and its -F substituted derivatives, namely, 2-FPN, 3-FPN, and 4-FPN. (b) UV-vis absorption spectra of 1 mM Li_2S_6 in DOL/DME, PN, and 3-FPN. (c) Digital photographs of lithium foil immersed in DOL/DME, 3-FPN, and PN after 30 min. Reproduced with permission.[79] Copyright 2022, American Chemical Society. (d) UV-vis spectra of polysulfide solution (nominally "Li_2S_4") diluted by 100 times in LiTFSI, LiTFSI/$LiNO_3$, $LiNO_3$, and LiBr electrolytes. (e) ^{7}Li NMR spectra of solution of Li salts with different anions vs. 3 M LiCl in D_2O standard. Reproduced with permission.[80] Copyright 2019, American Chemical Society. (f) Galvanostatic 1 h/1 h charge/discharge operation was conducted with 0.5 mA cm^{-2} current density for six different electrolyte systems. SEM images of Li_2S deposition morphology in electrolyte solutions with (g) LiTFSI, (h) LiTf, and (i) LiBr as supporting electrolytes. Scale bars, 10 µm. The Nyquist plots of the impedances measured at the points are provided in the insets. Reproduced with permission.[81] Copyright 2019 The Author(s), published by Springer Nature under the terms of the Creative Commons CC-BY 4.0 license. (j) The structures of different cations. (k, l) UV-vis spectra and photographs of the Li_2S_8 solution before and after contact with QASs T1Br, T2Br, T3Br, T4Br, T8Br and T3TFSI. (m, n) X-ray photoelectron spectroscopy (XPS) F 1s spectra of the cycled Li anodes in different electrolytes. (o) The discharge/charge profiles of KB/S at 0.05 C with a low E/S ratio 5 µL mg^{-1} and high sulfur loading of 4.6 mg cm^{-2}. (p) Long cycling performance at 1 C with low sulfur loading of ~2 mg cm^{-2} and under flooded electrolyte condition. Reproduced with permission.[82] Copyright 2023, Wiley-VCH.

This article is protected by copyright. All rights reserved.

Author Manuscript

15214095, 2024, 29, Downloaded from https://advanced.onlinelibrary.wiley.com/doi/10.1002/adma.202401263 by Office Of Scientific And Technical Information, Wiley Online Library on [19/08/2025]. See the Terms and Conditions (https://onlinelibrary.wiley.com/terms-and-conditions) on Wiley Online Library for rules of use; OA articles are governed by the applicable Creative Commons License

Another strategy to address the incompatibility while maintaining the features of high-DN electrolytes is to introduce supporting salt anions or cations. Since the Li cation is a strong Lewis acid with high tendency to accept electron, introducing anions with high donicity/Lewis base (such as F^-, Cl^-) will lead to strong cation-anion interaction that is difficult to dissociate. As in consideration of the electrochemical stability at the cathode side, the choice of anions with high donicity is limited, and trifluoroacetate (TFA^-),[83] triflate (Tf^-), Br^-, NO_3^-, and thiocyanate (SCN^-)[84] are generally studied. The donicity of anions follows the trend of $TFSI^- < Tf^- < Br^- < NO_3^- < SCN^-$, the increased donicity contributes to the higher polysulfide solubility, while only SCN^- is strong enough to stabilize the $S_3^{\bullet-}$ (Figure 7d).[80, 84] The anions with high donicity are also discovered to alleviate cathode passivation. The discharge product of electrolytes with weak donating anions of $TFSI^-$ grows with a 2D film morphology (Figure 7g).[81] In contrast, by replacing the anions with high DN anions including Tf^- (triflate) and Br^-, 3D particle-like Li_2S deposits are dominant (Figures 7h and 7i). The anions with high donicity alleviate cathode passivation thus promote the charge transfer kinetics. Yang *et al.*, through three-electrode EIS measurements, found that the charge-transfer resistance of cathodes is reduced in the roder from LiTFSI, LiTFSI/$LiNO_3$, $LiNO_3$ to LiBr, following the anion donicity trends (Figure 7g-i).[81]. Also, the high-DN anions with strong interaction of Li cations can hinder the participation of solvent molecules, thus dominating the first solvation shell (Figure 7e).[85] The anions dominated solvation structure suppress the solvent decomposition and form a stable inorganic SEI on the anode, alleviating the consumption of electrolytes with Li metal to expand the cycle lifespan (Figure 7f). Chu *et al.* studied the LiTFSI and $LiNO_3$ co-salt electrolytes with varying ratios of LiTFSI and $LiNO_3$ (from 95:5 to 40:60).[85] With the increase proportions of $LiNO_3$, the corresponding SEI with less organic but more N-rich inorganic components favor prolonged cycle performance of the Li metal. Also, the use of high-DN NO_3^- improves the solubility of the polysulfides and Li_2S, which facilitated solution-mediated sulfur redox reactions. The Li-S batteries with E/S ratio of 5 mL g_s^{-1} and sulfur loading of 4.5 mg cm^{-2} using highest proportion of $LiNO_3$ achieved high sulfur utilization of 1200 mAh g^{-1} and improved cycle lifespan up to 100 cycles.

Supporting cations with soft Lewis acid nature are alternative choice to facilitate the reversible reactions of sulfur. Strong Lewis acid Li cation is strongly solvated by solvents and exhibits a weak electrostatic interaction with short chain polysulfides, which retard the reduction of long-chain polysulfides to short-chain polysulfides.[86] The ammoniums stand out as potential additives for practical Li-S batteries (Figure 7j). By tailoring the ionic strength of the electrolyte and forming hydrogen bond between sulfide anions and ammonium cations, ammonium salts are capable of increasing the solubility of Li_2S and other short-chain species, thereby promoting the dissociation of Li_2S.[87] The dissociation also alternates the dense film Li_2S to porous three-dimensional flake, which leads to the delay of the cathode passivation.[88] By addressing the passivation issue, the ammonium additive NH_4TFSI improves the sulfur utilization and cycle lifespan of Li-S batteries with E/S of 5

This article is protected by copyright. All rights reserved.

Author Manuscript

15214095, 2024, 29, Downloaded from https://advanced.onlinelibrary.wiley.com/doi/10.1002/adma.202401263 by Office Of Scientific And Technical Information, Wiley Online Library on [19/08/2025]. See the Terms and Conditions (https://onlinelibrary.wiley.com/terms-and-conditions) on Wiley Online Library for rules of use; OA articles are governed by the applicable Creative Commons License

mL g_s^{-1}.[88] In addition, the additives composed of high-DN tetrapropylammonium or tetrabutylammonium cations and high-DN bromide anions are demonstrated to stabilize the $S_3^{\bullet-}$ radicals (Figures 7k and 7l).[82] With the radical pathway, the Li-S batteries with tetrapropylammonium bromide (T3Br) additive have a high initial specific capacity of 1150 mAh g^{-1} under E/S ratio of 5 mL g_s^{-1} and high sulfur loading of 4.6 mg cm^{-2} (Figure 7o).[82] Also, the cations with large ionic radius can work as cationic surfactant that promote the dense growth of Li.[114] During the lithium growth process, the electrostatic attraction force the cationic surfactant molecules to aggregate around protuberances and generate a nonpolar lithiophobic layer. The lithiophobic layer force the lithium cations to platting at adjacent regions, thus to enable uniform Li deposits.[89] Ascribed to the cationic surfactant feature along with the formation of LiF-rich SEI (Figures 7m and 7n), the incorporation of T3Br improve the stability of Li-S batteries (Figure 7p).[82]

Polysulfides is known undergoing disproportionation reaction, $Li_2S_x \rightleftharpoons Li_2S_y + (x-y)/8\ S_8$ ($x > y$), to insoluble elemental sulfur and lower order polysulfides. The generation of insoluble elemental sulfur within the liquid electrolytes or separator pores causes fast capacity attenuation and irreversible loss of sulfur.[56a, 90] The cations with weak Lewis acidity can entrap and stabilize the polysulfides which help hinder the sluggish disproportionation reaction and promote the electrochemical reactions.[91] It was demonstrated the soft acidic N-methyl-N-ethyl pyrrolidinium (MEP^+) cation prefers to coordinate with the soft base polysulfides through the deformation and overlap of electron clouds.[92] The strong absorbability of MEP cations towards polysulfides favors stable MEP-LiPSs complex, which has been demonstrated to drive the chemical reactions shift to electrochemical reactions with higher reaction kinetics. The stabilization of polysulfides and hinderance of polysulfide disproportion reactions are pivotal to deliver the 5-Ah Li-S batteries under a lean electrolyte ratio of 4 μL mg^{-1} with high energy density of 300 Wh kg^{-1} for 100 cycles.

3.4. Low-density electrolytes

Designing an electrolyte with low density provides a promising alternative to reduce the weight fraction of electrolyte, which enables higher energy density output at the same E/S volume ratio. As for the solid-liquid-solid conversion process, the conventional electrolyte (1 M LiTFSI and 2 wt% $LiNO_3$ in DME/DOL (v/v = 1/1) has a density of 1.17 g mL^{-1} at room temperature (**Figure 8**a).[93] The weakly solvating electrolytes composed of high concentration electrolyte with fluorinated ether dilutes typically have higher density of ~1.5 g mL^{-1}.[66, 94] This is due to the high density of fluorinated ethers (higher than 1.3 g mL^{-1}) and high concentration of Li salt. By adopting the electrolyte with low density of ~0.8 g mL^{-1} instead of the conventional electrolyte or weakly solvating electrolyte with fluorinated ethers, the energy density of Li-S batteries is expected to improve ~30% or ~40% at E/S ratio of 5 mL g_s^{-1} (Figure 8b).[95]

This article is protected by copyright. All rights reserved.

Author Manuscript

15214095, 2024, 29, Downloaded from https://advanced.onlinelibrary.wiley.com/doi/10.1002/adma.202401263 by Office Of Scientific And Technical Information, Wiley Online Library on [19/08/2025]. See the Terms and Conditions (https://onlinelibrary.wiley.com/terms-and-conditions) on Wiley Online Library for rules of use; OA articles are governed by the applicable Creative Commons License

Author Manuscript

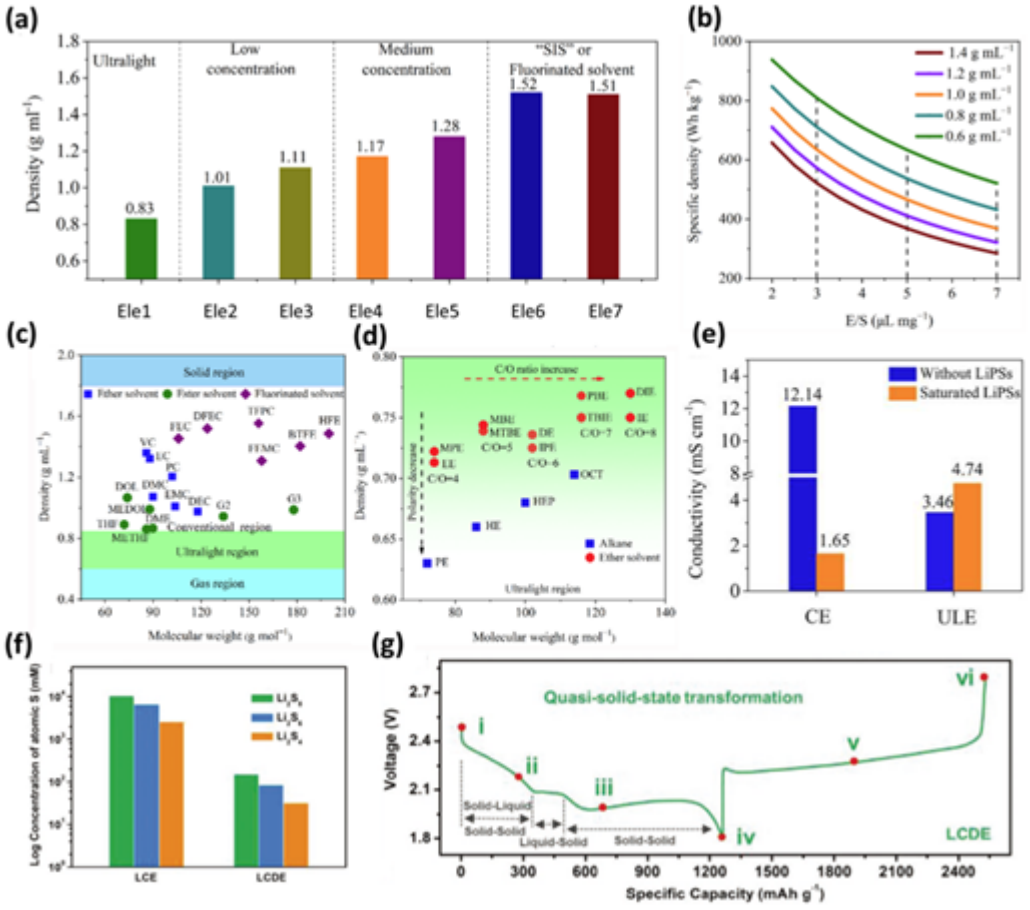

Figure 8. (a) The densities of different electrolytes (Ele1: 0.4 M $LiNO_3$ and 0.2 M LiTFSI in DME/MPE (48/52), Ele2: 0.1 M LiTFSI + 1 wt.% $LiNO_3$ in DME/DOL (50/50), Ele3: 0.6 M LiTFSI + 0.4 M $LiNO_3$ in DME/DOL (50/50), Ele4: 1.0 M LiTFSI + 2 wt.% $LiNO_3$ in DME/DOL (50/50), Ele5: 2.0 M LiTFSI in DOL, Ele6: 7 M LiTFSI in DME/DOL (50/50), Ele7: 1 M LiFSI in OFE/DME (95/5). (b) Relationship between the electrolyte density and the estimated specific energy of Li-S full cell. (c) Density diagram of common solvents. (d) Solvent density in the ultralight solvent region. (e) The comparison of conductivities of different electrolytes before and after dissolving saturated polysulfides. Reproduced with permission.[95] Copyright 2021, Wiley-VCH. (f) The GCD profiles of Li-S batteries with a high sulfur loading of 5.8 mg cm^{-2}. (g) Cycle performances of Li-S pouch cells with LCDE at 0.05 C. Reproduced with permission.[96] Copyright 2023, Wiley-VCH.

Alkanes and monoethers possess low density that is in the range of 0.6 to 0.8 g mL^{-1} (Figure 8d), presenting a possibility to design low-density Li-S electrolytes.[95] In comparison, common solvents such as ether, carbonate, and fluorinated solvents show a higher density from 1.0 to 1.6 g mL^{-1} (Figure 8c). Liu *et al.* presented an ultralight electrolyte (ULE, density of 0.83 g mL^{-1}) that consists of 0.4 M $LiNO_3$ and 0.2 M LiTFSI in DME/MPE (48/52) using methyl-propyl-ether (MPE) with a low density of 0.73 g mL^{-1} as a co-solvent. The content of DME and LiTFSI is also essential to keep a high degree of dissociation for a high ionic conductivity of 3.46 mS cm^{-1}. After dissolving

This article is protected by copyright. All rights reserved.

15214095, 2024, 29, Downloaded from https://advanced.onlinelibrary.wiley.com/doi/10.1002/adma.202401263 by Office Of Scientific And Technical Information, Wiley Online Library on [19/08/2025]. See the Terms and Conditions (https://onlinelibrary.wiley.com/terms-and-conditions) on Wiley Online Library for rules of use; OA articles are governed by the applicable Creative Commons License

polysulfides at saturation, the ionic conductivity of MPE based electrolyte increased to 4.74 mS cm^{-1} (Figure 8e) and the viscosity maintained at a moderate level (from 0.55 to 2.37 MPa s^{-1}). The good physical properties with saturated polysulfide ensured effective polysulfides redistribution and sulfur utilization, resulting in a discharge capacity of 1111 mAh g^{-1} in the Li-S cells. In comparison to Li-S cells with common electrolytes (CE), the ULE based Li-S cells shown a lower polarization and ~20% energy density. In addition to monoethers, alkanes also possess a low density below 0.8 g mL^{-1}. Also, nonpolar alkanes are capable of reducing the nucleation overpotential of Li to improve the Li plating/stripping reversibility.[97] Cheng *et al.* employed n-hexane (NH) to prepare a low-concentration and NH-diluted THF-based electrolyte (LCDE).[96] Benefiting from the low density of NH of 0.66 g $mL^{-1}$and the low salts concentration of 0.1 M, the LCDE had the lowest reported density of 0.79 g mL^{-1}. 0.1 M LiTFSI and 0.1 M $LiNO_3$ dissolved THF solution (LCE) showed high solubilities of Li_2S_8, Li_2S_6, and Li_2S_4 species of 10.4, 6.6, and 2.6 M_S (Figure 8f). Interestingly, by introducing 35% volume percentage of NH, the LCDE exhibited a sparing solvating electrolyte behavior with much decreased solubilities of Li_2S_8, Li_2S_6, and Li_2S_4 species at 152, 84, and 32 mM_S. Consequently, the LDCE based Li-S cells exhibited a different conversion process with three reduction plateaus (Figure 8g) dominated by solid-solid conversion pathway because of the low polysulfides solubility. Ascribe to the high sulfur utilization in quasi-solid-state transformation, the Li-S pouch cell with LCDE delivered a specific capacity of 1086 mAh g^{-1} under the condition of E/S ratio of 2.5 uL mg_s^{-1}. Fluorinated silane (Trifluoromethyl)trimethylsilane (TFMTMS) was also reported as a co-solvent for low-density electrolyte for its low density of 0.96 g mL^{-1}. The electrolyte composed of 0.4 M LiTFSI and 0.4 M $LiNO_3$ in DME/DOL/TFMTMS [48/17/35] solution has a low density of 1.02 g mL^{-1}.[7b] The introduction of TFMTMS contributed to a LiF and Li_xSi derivatives-rich SEI, which was demonstrated to effectively relieve the Li depletion and electrolyte consumption.

3.5. Electrolytes to optimize polysulfide solubility and Li anode stability

The unprotected Li metal constantly consumes the limited electrolytes via electrochemical and chemical parasitic reactions, and the resulting electrolyte consumption is identified to be one of the causes for the low cyclability of lean electrolyte Li-S batteries.[53] The weakly solvating electrolytes with sparing polysulfides dissolved represent as an effective solution to address such issues.[94] In common dilute electrolyte, the electrolyte consumption is mainly originated from the continuous decomposition of electrolyte solvent. While in weakly solvating electrolyte, the salt anions participate in formation of Li SEI dominated by inorganic species derived from anions, and the consumption of electrolyte can be reduced. Zheng *et al.* reported inert 1H,1H,5H-octafluoropentyl-1,1,2,2-tetrafluoroethyl ether (OFE) as main solvent for solubilizing few polysulfides while use 5 vol.% of DME to regulate the solvent solvating power strong enough to dissolve LiFSI.[94, 98] The optimal solvating power ensured an acceptable ionic conductivity of 1.24 mS cm^{-1} and low polysulfide solubility. Also, the fluorinated ether is beneficial for the formation of LiF-rich SEI, which promotes

This article is protected by copyright. All rights reserved.

Author Manuscript

15214095, 2024, 29, Downloaded from https://advanced.onlinelibrary.wiley.com/doi/10.1002/adma.202401263 by Office Of Scientific And Technical Information, Wiley Online Library on [19/08/2025]. See the Terms and Conditions (https://onlinelibrary.wiley.com/terms-and-conditions) on Wiley Online Library for rules of use; OA articles are governed by the applicable Creative Commons License

the cyclability in a lean electrolyte Li-S cell. The electrolyte of 1 M LiFSI in OFE/DME (v/v 95:5) was proved to suppress Li dendrite growth and promote Li plating/stripping reversibility, resulting in a high CE of 99.3% for 250 cycles at a current of 1 mA cm^{-2} with the deposition capacity of 1.0 mAh cm^{-2} in the Li|Cu cells. As ascribed to the two benefits, the Li-S cells with a lean electrolyte of 4.56 g $(Ah)^{-1}$ are cable to maintain a specific capacity of 775 mAh g^{-1} for 150 cycles.

In electrolytes enabling the conventional solid-liquid-solid sulfur conversion pathway, co-solvents or additives that can form a stable SEI are developed to protect Li metal, typically DOL and $LiNO_3$ are widely used. DOL can generate a robust polymer-based SEI layer through the cleavage of the cyclic structures.[24] NO_3^- anion prefer to enter the inner solvation shell of Li^+ so that it is reduced during Li depostion to form a stable passivation LiN_xO_y layer to alleviate the parasitic reactions.[47] It is found that manipulating the solvation structure is an effective approach to mitigate the side reactions while still maintaining the kinetically favorable solid-liquid-solid reactions.[99] The solvation structure of LiPSs can be predicted by the DN number that solvents with high donicity have strong ion-dipole interactions with cations that prefer to enter the inner solvation shells.[57a] Solvents with medium to high DN such as DME are applied to dissolve certain polysulfides and the strong cation-solvent interaction with Li cation guarantees that DME prefer to occupy the inner solvent shell. While the solvent with low DN and high reductive resistance can be incorporated to design encapsulating lithium polysulfide electrolytes (**Figure 9a**).[99] Such co-solvents occupying the outer solvation shell with high reductive stability are crucial for alleviating the parasitic reaction with Li. Hou *et al.* incorporated di-isopropyl sulfide (DIPS) to realize such heterogeneous solvation shell and the corresponding electrolyte that composed of 1M LiTFSI in DIPS/DME/DOL (1:2:2 by volume) is denoted as DIPS-EPSE(20%).[99b] The cation-solvent interaction between Li^+ and S atoms of DIPS is much weaker than that between Li^+ and O atoms of DME or DOL. Thus, a de-shielding phenomenon is reserved in the DIPS-EPSE electrolyte because of the reduction in electron cloud density around Li^+ (Figure 9b). The inferior coordination ability of the S atom compared with that of the O atom and the large steric hindrance of isopropyl result in the DIPS to emerge at the outer solvation shell (Figures 9c and 9d). Encapsulation lithium polysulfide structure alleviates the parasitic reactions between lithium polysulfide and Li metal in DIPS-EPSE. The Li_2S_8 in DME/DOL continuously is consumed after the Li metal in immersed (Figure 9e); on the contrary, DIPS-EPSE containing Li_2S_8 is more stable with Li metal (Figure 9f). The less S atomic content in the SEI of cells cycled with DIPS-EPSE (Figure 9g) validates that DIPS promotes the reduction stability of the encapsulated LiPSs. Such electrolyte with $LiNO_3$ enables a 1.2Ah Li-S battery to maintain 50% capacity after 103 cycles under lean electrolyte of E/S ratio of 3 mL g_s^{-1} and sulfur loading of 6.3 mg cm^{-2} (Figure 9h), which is one of the best demonstrations of Li-S batteries with long cycle stability under practical conditions.

This article is protected by copyright. All rights reserved.

Author Manuscript

15214095, 2024, 29, Downloaded from https://advanced.onlinelibrary.wiley.com/doi/10.1002/adma.202401263 by Office Of Scientific And Technical Information, Wiley Online Library on [19/08/2025]. See the Terms and Conditions (https://onlinelibrary.wiley.com/terms-and-conditions) on Wiley Online Library for rules of use; OA articles are governed by the applicable Creative Commons License

Author Manuscript

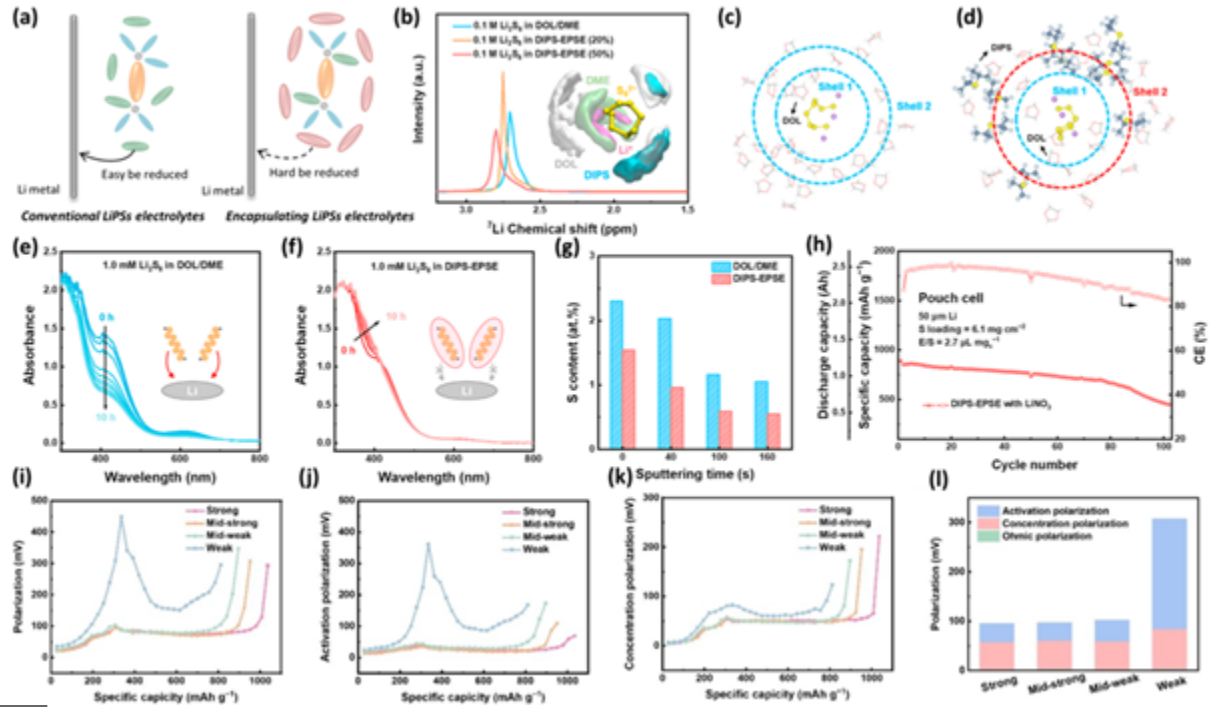

Figure 9. Encapsulating LiPSs electrolyte strategies to protect Li metal. (a) Scheme of the solvation structure of LiPSs in conventional electrolytes and encapsulating lithium polysulfide electrolytes. (b) ^{7}Li-NMR spectra of 0.1 M Li_2S_8 in DOL/DME and DIPS-EPSE. DOL/DME and DIPS-EPSE are pure solvent mixtures without LiTFSI. The illustration inside is the spatial distribution functions (SDFs) of DIPS-EPSE. (c, d) Snapshots of the molecular distributions around S_8^{2-} in (c) DOL/DME and (d) DIPS-EPSE. DME and $TFSI^-$ are omitted for a clear comparison. (e, f) *In situ* UV-vis spectra of (e) DOL/DME and (f) DIPS-EPSE with 1.0 mM Li_2S_8, in which fresh Li foils were immersed. The insects in (e) and (f) represent the different interactions between LiPSs and Li metal anodes in DOL/DME and DIPS-EPSE. (g) The S atomic content on the surface of Li metal anodes after the 5th cycle at a sputtering time of 0, 40, 100, and 160 s. (h) Cycle performance of the Li-S pouch cell. Reproduced with permission.[99b] Copyright 2022, Cell Press. (i-k) Decoupled polarization at different depths of discharge for (i) total polarization, (j) concentration polarization, and (k) activation polarization. (l) Decoupled polarization at the specific capacity of 308 mAh g^{-1}. Reproduced with permission.[100] Copyright 2023, Wiley-VCH.

Notably, the incorporation of solvents with weak solvation power can indeed maintain the kinetic favorable solid-liquid-solid reactions but the overall reaction kinetics is impaired.[100] The 1M LiTFSI in DME/DOL electrolytes shows a strong solvating power and is capable of dissolving 4.3 M_s Li_2S_8. Adding 10 vol.%, 20 vol.%, and 30 vol.% of TTE into the LiTFSI in DME/DOL electrolyte can reduce the overall solvating powers so that only 2.9 M_s Li_2S_8, 2.6 M_s Li_2S_8, 1.8 M_s Li_2S_8 can be dissolved, respectively. As the TTE content increases, the coordination number of TTE at the outer solvation shell increases with the increased Li anode stability. However, the decreased solvating

This article is protected by copyright. All rights reserved.

15214095, 2024, 29, Downloaded from https://advanced.onlinelibrary.wiley.com/doi/10.1002/adma.202401263 by Office Of Scientific And Technical Information, Wiley Online Library on [19/08/2025]. See the Terms and Conditions (https://onlinelibrary.wiley.com/terms-and-conditions) on Wiley Online Library for rules of use; OA articles are governed by the applicable Creative Commons License

power of electrolytes in Li-S batteries contribute to increased voltage polarization. The GITT-EIS technology revealed a drastic increase in the activation polarization than concentration polarization in the electrolyte with weak solvation power (Figures 9i to 9l). The sluggish kinetics of phase conversion process is a consequence of the inadequacies of solvation power. Therefore, the solvation ability of electrolytes has a trade-off impact on the cathode kinetics and anode stability. The Li-S pouch cells using 1M LiTFSI with 2 wt.% $LiNO_3$ in DME/DOL/TTE (20 vol.% TTE) exhibits a medium weak solvation power, which are able to maintain a specific capacity of ~1000 mAh g^{-1} after 30 cycles under lean electrolyte of E/S mass ratio of 3.5 and sulfur loading of 7.4 mg cm^{-2}.

4. Electrolyte Design to Improve the Intrinsic Kinetics

4.1 Redox mediator

Introducing redox mediators is an effective strategy to address the retard kinetic. Redox mediators are reversible redox couples that undergo surface electro-oxidation or electro-reduction and diffuse to electrolyte to oxidize/reduce the active material.[55] This unique feature is significant because the discharge product Li_2S are nearly electronic insulating, and the deposited Li_2S on the cathode surface hinders the further reduction of polysulfides. Redox mediators can facilitate electrons shuttle between current collectors and the surfaces of inactive sites, resulting in decrease of electron/ion-transfer resistances and improvement of the redox kinetics (**Figure 10**a). Moreover, the redox mediators facilitate polysulfides reduction without relying on conductive surfaces, allowing Li_2S to grow on previous deposited sites in a 3D particle morphology.

Polycyclic aromatic hydrocarbons are potential redox mediators. Because the conjugated aromatic rings have low HOMO-LUMO gap, polycyclic aromatic hydrocarbons require low activation energy for reduction and oxidation.[101] Their molecular structure can tuned to render different redox potential, such as introducing the electron-withdrawing groups onto the aromatic core to raise the reduction potential, or increasing the electro-donating group to lower the reduction potential (Figure 10b).[102] Through structural design, benzo[ghi]peryleneimide was used to accelerate the liquid-solid conversion process of Li_2S,[102b] and 1,5-bis(2-(2-(2-methoxyethoxy)ethoxy)ethoxy) anthra-9,10-quinone was designed to facilitate Li_2S cathodes activation.[49] Shen *et al.* applied fluorenone as an additive in Li-S batteries to achieve a discharge capacities of 1099.7 mAh g^{-1} at an E/S ratio of 5 µL mg^{-1}.[103] Fluorenone can stabilize the $S_3^{\bullet-}$ radicals to improve the sulfur conversion. It can also be reduced to radical at the similar reduction potential of Li_2S_4 to Li_2S, thus improving the deposition of Li_2S. Redox mediator can also shuttle electrons to the "dead" sulfur species as a scavenger to reutilize them. Ethyl viologen diperchlorate ($EV(ClO_4)_2$) features with two pairs of redox peaks in cyclic voltammogram.[104] One of the redox peaks around 2.03 V versus Li^+/Li corresponds to the EV^+/EV^0 pair, which is lower than the peaks of the solid-liquid sulfur conversion but higher than the peak of the

This article is protected by copyright. All rights reserved.

Author Manuscript

15214095, 2024, 29, Downloaded from https://advanced.onlinelibrary.wiley.com/doi/10.1002/adma.202401263 by Office Of Scientific And Technical Information, Wiley Online Library on [19/08/2025]. See the Terms and Conditions (https://onlinelibrary.wiley.com/terms-and-conditions) on Wiley Online Library for rules of use; OA articles are governed by the applicable Creative Commons License

liquid-solid conversion, facilitating the reduction of solid S to form soluble polysulfides (Figure 10d). The other redox peak of $EV(ClO_4)_2$ is around 2.46V (EV^{2+}/EV^{+}). The anodic peak is higher than the Li_2S oxidation reaction promotes the oxidation of solid Li_2S to soluble polysulfides. In addition to experimental measurements, the frontier molecular orbital theory is applied to predict the redox capability. The LUMO of EV^{2+} is below that of Li_2S, indicating higher electron receptivity and stronger oxidation capability (Figure 10c). The HOMO of EV^{0} is above that of sulfur indicating a stronger reduction capability. Thus, $EV(ClO_4)_2$ reutilized the inactive S and Li_2S in the cathode, contributing to the increased sulfur utilization and reaction kinetics. The mediator-assisted Li-S batteries provided a high sulfur utilization of about 61% and rate performance 780 mAh g^{-1} at 1 mA cm^{-2} with E/S ratio of 5 µL mg^{-1}.

Metallocenes also stand out as potential redox mediators due to their high stability and features as reversible redox couples. By tuning the metal ion or the ligand, the electrochemical properties of metallocenes can be modified to realize electrochemical active characteristic within the polysulfides reduction/oxidation range. Ferrocene $Fe(\eta^5\text{-}C_5H_5)_2$, and decamethylferrocene $Fe(\eta^5\text{-}C_5Me_5)_2$ with a voltage window covering most of the charge domain are applied as redox mediators to decrease the initial activation overpotential in solid-state Li_2S cathodes.[105] Dibenzenechromium $Cr(\eta^6\text{-}C_6Me_6)_2$ can be used as redox mediator to accelerate the liquid-liquid chemical conversion because its reduction peak is lower than polysulfides but higher than that of Li_2S. Cobaltocene $Co(\eta^5\text{-}C_5H_5)_2$ ($CoCp_2$) has been demonstrated as effective redox mediator to boost the liquid-solid conversion process.[106] $CoCp_2$ is capable to chemically reduce polysulfides to Li_2S and showing better chemical conversion kinetics than that of electrochemical reduction, demonstrating $CoCp_2$ can serve as a kinetically favorable redox mediator in Li-S batteries.[106b] Also, $CoCp_2$ redox mediators are able to alternate the growing pathway to 3D Li_2S growth. The growth morphologies of Li_2S at different depths of discharge were studied to provide insight into the effect of $CoCp_2$ redox mediator (Figure 10e). A conventional 2D growth mode is observed at the absence of $CoCp_2$ (Figures 10f to 10h). While the presence of $CoCp_2$ promoted porous 3D growth of Li_2S, which can slow the impingement of insulating Li_2S islands on cathode (Figures 10i to 10k). With the regulation of $CoCp_2$, the Li-S cell delivers a high initial specific capacity of ~1200 mAh g^{-1} at 0.05 C with sulfur loading of 4.8 mg cm^{-2} under a lean electrolyte condition of 4.7 µL mg_s^{-1} (Figure 10l).

This article is protected by copyright. All rights reserved.

Author Manuscript

15214095, 2024, 29, Downloaded from https://advanced.onlinelibrary.wiley.com/doi/10.1002/adma.202401263 by Office Of Scientific And Technical Information, Wiley Online Library on [19/08/2025]. See the Terms and Conditions (https://onlinelibrary.wiley.com/terms-and-conditions) on Wiley Online Library for rules of use; OA articles are governed by the applicable Creative Commons License

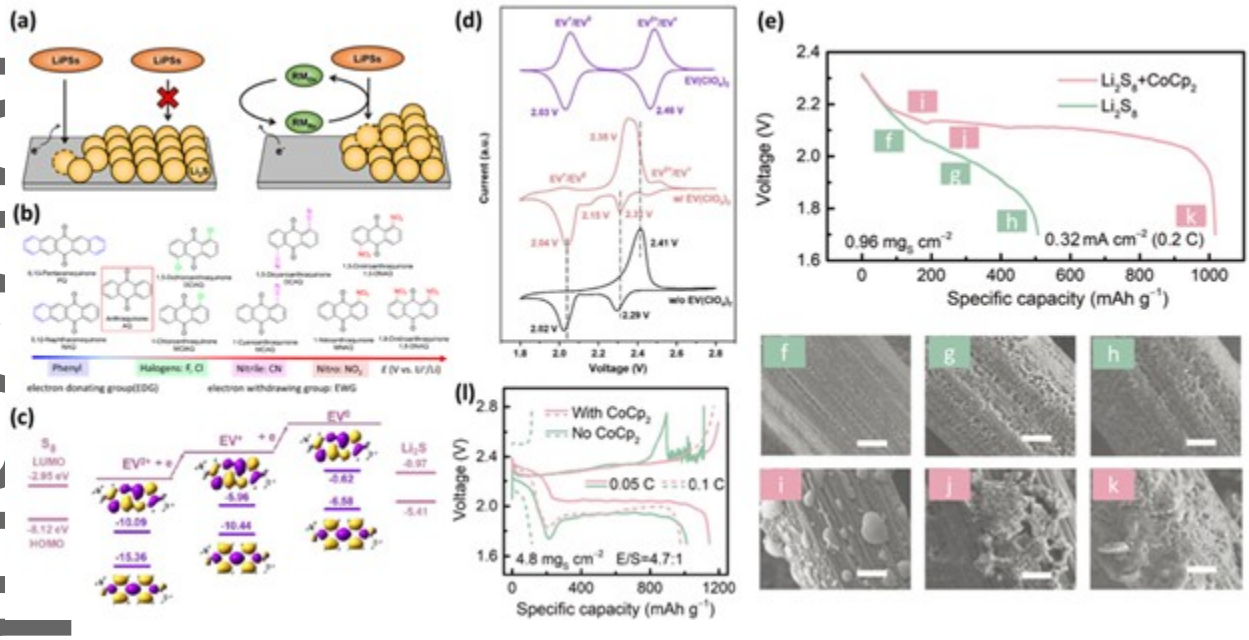

Figure 10. Redox mediators boost the reaction kinetic of Li-S batteries. (a) Schematic illustration of redox mediators facilitating electrons shuttle between current collectors and the inactive sites to improve the redox kinetics. (b) Structures of anthraquinone and its derivatives. The introduction of electron withdrawing group increases the reduction potential. Reproduced with permission.[102a] Copyright 2020, American Chemical Society. (c) Energy levels of $EV(ClO_4)_2$ in different redox states in comparison with those of sulfur and Li_2S. (d) Cyclic voltammograms of MoS_{2-x}/rGO/S electrodes with and without $EV(ClO_4)_2$ at 0.2 mV s^{-1}. Reproduced with permission.[104] Copyright 2021, Elsevier. (e) The first discharge profile at 0.2 C. Cells were stopped at different depths of discharge indicated as points f to k to characterize the Li_2S deposits. (f-h) SEM images of Li_2S deposits on carbon paper with $CoCp_2$ absent (upper panel f to h) and present (bottom panel i to k). Scale bar is 1 µm. (l) Galvanostatic discharge-charge profiles of electrolytes with and without the $CoCp_2$ at various current densities. Reproduced with permission.[106b] Copyright 2020, Wiley-VCH.

4.2. Exogeneous redox active ingredients

Exogeneous redox active ingredients such as organopolysulfides ($R_1S_nR_2$, R_1 and R_2 are different organic groups), thiols (R_1SH), organopolyselenides ($R_1Se_nR_2$), and organopolytellurides ($R_1Te_nR_2$) that can in situ react with polysulfides to generate new intermediates represent a promising strategy to address the challenge of lean electrolyte condition (**Figure 11**a). The thiols can react with sulfur species with hydrogen abstractions to form thioether oligomers,[107] and react with polysulfides in the same reaction mechanism as other organopolysulfides, organopolyselenides and organopolytelluride compounds. For simplicity, the mechanism of exogeneous redox active ingredients is presented in organopolysulfides. Organopolysulfides can react with elemental sulfur as follows (Reaction 18):[108]

This article is protected by copyright. All rights reserved.

Author Manuscript

15214095, 2024, 29, Downloaded from https://advanced.onlinelibrary.wiley.com/doi/10.1002/adma.202401263 by Office Of Scientific And Technical Information, Wiley Online Library on [19/08/2025]. See the Terms and Conditions (https://onlinelibrary.wiley.com/terms-and-conditions) on Wiley Online Library for rules of use; OA articles are governed by the applicable Creative Commons License

$$R_1S_nR_2 + \frac{m}{8}S_8 \leftrightarrow R_1S_{n+m}R_2 \quad \text{(Reaction 18)}$$

$R_1S_{n+m}R_2$ can dissociate into short-chain lithium organopolysulfides, which can be further reduced to Li_2S and other final products (Reaction 19).[109]

$$R_1S_{n+m}R_2 + 2(n+m-1)Li^+ + 2(n+m-1)e^- \rightarrow R_1SLi + R_2SLi + (n+m-2)Li_2S \quad \text{(Reaction 19)}$$

The exogeneous redox active ingredients are capable of alternating and accelerating the electrochemical reaction pathway by facilitating the cleavage and recombination of S-S bonds of polysulfides. The increase of the number of middle sulfur atoms promotes the dissociation of S-S bond. As for the AMDS (CH_2=$CHCH_2SSCH_3$), the trisulfide discharge intermediate, CH_2=$CHCH_2SSSCH_3$, is the most stable and main intermediates during discharge based on DFT calculations.[109a] The low bond dissociation energy of S-S near the allyl results in the first product of CH_2=$CHCH_2SLi$ and $LiSSCH_3$, the latter is finally reduced to Li_2S and CH_3LiS. Also, the ex situ ^1H NMR characterization at different depths of discharge reveals the intermediate process involved (Figures 11b and 11c). The peaks at 2.32 and 2.44 ppm corresponding to the discharge intermediates of CH_2=$CHCH_2SLi$ and $LiSSCH_3$ decrease at the end of discharge; and the final discharge product of CH_3LiS emerges at the early stage of discharge with corresponding peak at 1.91 ppm. AMDS are present throughout the discharge process that the ascribed signal peaks at 2.30, 2.41, and 5.1 ppm are constant. Trisulfide (DMTS, CH_3SSSCH_3) is demonstrated to partially dissolve Li_2S with color change to dark red (Figure 11d), indicating the formation of polysulfides (Reaction 20):[109b]

$$(x-1)R_1S_{n+m}R_2 + Li_2S \leftrightarrow (x-1)R_1S_{n+m-1}R_2 + Li_2S_x \ (x = 2-8) \quad \text{(Reaction 20)}$$

The improved reversibility of Li_2S can significantly improve the capacity retention with less "dead" sulfur formed. Overall, the exogeneous redox active ingredients are capable of alternating and accelerating the electrochemical reaction pathway by facilitating the cleavage and recombination of S-S bonds of polysulfides.

This article is protected by copyright. All rights reserved.

Author Manuscript

15214095, 2024, 29, Downloaded from https://advanced.onlinelibrary.wiley.com/doi/10.1002/adma.202401263 by Office Of Scientific And Technical Information, Wiley Online Library on [19/08/2025]. See the Terms and Conditions (https://onlinelibrary.wiley.com/terms-and-conditions) on Wiley Online Library for rules of use; OA articles are governed by the applicable Creative Commons License

Author Manuscript

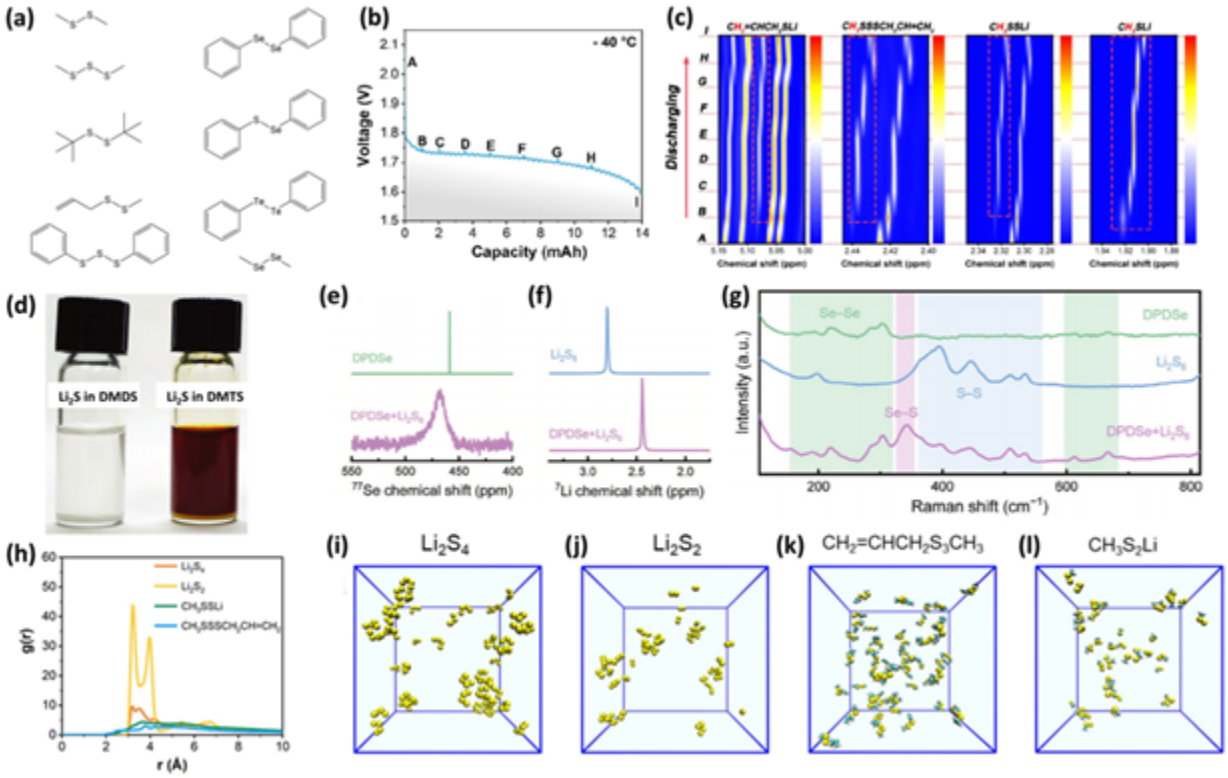

Figure 11. The reaction mechanism of exogeneous redox active ingredients. (a) Chemical structure of organopolysulfides and organodiselenides and organoditelluride compounds. (b) Initial discharge profiles of the flask battery with the AMDS-modified electrolyte. And the corresponding (c) ^{1}H NMR spectra of the AMDS-modified electrolyte at varying discharging stages at -40 °C. Reproduced with permission.[109a] Copyright 2021, American Chemical Society. (d) Solubility test of Li_2S in DMDS- and DMTS-containing electrolyte systems demonstrated by adding 12 mg Li_2S to 1 mL of 50 vol.% DMDS- and 25 vol.% DMTS-containing electrolyte and stirring overnight before photos were taken. Reproduced with permission.[109b] Copyright 2018, Wiley-VCH. (e) ^{77}Se and (f) ^{7}Li NMR spectra of the DPDSe solution, the Li_2S_6 solution, and the mixed DPDSe + Li_2S_6 solution. (g) Raman spectra of DPDSe and Li_2S_6 solutions before and after chemical reaction. Reproduced with permission.[110] Copyright 2021, Wiley-VCH. (h) Radial distribution fucntion of S-S from intermediates and corresponding snapshots of MD simulation boxes highlighting the four intermediates of Li_2S_4 (i), Li_2S_2 (j), CH_2=$CHCH_2S_3CH_3$ (k), and CH_3S_2Li (l), respectively. Reproduced with permission.[109a] Copyright 2021, American Chemical Society.

Organopolysulfides such as DMDS, CH_3SSCH_3,[111] dimethyl trisulfide (DMTS, CH_3SSSCH_3),[109b, 112] di-t-butyl disulfide (DtbDS, $C(CH_3)_3SSC(CH_3)_3$),[50] diphenyl trisulfide ($C_6H_5SSSC_6H_5$),[113] and allyl methyl disulfide (AMDS, CH_2=$CHCH_2SSCH_3$)[109a] are demonstrated with improved sulfur redox kinetics, as well as organodiselenides and organoditelluride compounds such as diphenyl diselenide (DPDSe),[110] dimethyl diselenide (Me-Se),[114] diphenyl diselenide (Ph-Se),[114] diphenyl ditelluride

This article is protected by copyright. All rights reserved.

15214095, 2024, 29, Downloaded from https://advanced.onlinelibrary.wiley.com/doi/10.1002/adma.202401263 by Office Of Scientific And Technical Information, Wiley Online Library on [19/08/2025]. See the Terms and Conditions (https://onlinelibrary.wiley.com/terms-and-conditions) on Wiley Online Library for rules of use; OA articles are governed by the applicable Creative Commons License

(DPDTe),[115] phenyl selenosulfide (PhS-SePh)[116] (Figure 11a). Tellurium and selenium are *d*-electron-containing members of group 16 in the periodic table. As congeners of sulfur, their stronger metallicity and higher electrical conductivity enhance the reactivity of organodiselenides or organoditelluride towards polysulfides.[117] After the reaction, the interaction of Se-S contributes to the upshifted Se-Se peaks and downshifted Li-S peaks (Figures 11e and 11f). DPDSe reacts with LiPSs and convert to soluble lithium phenylseleno polysulfides (LiPhSePSs), supporting by the new peak at 341 cm^{-1} ascribed to Se-S vibration (Figure 11g).[110]

Generating intermediates from chemical reactions between polysulfides and organopolysulfides/organopolyselenides/organoditellurides rather than the short-chain polysulfides from direct electrochemical reduction with poor solubility promotes in-depth sulfur reduction. High aggregation state of Li_2S_4 and Li_2S_2 is observed in conventional electrolytes (Figures 11h to 11j).[109a] The clustered aggregate of short-chain polysulfides obstacles the sulfur reduction reaction process in a liquid-solid or solid-solid pathway.[118] The activation energy required to enable the charge transfer increases significantly during the conversion from soluble lithium polysulfide intermediates into insoluble final Li_2S in conventional electrolytes (**Figures 12**a to 12c). In comparison, the discharge intermediates of CH_2=$CHCH_2SLi$ and $LiSSCH_3$ exhibit a better distribution in a highly decentralized state (Figures 10k and 10l), validating higher solubilities. The new intermediates demonstrated with higher solubility enable liquid-liquid conversion till the generation of final precipitates. The activation energy for reducing short-chain polysulfides decreases significantly compared to that without AMDS (Figures 12a to 12c). Also, the higher peak current and earlier peak time are observed in the cells with DPDSe from chronoamperometry test, validating a fast deposition kinetic (Figure 12d). The exogeneous redox active ingredients also alter the Li_2S deposition behavior with a 3D growth characteristic with improved sulfur reduction kinetic and utilization (Figure 12e).[109a] This approach effectively circumvents the typically sluggish liquid-solid or solid-solid conversion process.

This article is protected by copyright. All rights reserved.

Author Manuscript

15214095, 2024, 29, Downloaded from https://advanced.onlinelibrary.wiley.com/doi/10.1002/adma.202401263 by Office Of Scientific And Technical Information, Wiley Online Library on [19/08/2025]. See the Terms and Conditions (https://onlinelibrary.wiley.com/terms-and-conditions) on Wiley Online Library for rules of use; OA articles are governed by the applicable Creative Commons License

Author Manuscript

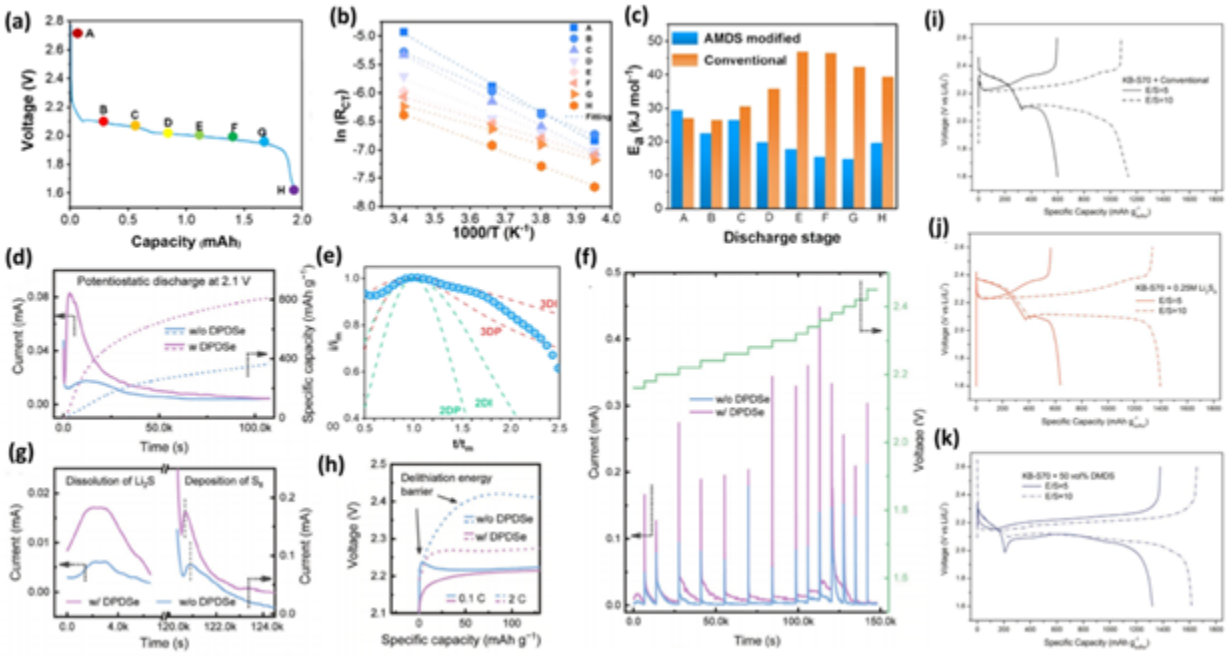

Figure 12. The impact of exogeneous redox active ingredients on sulfur reaction kinetics. (a) EIS measurements of the Li-S cell with AMDS-modified electrolyte at different stages. (b)Arrhenius linear relationship between logarithmic values of the charge transfer resistance (R_{CT}) and the reciprocal of temperatures in the AMDS electrolyte. (c) Comparison of activation energies between conventional and AMDS-modified electrolytes. Reproduced with permission.[109a]Copyright 2021, American Chemical Society. (d) Chronoamperometry curves of Li | Li_2S_8 cells, showing the kinetics of Li_2S deposition. Reproduced with permission.[110] Copyright 2021, Wiley-VCH. (e) Current-time transients obtained at 2.08 V and corresponding dimensionless transient model. Reproduced with permission.[109a] Copyright 2021, American Chemical Society. (f) PITT (potentiostatic intermittent titration technique) profiles of Li | Li_2S cells, (g) Partially enlarged view of showing the current responses during Li_2S dissolution and S_8 deposition. (h) Initial galvanostatic charge profiles at various current densities. Reproduced with permission.[110] Copyright 2021, Wiley-VCH. Initial discharge-charge profiles of KB-S70 cathodes in (i) conventional, (j) 0.25 M polysulfide-containing, and (k) 50 vol.% DMDS-containing electrolytes with E/S=5 and 10 mL g^{-1} at a current density of 0.2 mA cm^{-2}. Reproduced with permission.[111b] Copyright 2017, Elsevier.

The insulating nature of the final discharge products of Li_2S passivate the conductive surface contributes to the large energy barrier for electrochemical oxidation of Li_2S (Figures 12f and 12g). The charge process is also generally considered as solid-solid conversion without polysulfides intermediates as mediators, which aggravate the sluggish delithiation process.[119] Organopolysulfides are able to react with Li_2S to generate polysulfides to alleviate the passivation issues,[111a] and the organodiselenides and organoditelluride compounds are also demonstrated with the same functions. Exogeneous redox active ingredients are found to improve the reversibility of Li_2S and partially

This article is protected by copyright. All rights reserved.

15214095, 2024, 29, Downloaded from https://advanced.onlinelibrary.wiley.com/doi/10.1002/adma.202401263 by Office Of Scientific And Technical Information, Wiley Online Library on [19/08/2025]. See the Terms and Conditions (https://onlinelibrary.wiley.com/terms-and-conditions) on Wiley Online Library for rules of use; OA articles are governed by the applicable Creative Commons License

dissolve Li_2S.[109b] The comedication of DPDSe eliminates the reaction barrier and contributes to the enhanced dissolution of Li_2S and deposition of S_8 (Figures 12f and 12g), reflecting in a much smoother charging curve (Figure 12h). The DPDSe-containing electrolyte resulted in a high initial specific capacity of sulfur at 1322 mAh g^{-1} with high sulfur loading of 4.9 mg_s cm^{-2} and E/S ratio of 4.0 µL mg_S^{-1} in a 1.5Ah pouch cell.[110] Similarly, DPDTe and the mixture of Me-Se and Ph-Se are applied as additives to enable the Li-S batteries with high sulfur loading and low E/S ratio (> 5 mg_s cm^{-2} and E/S ratio < 5 µL mg_S^{-1}) with a high initial specific capacity of over 1300 mAh g^{-1}.[114-115]

The multi-electron transfer reactions of S-S bonds endow exogeneous redox active ingredients to provide additional capacity.[112a] The increase in the number of middle sulfur atoms increases the overall capacity, such as DMDS with theoretical specific capacity of 570 mAh g^{-1} and DMTS with theoretical specific capacity of 851 mAh g^{-1}. Although the capacity rises with the increasing sulfur atoms, the dissociation energy of the S-S bond decreases thus leading to the instability.[120] The exogeneous redox active ingredients are introduced as additives in DME/DOL electrolytes with a concentration about 0.1 M. Under 5 mL g^{-1} E/S ratio and 60% sulfur utilization (1000 mAh g^{-1}), 0.1M DMTS can contribute ~4% extra capacity. Li_2S_8 is the intrinsic active material that undergoes redox reaction to provide such capacity. Simply adding Li_2S_8 into Li-S batteries under E/S ratio of 10 mL g^{-1} can provide ~30% extra capacity, but the extra Li_2S_8 is ineffective under low E/S ratio of 5 mL g^{-1} (Figures 12i and 12k),[111b] due to high viscosity induced sluggish mass transport under lean electrolyte condition. As a stark comparison, with the addition of DMDS, about a 100% increase in capacity is observed under E/S ratio of 5 mL g^{-1} (Figures 12i and 12j). The exogeneous redox active ingredients provide extra capacity meanwhile avoiding the sluggish mass transport challenge.

Thiols are another exogeneous redox active compounds that can react with sulfur species with hydrogen abstraction to form thioether oligomers (**Figures 13**a and 13b).[107, 121] Thiols are first reported as polysulfide-scission reagents to boost the chain-shortening reactions,[122] and dithiothreitol (DTT) is studied in biochemistry to cleave the S-S bonds to prevent proteins from polymerization.[123] Thioether itself will convert to oligomers that possess the same characteristics of S-S bonds like organopolysulfides (Figures 13c and 13d). Sulfydryl groups of thiols possess a common characteristic of cleaving the S-S bond, such as dithiothreitol can split the S_4^{2-} species to form solid Li_2S or Li_2S_2, thus eliminating the accumulation of LiPSs and directing to more favorable kinetics.[122, 124] Biphenyl-4,4'-dithiol (BPD) can combine short chain polysulfide through the delocalization of the S-S bond to slow the formation of nearly insoluble short-chain polysulfides.[125] Such combination with a higher solubility than that of short-chain polysulfides benefits the kinetics of the dissolution process.

This article is protected by copyright. All rights reserved.

Author Manuscript

15214095, 2024, 29, Downloaded from https://advanced.onlinelibrary.wiley.com/doi/10.1002/adma.202401263 by Office Of Scientific And Technical Information, Wiley Online Library on [19/08/2025]. See the Terms and Conditions (https://onlinelibrary.wiley.com/terms-and-conditions) on Wiley Online Library for rules of use; OA articles are governed by the applicable Creative Commons License

Author Manuscript

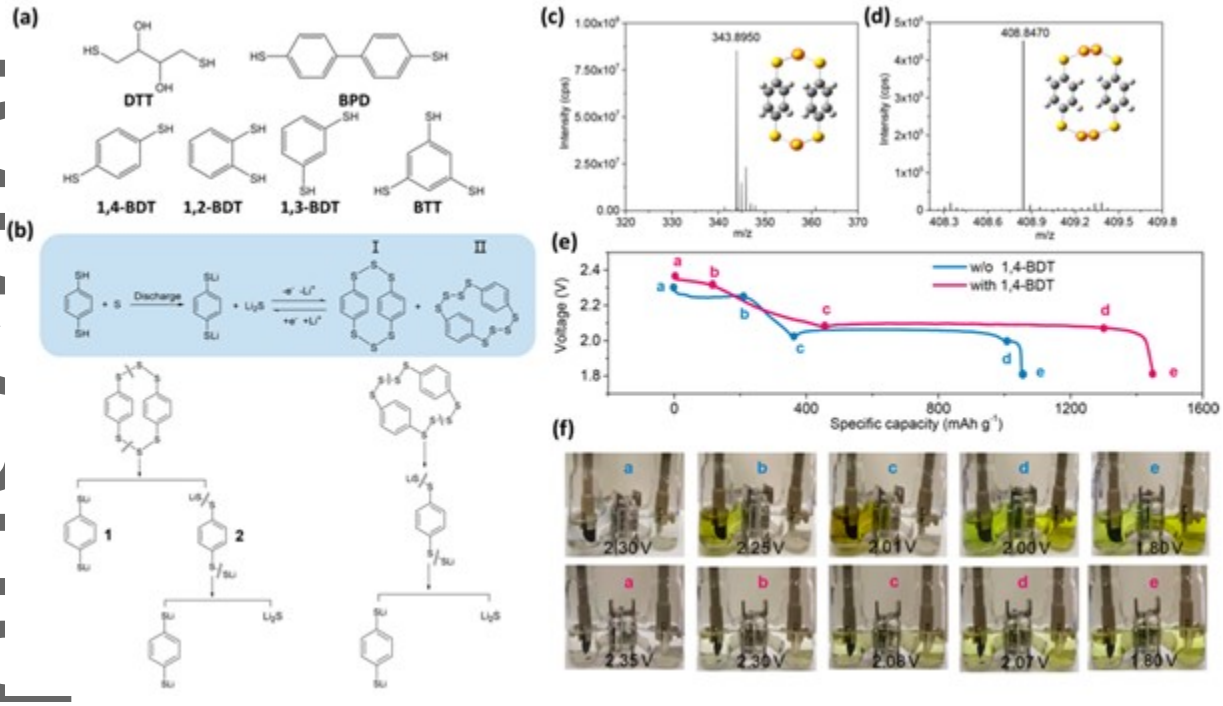

Figure 13. Thiols represent as another type of exogeneous redox active ingredients. (a) The chemical structure of thioethers. (b) Reaction Mechanism in the Initial Discharge and Recharge Processes of the Li-S cell with 1,4-BDT and possible reduction reaction of the oligomer I and oligomer II. (c, d) MS of the charged products of the Li-S cell with 1,4-BDT. (e) First cycle discharge curve of the visual Li-S cells with and without 1,4-BDT and (f) corresponding photographs of the cells at different discharge voltages; blue refer to the control cell and red refer to the Li-S cell with 1,4-BDT electrolyte; the sulfur cathode is on the left and the lithium metal anode is on the right in these photographs. Reproduced with permission.[121] Copyright 2021, American Chemical Society.

Benzenetrithiol (BTT) and benzenedithiols (BDT) have been demonstrated to be able to activate dead sulfur and facilitate homogeneous chemical reactions to improve the overall electrochemical kinetics.[107, 121] Organthiols can incorporate with sulfur species, the corresponding structure change alternates the redox path of sulfur. Benefiting from the combination, organdithiols can also postpone the accumulation of LiPSs, which is verified by the visual cell tests and the corresponding initial discharge profile of the two cells (control cell and Li-S cell with 1,4-BDT in Figures 13e and 13f).[121] Changes in the sulfur-chain length and concentration of polysulfides lead to a progressive alteration in color on the cathode side, transitioning from a clear to a deep yellow and eventually to a light yellow-green color in control cell. While in the cells with 1,4-BDT, only a pale-yellow color is observed throughout the discharge process, indicating a reduced formation of LiPSs. With the electrolyte containing 1,4-BDT, the Li-S cell delivers a high initial specific capacity of 943 mAh g^{-1} at 0.1 C with sulfur loading of 3.5 mg cm^{-2} and a lean electrolyte condition of 3.5 μL mg_s^{-1}.[121] The Li-S cells with

This article is protected by copyright. All rights reserved.

15214095, 2024, 29, Downloaded from https://advanced.onlinelibrary.wiley.com/doi/10.1002/adma.202401263 by Office Of Scientific And Technical Information, Wiley Online Library on [19/08/2025]. See the Terms and Conditions (https://onlinelibrary.wiley.com/terms-and-conditions) on Wiley Online Library for rules of use; OA articles are governed by the applicable Creative Commons License

BTT additives exhibit a higher specific capacity of 1022 mAh g^{-1}, which may be attributed to 3 sulfydryl groups in BTT comparing to 2 sulfydryl groups in 1,4-BDT.[107]

4.3. Homogeneous catalysts

Catalysis is a widely adopted strategy to improve intrinsically sluggish reaction kinetics, hence it is a rational direction to improve electrochemical reduction of polysulfides under lean electrolyte condition. Catalytical approaches generally include heterogeneous catalysis and homogeneous catalysis to promote the S_8/Li_2S conversion kinetics.[126] Heterogeneous catalysts have been widely studied and demonstrated with great potential to enable the practical Li-S batteries.[118, 127] The biggest constrain for heterogeneous catalysts is that the catalytic efficiency is highly dependent on the limited accessible catalyst surface and the durability towards the catalyst inactivation.[128] On the opposite, homogeneous catalysts are dissolved in the electrolytes to achieve homogeneous interaction with polysulfides. Such feature guarantees the long-lasting catalytic activity to enable the polysulfides undergo at the homogeneous interface, which is less dependent on the conductive cathode surface.[128a]

The sluggish reaction kinetics is attributed to both electrochemical and chemical reactions in Li-S cells. As aforementioned, polysulfides undergo chemical reaction $Li_2S_x \rightleftharpoons Li_2S_y + (x\text{-}y)/8S_8$ ($x > y$) that the polysulfides disproportionate in electrolytes to insoluble elemental sulfur and lower order polysulfides. The generation of insoluble elemental sulfur within the liquid electrolytes or separator pores causes fast capacity attenuation and irreversible loss of sulfur.[56a, 90] The sluggish disproportionation reaction can also be turned into an advantage by employing efficient catalysts with enhanced reaction kinetics.[129] Lin *et al.* proposed a homogeneous catalyst $LiPO_2F_2$ that is able to selectively "carry" the soluble polysulfides back to cathode surface and then facilitate the disproportionation reaction of polysulfides.[130] The open circuit voltage and the color change of the electrolyte with 2 wt.% $LiPO_2F_2$ and saturated polysulfides were monitored (**Figure 14**a). After an extended period of rest, the concentration of polysulfides in the electrolyte significantly decreased. Interestingly, "self-charge" behavior was observed that the open circuit voltage increased from 2.4 V to 2.8 V (Figure 14b), indicating the transformation from Li_2S_8 to S_8. Further XPS and EDS (energy dispersive X-ray spectroscopy) analysis demonstrated the sulfur species were S_8 and Li_2S_2/Li_2S sedimented on the cathode surface (Figures 14c to 14e). The $LiPO_2F_2$ works as a homogeneous catalyst to accelerate the chemical transformation of polysulfides through the biradical mechanism. The combination of electron-deficient catalysis and Li_2S_n leads to the formation of highly oxidative $1LiPO_2F_2$-$1Li_2S_n$ or $2LiPO_2F_2$-$1Li_2S_n$ (Figure 14f). The $1LiPO_2F_2$-$1Li_2S_n$ with reduced energy barrier induces the generation of biradicals of $^{\bullet}S_x$Li-$LiPO_2F_2$-$LiS_y^{\bullet}$ and pseudo biradical of $LiPO_2F_2$-LiS_x-LiS_y ($x + y = n$). The $LiPO_2F_2$ catalyst initiates the production of biradicals, facilitating a different disproportionation reaction of LiPSs through the transfer of radicals between these biradicals (Figure

This article is protected by copyright. All rights reserved.

Author Manuscript

15214095, 2024, 29, Downloaded from https://advanced.onlinelibrary.wiley.com/doi/10.1002/adma.202401263 by Office Of Scientific And Technical Information, Wiley Online Library on [19/08/2025]. See the Terms and Conditions (https://onlinelibrary.wiley.com/terms-and-conditions) on Wiley Online Library for rules of use; OA articles are governed by the applicable Creative Commons License

14g). With the electrolyte additive of $LiPO_2F_2$, the 14.5-Ah Li-S pouch cells exhibit high energy density up to 400 Wh kg^{-1}, under E/S ratio of 2.7 μL mg^{-1} (Figure 14h).

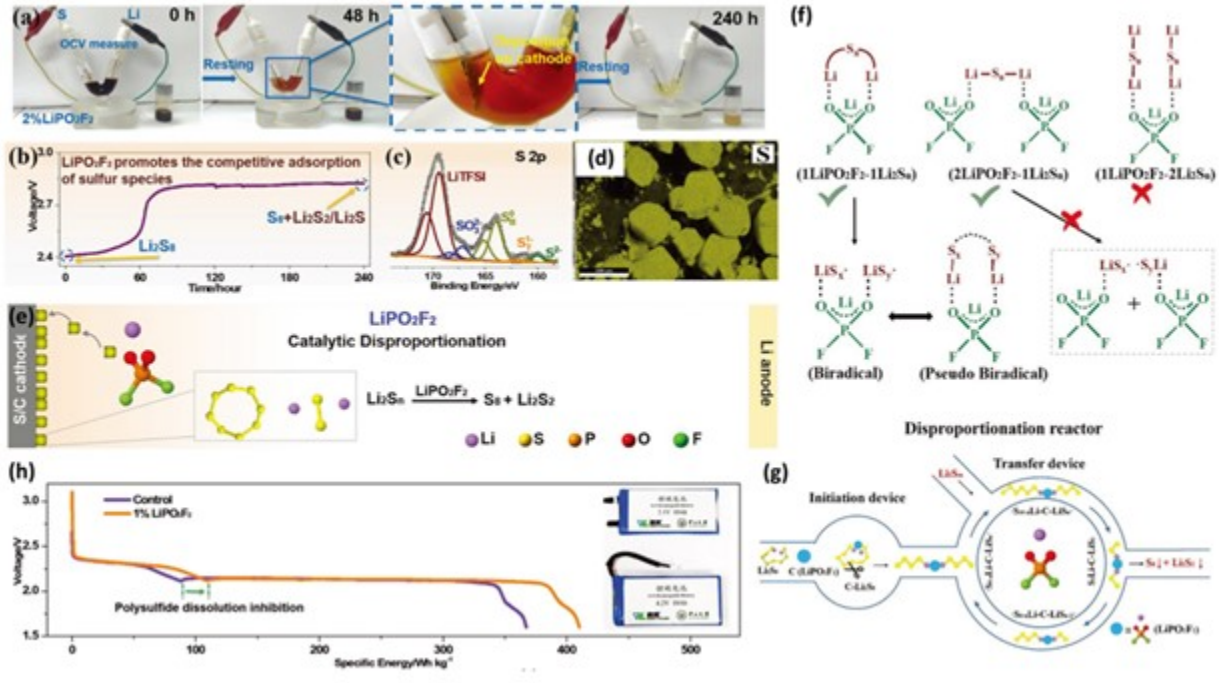

Figure 14. Homogeneous catalysts for promoting chemical reactions. (a) Visual change of V-type glass Li/S cell with LiPS-containing electrolyte after adding 2 wt.% $LiPO_2F_2$. (b) Open circuit voltage profile versus time of the V-type Li/S cell after adding 2 wt.% $LiPO_2F_2$. (c) S 2p XPS spectrum and (d) EDS elemental mapping of the precipitate products from the glass cell. (e) Schematic diagram for LiPSs in Li-S batteries with $LiPO_2F_2$-containing electrolyte. (f) Radical initiation mechanism by $LiPO_2F_2$ with Li_2S_n. (g) Schematic diagram of biradicals in polysulfide disproportionation by $LiPO_2F_2$ under discharge or self-discharge of Li-S batteries. (h) Specific energy of Li-S pouch cells (5 mg cm^{-2} areal sulfur loading) with $LiPO_2F_2$-containing electrolyte (1wt.%) under lean electrolyte condition. Reproduced with permission.[130] Copyright 2022, Wiley-VCH.

Soluble metallocenes such as titanocene ($TiCp_2$), nickelocene ($NiCp_2$) and 1,1'-bis(diphenylphosphino)ferrocene (DPPF) are identified as protentional homogeneous catalysts because of their electrochemical inert characteristic within the polysulfides reduction range.[131] Based on DFT calculation, $TiCp_2$ exhibits a high affinity to polysulfides to form the $TiCp_2$-LiPs complexes. The complexes are capable of lowering the activation energy barrier for further reduction, thus promoting the overall reaction kinetics. Also, organometallic compounds are potential candidates as homogeneous catalysts such as nickel chloride dimethoxyethane adduct ($NiCl_2$-DME, abbreviated as NiDME).[132] DME ligand renders acceptable solubility of NiDME in electrolytes and $NiCl_2$ serves as catalytic sites for trapping the polysulfides and enhancing the conversion kinetic (**Figure 15**a). $NiCl_2$ exhibits stronger attraction to polysulfides than to DME that facilitates the formation of $NiCl_2$-LiPSs

This article is protected by copyright. All rights reserved.

Author Manuscript

15214095, 2024, 29, Downloaded from https://advanced.onlinelibrary.wiley.com/doi/10.1002/adma.202401263 by Office Of Scientific And Technical Information, Wiley Online Library on [19/08/2025]. See the Terms and Conditions (https://onlinelibrary.wiley.com/terms-and-conditions) on Wiley Online Library for rules of use; OA articles are governed by the applicable Creative Commons License

complex (Figure 15b), which shows a lower activation energy for reduction comparing to free LiPSs (Figure 15c). NiDME also drastically enhances the transient liquid-solid conversion process indicated by the higher activation energy drop. The higher ratio between low- and high-plateau capacities also verifies the much-improved Li_2S conversion efficiency (Figure 15d). Benefiting from the NiDME catalysts, the Li-S batteries with NiDME-containing electrolyte are able to maintain a high specific capacity of more than 600 mAh g^{-1} after 100 cycles at high discharge rate under a lean electrolyte ratio of 5 μL mg^{-1}. Those results highlight the significant kinetics improvement of the sulfur reduction reaction facilitated by the homogeneous catalysts.

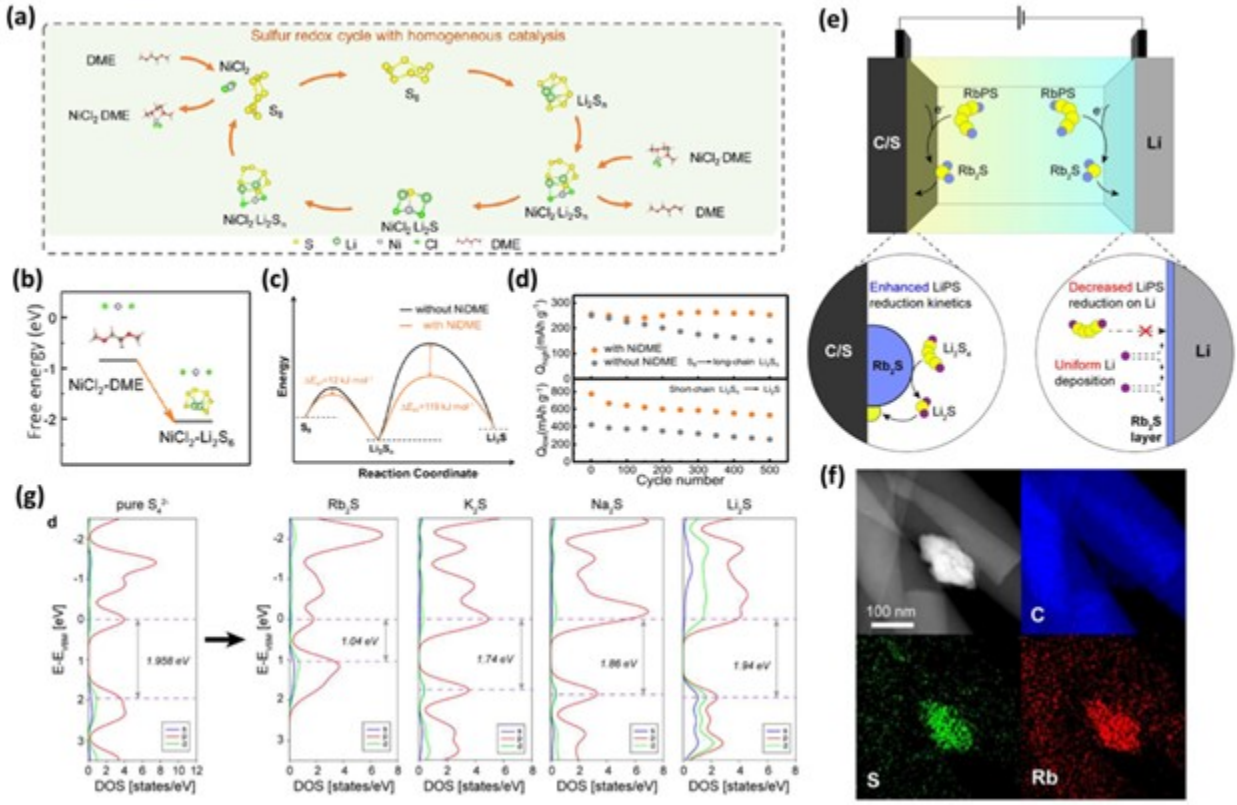

Figure 15. Homogeneous catalysts to promote Li-S electrochemical reactions. (a) Schematic of a LiPS conversion cycle with NiDME catalyst. (b) The calculated binding energy between $NiCl_2$ and DME or Li_2S_6. (c) The activation energies (E_a) of the discharge processes with and without NiDME catalyst. (d) Capacities at different cell plateau with/without the NiDME additive. Reproduced with permission.[132] Copyright 2020, Elsevier. (e) Scheme of the dual roles of Rb^+ additive at sulfur and Li electrodes. (f) STEM-EDAX images of Rb_2S formed on cathode. (g) Comparison of partial DOS of S_4^{2-} on different substrates (X_2S, X=Rb, K, Na, Li). The band gaps of S_4^{2-} are indicated by purple lines. Reproduced with permission.[133] Copyright 2023, Elsevier.

A unique method is to *in situ* generate catalysts through electrochemical reactions from the electrolyte additives.[118, 127] Jung *et al.* proposed rubidium cation (Rb^+) as an electrolyte additive to improve the kinetics of sulfur reduction.[133] Rb_2S possess a higher standard redox potential at 2.22 V versus

This article is protected by copyright. All rights reserved.

Author Manuscript

15214095, 2024, 29, Downloaded from https://advanced.onlinelibrary.wiley.com/doi/10.1002/adma.202401263 by Office Of Scientific And Technical Information, Wiley Online Library on [19/08/2025]. See the Terms and Conditions (https://onlinelibrary.wiley.com/terms-and-conditions) on Wiley Online Library for rules of use; OA articles are governed by the applicable Creative Commons License

Li^+/Li, which is higher than that of Li_2S. Such characteristics ensures that Rb_2S form before Li_2S during discharge. The product formed on the cathode after galvanostatic discharge to 2.15 V is verified as Rb_2S by STEM-EDAX analysis (Figure 15f). Computational study indicates hen adsorbed on the Rb_2S surface, the band gap of S_4^{2-} decreases from 1.96 eV to 1.04 eV (Figure 15g). In comparison, adsorption of S_4^{2-} on Li_2S, Na_2S, and K_2S surfaces only results in negligible band gap decrease. This suggests the in situ formed Rb_2S can function as a catalyst to improve the charge transfer in reducing S_4^{2-}. The $RbNO_3$ additive also contributes to a Rb_2S-rich SEI layer on Li anode, which is found to alleviate irregular Li deposition. Benefiting from those features, the Rb^+ additive enables Li-S batteries with a high initial specific capacity of 1175 mAh g^{-1} with 3.8 mg cm^{-2} sulfur loading under a lean condition of 2.5 μL mg^{-1}.

5. Conclusion and Perspective

Lean electrolyte is a mandatory condition to realize Li-S batteries with high specific energy (gravimetric energy density), and dissolution of polysulfides is an indispensable step in the overall operation of Li-S batteries using bulk sulfur cathode. The electrolyte properties particularly the Li^+ solvation has a strong, if not decisive, influence on the polysulfides dissolution and sequentially the fate of polysulfides via complex and intertwined pathways such as electrochemical reduction, self-disproportionation, chemical reduction enabled by intrinsically generated radical ($S_3^{\bullet-}$) and/or added redox mediators. Catalysis is also a theoretically viable means to improve the kinetics of polysulfides redox either electrochemically or chemically. The current electrolyte designs to address the challenges under lean electrolyte condition can be generally put in two categories: (1) Changing the type of salts, salt concentration, solvents, and co-solvents to manipulating the solvation strength of the electrolytes thus control the dissolution of polysulfides; using co-solvents with low density brings additional benefit of reducing the mass of the electrolyte. (2) Developing redox mediators to replace the sluggish electrochemical reactions of polysulfides with facial chemical reactions. Catalyst design can also help either electrochemical or chemical redox of the polysulfides. **Table 3** summarize the reported Li-S cells under lean electrolyte condition and their electrolyte compositions.

Table 3. Reported Li-S cells under lean electrolyte condition and their electrolyte compositions.

Electrolytes	E/S ratio (μL mg^{-1})	Sulfur loading (mg cm^{-2})	Specific capacity of sulfur (mAh g^{-1})	Cycle number & Retention	Specific energy (Wh kg^{-1})	Ref
Low concentration electrolytes:						
0.5M LiTFSI and 0.1M $LiNO_3$ in DME/DOL	4	5.6	1000 (0.1C 0ºC)	30 (~90%)	350	[59]
0.2M LiTFSI and 1.5 wt.% $LiNO_3$ in DME/DOL	2.4	6	1050 (0.02C)	10 (~80%)	300	[5]
Weakly solvating electrolytes:						
1.2M LiTFSI in F4DMB	5	1-2	1054 (0.2C 60ºC)	150 (47.4%)	Not reported	[64]

This article is protected by copyright. All rights reserved.

Author Manuscript

15214095, 2024, 29, Downloaded from https://advanced.onlinelibrary.wiley.com/doi/10.1002/adma.202401263 by Office Of Scientific And Technical Information, Wiley Online Library on [19/08/2025]. See the Terms and Conditions (https://onlinelibrary.wiley.com/terms-and-conditions) on Wiley Online Library for rules of use; OA articles are governed by the applicable Creative Commons License

	7	5.3	1309 (0.05C 60°C)	20 (~46%)	Not reported	
ACN_2LiTFSI in TTE (1:1 by volume)	5	1.2	1150 (0.03C 55°C)	Not reported	Not reported	[41]
G2:LiTFSI (0.8:1)	5	2	1300 (0.2C 55°C)	100 (~55%)	Not reported	[66]
$(THF)_2$LiTFSI-Toluene (3:7 by volume)	5	3	~800 (0.1C 55°C)	160 (~100%)	Not reported	[67]
	3	6.3	~750 (0.1C 55°C)	20 (~93%)	Not reported	
1M LiFSI in OFE/DME (95:5 by volume)	4.5 g Ah^{-1}	2	1012 (0.1C)	150 (~80%)	Not reported	[94]
Highly solvating electrolytes:						
1M LiTFSI in DOL/TMU	3 (mass ratio)	2.5	1524 (0.05C)	7 (~100%)	324	[78]
1M LiTFSI and 0.5M $LiNO_3$ in DMI	5	1	1595 (0.03C)	30 (~60%)	Not reported	[27]
1M LiTFSI in 3-FPN	7	1	~910 (0.1C)	100 (~88%)	Not reported	[79]
0.4M LiTFSI and 0.6M $LiNO_3$ in DME/DOL	5	3	1200 (0.1C)	100 (~80%)	Not reported	[85]
0.8M LiSCN, 0.2M LiTFSI and 0.2M $LiNO_3$ in DME/DOL	4	3.17	~1050 (0.09C)	45 (~75%)	Not reported	[84]
0.8M LiTFSI and 0.2M $LiNO_3$ in DME/DOL with 0.2M CH_3TFA	4.5	4.8	750 (0.1C)	40 (~45%)	Not reported	[83]
1M LiTFSI and 2 wt.% $LiNO_3$ in DME/DOL with 10% NH_4TFSI	5	4	900 (0.1C)	50 (~40%)	Not reported	[88]
1M LiTFSI and 5 wt.% $LiNO_3$ in DME/DOL with 5% MEP-Br	4	4	Not reported	100 (~65%)	300	[92]
1M LiTFSI and 2 wt.% $LiNO_3$ in DME/DOL with 0.1M T3Br	5	1.5-2	1200 (0.05C)	15 (~83%)	Not reported	[82]
Low density electrolytes:						
0.4M $LiNO_3$ and 0.2M LiTFSI in DME/MPE (48/52)	3	4.75	1134 (0.05C)	10 (~80%)	Not reported	[95]
0.4M LiTFSI, 0.1MLiHDFD and 0.4M $LiNO_3$ in DME/DOL/TFMTMS (48/17/35)	4.5	4	1024	100 (~60%)	276	[7b]
0.1M LiFSI and 0.1M $LiNO_3$ in THF/NH (65:35 by volume)	2.5	5.2	920 (0.05C)	40 (~90%)	Not reported	[96]
Electrolytes to optimize polysulfide solubility and Li anode stability:						
1M LiTFSI and 2 wt.% $LiNO_3$ in DIPE/DME/DOL (3:3.5:3.5 by vol.)	3	6.1	~1100 (0.025C)	23 (~81%)	300	[99a]
1M LiTFSI and 2 wt.% $LiNO_3$ in DIPS/DME/DOL (1:2:2 by volume)	2.7	6.1	~900 (0.025C)	103 (~50%)	Not reported	[99b]
1M LiTFSI and 2 wt.% $LiNO_3$ in DME/DOL adding 20% TTE by volume	3.5 (mass ratio)	7.4	~1150 (0.05C)	30 (~87%)	338	[100]
Redox mediators:						
1M LiTFSI and 0.3M $LiNO_3$ in DME/DOL with 0.02M $CoCP_2$	4.7	4.8	1148 (0.05C)	20 (~70%)	Not reported	[106b]
1M LiTFSI and 0.2M $LiNO_3$ in DME/DOL with 0.05M $EV(ClO_4)_2$	5	5.6	1022 (0.1C)	100 (~80%)	Not reported	[104]
1M LiTFSI and 0.3M $LiNO_3$ in DME/DOL with 0.1M fluorenone	5	4.6	~1400 (0.05C)	50 (~60%)	Not reported	[103]
Exogeneous redox active ingredients:						
1M LiTFSI and 0.1M $LiNO_3$ in DME/DOL/DMMS (1/1/2)	5	4	1319 (0.04C)	25 (~75%)	Not reported	[111b]
1M LiTFSI and 2 wt.% $LiNO_3$ in DME/DOL with 0.1M DtbDS	4	4.9	1313 (0.05C)	40 (~85%)	300	[50]
1M LiTFSI and 2 wt.% $LiNO_3$ in DME/DOL with 0.05M DPDTe	5	5	1322 (0.05C)	50 (~60%)	207	[115]

This article is protected by copyright. All rights reserved.

Author Manuscript

15214095, 2024, 29, Downloaded from https://advanced.onlinelibrary.wiley.com/doi/10.1002/adma.202401263 by Office Of Scientific And Technical Information, Wiley Online Library on [19/08/2025]. See the Terms and Conditions (https://onlinelibrary.wiley.com/terms-and-conditions) on Wiley Online Library for rules of use; OA articles are governed by the applicable Creative Commons License

1M LiTFSI and 2 wt.% $LiNO_3$ in DME/DOL with 0.05M MeSe and 0.05M PhSe	3	6.1	1399 (0.025C)	25 (~75%)	384	[114]
1M LiTFSI and 2 wt.% $LiNO_3$ in DME/DOL with 0.1M DPDSe	4.9	4	1322 (0.05C)	30 (~90%)	301	[110]
1M LiTFSI and 0.15M $LiNO_3$ in DME/DOL with 0.15M BTT	2.6	4.8	1022 (0.1C)	17 (~80%)	Not reported	[107]
1M LiTFSI and 0.1M $LiNO_3$ in DME/DOL with 0.15M 1,4-BDT	3.5	3.5	943 (0.1C)	25 (~85%)	Not reported	[121]
Homogeneous catalyst:						
1M LiTFSI and 1 wt.% $LiNO_3$ in DME/DOL with 0.5% NiDME	5	1	650 (0.5C)	100 (~85%)	Not reported	[132]
0.5M LiTFSI and 0.4M $LiNO_3$ and in DME/DOL with 0.05M $RbNO_3$	3	3.8	~1400 (0.15C)	79 (~50%)	Not reported	[133]
1M LiTFSI and 2 wt.% $LiNO_3$ in DME/DOL with 1% $LiPO_2F_2$	2.7	5	Not reported	Not reported	410	[130]
	4.5	3	740 (0.2C)	70 (~77%)	Not reported	

The weakly solvating electrolytes (including low concentration electrolytes) force the electrochemical reduction of sulfur into a reaction pathway with simplicity: low solubility of polysulfides in the electrolyte largely prevent complex phenomena including massive and uncontrolled Li_2S and sulfur precipitation via polysulfide disproportionation and chemical reactions between different polysulfides, poor mass transfer due to high viscosity, and parasitic reactions with Li anode. On the other hand, low polysulfide solubility can easily induce kinetic bottleneck if the kinetics of each step in the cascade reduction of sulfur are not well aligned. In other words, the charge transfer rate, which heavily depended on current, of each elementary reaction including reduction of elemental sulfur, reduction of S_8^{2-}, reduction of polysulfides with lower order than S_8^{2-} must be the same or very close to make the weakly solvating electrolytes work. This is very difficult to achieve, or at least it is safe to say that there is a lack of fundamental understanding of the kinetics of elementary reactions of sulfur reduction in Li electrolytes. The current literatures suggest weakly solvating electrolytes only work well at elevated temperature with low current and/or low sulfur loading. This observation clearly indicates the inherent kinetic bottleneck induced by weakly solvating electrolyte.

Highly solvating electrolytes are at the opposite side of the spectrum of controlling polysulfide dissolution. They essentially enable a “catholyte” scenario by maximizing the solubility of polysulfides in the electrolytes. Kinetics is not the main concern since the electrolyte serves as a sufficient polysulfide reservoir although the viscosity of the high-polysulfide-concentration may bring inferior mass transfer. However, the reaction pathways in highly solvating electrolytes are complex and intertwined as mentioned in the previous paragraph. The redox mediators and catalysts are developed to mainly address the challenges associated with electrolyte having high

This article is protected by copyright. All rights reserved.

Author Manuscript

15214095, 2024, 29, Downloaded from https://advanced.onlinelibrary.wiley.com/doi/10.1002/adma.202401263 by Office Of Scientific And Technical Information, Wiley Online Library on [19/08/2025]. See the Terms and Conditions (https://onlinelibrary.wiley.com/terms-and-conditions) on Wiley Online Library for rules of use; OA articles are governed by the applicable Creative Commons License

polysulfide solubility. The idea is to chemically promote the formation and porous deposition of Li_2S so that in-depth reduction of sulfur is not passivated; and the key to design effective redox mediators is to ensure facile chemical charge transfer with polysulfides and facile electrochemical charge transfer from or to the electrode. Li anode protection is also crucial to highly solvating electrolytes.

A rational direction is to design electrolytes striking a balance of proper solvating strength with sufficient polysulfide solubility and the reactions associated with the dissolved polysulfides can be managed by mediators and/or catalysts design. Fluorinated ethers have emerged as effective co-solvents to tune the solvating strength and they also enable the formation of LiF-rich SEI layer to protect Li anode and enhance plating/stripping reversibility. Partially fluorinated ethers offer easy manipulation of polysulfide solubility while maintaining excellent compatibility with lithium due to their solvating and non-solvating segments within the same molecules. For catalyst design, heterogeneous catalysts decorated on the cathode have been widely reported. However, heterogeneous catalysts are ill-suited for Li-S electrochemical reaction, since the final product Li_2S will deposit on the surface of the catalysts. Homogeneous catalysts should be the direction of future investigation.

Electrolyte design for lean electrolyte Li-S batteries requires a fundamental understanding of the electrochemical and chemical evolution pathways of polysulfide in the electrolyte, kinetics of each elementary reactions, mass transfer, and the crosstalk with lithium anode. These processes are complex and intertwined and can be exacerbated with limited electrolyte reservoir. Therefore, characterization tool development, particularly operando spectroscopic methods combined with electrochemical analysis will be crucial. Furthermore, it is clear that the performance of Li-S coin cells can be unrealistic comparing to pouch cells, and a main reason can be that accurate E/S ratio is difficult to implement in coin cells. It is critical to accurately evaluate the lean electrolyte Li-S behavior using pouch cells with realistic parameters.

Finally, theoretical simulation may provide atomic insights for Li-S reaction mechanisms that cannot be probed by experimental means due to spatial and temporal limitation. Density functional theory (DFT) provides a robust way for studying the electronic structure and thus the intrinsic properties of the electrolyte and the thermodynamics of the reaction. Yet with much simplification to the model, it is often limited to qualitative comparison. Molecular dynamics (MD) simulation instead provides a direct atomic picture of the bulk electrolyte and the dissolved polysulfide. With ab initio MD, one can address both the reaction thermodynamics and kinetics within a well-defined system. But the computational cost of ab initio MD is the bottleneck for its accuracy in good statistical mechanical average that requires sufficient simulation time and model size. One way of circumventing the issue is

This article is protected by copyright. All rights reserved.

Author Manuscript

15214095, 2024, 29, Downloaded from https://advanced.onlinelibrary.wiley.com/doi/10.1002/adma.202401263 by Office Of Scientific And Technical Information, Wiley Online Library on [19/08/2025]. See the Terms and Conditions (https://onlinelibrary.wiley.com/terms-and-conditions) on Wiley Online Library for rules of use; OA articles are governed by the applicable Creative Commons License

by degrading the computational method with care, *e.g.* QM/MM MD simulation which uses DFT for only the species of interest and classical force field for relatively distant solvent environment, or DFTB which approximates DFT method. Another promising solution to high computational cost is the use of machine learning (ML) force field, in which one can train a force field with ab initio MD simulations. The trained force field captures the underlying physics of the system while proceeding with the MD simulation much faster than quantum mechanical calculations. Despite the promising solution, systematic studies on the stability of these methods should be carried out before their application. Often the trade-off between model size and computation accuracy limits the consideration of more complex solvation environments, which had been shown critical in the thermodynamics and kinetics of the electrochemical processes. In addition to solvation, the nature of polysulfides is often simplified to crystalline or pure Li_2S_n species instead of amorphous network of multiple polysulfide species, which may exhibit distinctively different mechanics that better explains the experimental finding in Li-S batteries.

Declaration of Competing Interest

The authors declare that they have no known competing financial interests or personal relationships that could have appeared to influence the work reported in this paper.

Acknowledgment

J. C. and J. G. are grateful to the support from Department of Energy (DE-SC0020872) through subaward from Automat Solutions, Inc. Y. F. is thankful to the support University of California – Riverside.

References

[1] J. B. Goodenough, *Energy. Environ. Sci.* **2014**, 7, 14.

[2] a)M. Armand, J. M. Tarascon, *Nature* **2008**, 451, 652; b)J. Liu, Z. Bao, Y. Cui, E. J. Dufek, J. B. Goodenough, P. Khalifah, Q. Li, B. Y. Liaw, P. Liu, A. Manthiram, Y. S. Meng, V. R. Subramanian, M. F. Toney, V. V. Viswanathan, M. S. Whittingham, J. Xiao, W. Xu, J. Yang, X.-Q. Yang, J.-G. Zhang, *Nat. Energy* **2019**, 4, 180.

[3] a)M. Winter, B. Barnett, K. Xu, *Chem. Rev.* **2018**, 118, 11433; b)K. Zhang, G.-H. Lee, M. Park, W. Li, Y.-M. Kang, *Adv. Energy Mater.* **2016**, 6, 1600811.

[4] a)P. Bonnick, J. Muldoon, *Energy. Environ. Sci.* **2020**, 13, 4808; b)M. Zhao, B.-Q. Li, X.-Q. Zhang, J.-Q. Huang, Q. Zhang, *ACS Cent. Sci.* **2020**, 6, 1095; c)W. M. Haynes, *CRC handbook of chemistry and physics*, CRC press, **2014**; d)M. Zhao, B.-Q. Li, H.-J. Peng, H. Yuan, J.-Y. Wei, J.-Q. Huang, *Angew. Chem. Int. Ed.* **2020**, 59, 12636.

[5] Y. Zhao, J. Zhang, J. Guo, *ACS Appl. Mater. Interfaces* **2021**, 13, 31749.

This article is protected by copyright. All rights reserved.

Author Manuscript

15214095, 2024, 29, Downloaded from https://advanced.onlinelibrary.wiley.com/doi/10.1002/adma.202401263 by Office Of Scientific And Technical Information, Wiley Online Library on [19/08/2025]. See the Terms and Conditions (https://onlinelibrary.wiley.com/terms-and-conditions) on Wiley Online Library for rules of use; OA articles are governed by the applicable Creative Commons License

[6] a)L. Cheng, L. A. Curtiss, K. R. Zavadil, A. A. Gewirth, Y. Shao, K. G. Gallagher, *ACS Energy Lett.* **2016**, 1, 503; b)H. Yang, J. Chen, J. Yang, J. Wang, *Angew. Chem. Int. Ed.* **2020**, 59, 7306.
[7] a)M. Wild, L. O'Neill, T. Zhang, R. Purkayastha, G. Minton, M. Marinescu, G. J. Offer, *Energy. Environ. Sci.* **2015**, 8, 3477; b)T. Liu, Z. Shi, H. Li, W. Xue, S. Liu, J. Yue, M. Mao, Y.-s. Hu, H. Li, X. Huang, L. Chen, L. Suo, *Adv. Mater.* **2021**, 33, 2102034.
[8] K. Izutsu, in *Electrochemistry in Nonaqueous Solutions*, 2002.
[9] V. Gutmann, *Coord. Chem. Rev.* **1976**, 18, 225.
[10] C. Zhang, A. Yamazaki, J. Murai, J.-W. Park, T. Mandai, K. Ueno, K. Dokko, M. Watanabe, *J. Phys. Chem. C* **2014**, 118, 17362.
[11] C. Fu, L. Xu, F. W. Aquino, A. v. Cresce, M. Gobet, S. G. Greenbaum, K. Xu, B. M. Wong, J. Guo, *J. Phys. Chem. Lett.* **2018**, 9, 1739.
[12] a)H. Cheng, Q. Sun, L. Li, Y. Zou, Y. Wang, T. Cai, F. Zhao, G. Liu, Z. Ma, W. Wahyudi, Q. Li, J. Ming, *ACS Energy Lett.* **2022**, 7, 490; b)Z. Piao, R. Gao, Y. Liu, G. Zhou, H.-M. Cheng, *Adv. Mater.* **2023**, 35, 2206009.
[13] K. Xu, *Chem. Rev.* **2014**, 114, 11503.
[14] K. Xu, Y. Lam, S. S. Zhang, T. R. Jow, T. B. Curtis, *J. Phys. Chem. C* **2007**, 111, 7411.
[15] J. Ming, Z. Cao, W. Wahyudi, M. Li, P. Kumar, Y. Wu, J.-Y. Hwang, M. N. Hedhili, L. Cavallo, Y.-K. Sun, L.-J. Li, *ACS Energy Lett.* **2018**, 3, 335.
[16] Y. Wang, Z. Li, Y. Hou, Z. Hao, Q. Zhang, Y. Ni, Y. Lu, Z. Yan, K. Zhang, Q. Zhao, F. Li, J. Chen, *Chem. Soc. Rev.* **2023**, 52, 2713.
[17] D. Aurbach, Y. Talyosef, B. Markovsky, E. Markevich, E. Zinigrad, L. Asraf, J. S. Gnanaraj, H.-J. Kim, *Electrochim. Acta* **2004**, 50, 247.
[18] T. Yim, M.-S. Park, J.-S. Yu, K. J. Kim, K. Y. Im, J.-H. Kim, G. Jeong, Y. N. Jo, S.-G. Woo, K. S. Kang, I. Lee, Y.-J. Kim, *Electrochim. Acta* **2013**, 107, 454.
[19] a)C. Fu, B. M. Wong, K. N. Bozhilov, J. Guo, *Chem. Sci.* **2016**, 7, 1224; b)C. Fu, G. Li, J. Zhang, B. Cornejo, S. S. Piao, K. N. Bozhilov, R. C. Haddon, J. Guo, *ACS Energy Lett.* **2016**, 1, 115.
[20] a)J. Chen, H. Zhang, M. Fang, C. Ke, S. Liu, J. Wang, *ACS Energy Lett.* **2023**, 8, 1723; b)H. J. Gores, J. Barthel, S. Zugmann, D. Moosbauer, M. Amereller, R. Hartl, A. Maurer, in *Handbook of Battery Materials*, 2011.
[21] a)J. Scheers, S. Fantini, P. Johansson, *J. Power Sources* **2014**, 255, 204; b)S. Zhang, K. Ueno, K. Dokko, M. Watanabe, *Adv. Energy Mater.* **2015**, 5, 1500117; c)M. R. Kaiser, S. Chou, H.-K. Liu, S.-X. Dou, C. Wang, J. Wang, *Adv. Mater.* **2017**, 29, 1700449; d)L. Wang, Y. Ye, N. Chen, Y. Huang, L. Li, F. Wu, R. Chen, *Adv. Funct. Mater.* **2018**, 28, 1800919.
[22] a)H. S. Ryu, H. J. Ahn, K. W. Kim, J. H. Ahn, K. K. Cho, T. H. Nam, *Electrochim. Acta* **2006**, 52, 1563; b)S. Kim, Y. Jung, H. S. Lim, *Electrochim. Acta* **2004**, 50, 889.
[23] a)C. Fu, M. B. Oviedo, Y. Zhu, A. von Wald Cresce, K. Xu, G. Li, M. E. Itkis, R. C. Haddon, M. Chi, Y. Han, B. M. Wong, J. Guo, *ACS Nano* **2018**, 12, 9775; b)C. Barchasz, J.-C. Leprêtre, S. Patoux, F. Alloin, *Electrochim. Acta* **2013**, 89, 737.
[24] D. Aurbach, E. Pollak, R. Elazari, G. Salitra, C. S. Kelley, J. Affinito, *J. Electrochem. Soc.* **2009**, 156, A694.
[25] C. B. Bucur, J. Muldoon, A. Lita, *Energy. Environ. Sci.* **2016**, 9, 992.
[26] a)J.-W. Choi, J.-K. Kim, G. Cheruvally, J.-H. Ahn, H.-J. Ahn, K.-W. Kim, *Electrochim. Acta* **2007**, 52, 2075; b)Z. Yu, B. Wang, X. Liao, K. Zhao, Z. Yang, F. Xia, C. Sun, Z. Wang, C. Fan, J. Zhang, Y. Wang, *Adv. Energy Mater.* **2020**, 10, 2000907.
[27] M. Baek, H. Shin, K. Char, J. W. Choi, *Adv. Mater.* **2020**, 32, 2005022.

This article is protected by copyright. All rights reserved.

Author Manuscript

15214095, 2024, 29, Downloaded from https://advanced.onlinelibrary.wiley.com/doi/10.1002/adma.202401263 by Office Of Scientific And Technical Information, Wiley Online Library on [19/08/2025]. See the Terms and Conditions (https://onlinelibrary.wiley.com/terms-and-conditions) on Wiley Online Library for rules of use; OA articles are governed by the applicable Creative Commons License

[28] H. Pan, X. Wei, W. A. Henderson, Y. Shao, J. Chen, P. Bhattacharya, J. Xiao, J. Liu, *Adv. Energy Mater.* **2015**, 5, 1500113.
[29] J. Chen, K. S. Han, W. A. Henderson, K. C. Lau, M. Vijayakumar, T. Dzwiniel, H. Pan, L. A. Curtiss, J. Xiao, K. T. Mueller, Y. Shao, J. Liu, *Adv. Energy Mater.* **2016**, 6, 1600160.
[30] M. Yanagi, K. Ueno, A. Ando, S. Li, Y. Matsumae, J. Liu, K. Dokko, M. Watanabe, *J. Electrochem. Soc.* **2020**, 167, 070531.
[31] K. Dokko, N. Tachikawa, K. Yamauchi, M. Tsuchiya, A. Yamazaki, E. Takashima, J.-W. Park, K. Ueno, S. Seki, N. Serizawa, M. Watanabe, *J. Electrochem. Soc.* **2013**, 160, A1304.
[32] K. Ueno, J.-W. Park, A. Yamazaki, T. Mandai, N. Tachikawa, K. Dokko, M. Watanabe, *J. Phys. Chem. C* **2013**, 117, 20509.
[33] C. Weller, S. Thieme, P. Härtel, H. Althues, S. Kaskel, *J. Electrochem. Soc.* **2017**, 164, A3766.
[34] a)X. Yu, A. Manthiram, *Phys. Chem. Chem. Phys.* **2015**, 17, 2127; b)X. Ji, S. Evers, R. Black, L. F. Nazar, *Nat. Commun.* **2011**, 2, 325.
[35] K. A. See, Y.-S. Jun, J. A. Gerbec, J. K. Sprafke, F. Wudl, G. D. Stucky, R. Seshadri, *ACS Appl. Mater. Interfaces* **2014**, 6, 10908.
[36] R. Demir-Cakan, M. Morcrette, Gangulibabu, A. Guéguen, R. Dedryvère, J.-M. Tarascon, *Energy. Environ. Sci.* **2013**, 6, 176.
[37] X. Ji, K. T. Lee, L. F. Nazar, *Nat. Mater.* **2009**, 8, 500.
[38] a)X. Ren, S. Chen, H. Lee, D. Mei, M. H. Engelhard, S. D. Burton, W. Zhao, J. Zheng, Q. Li, M. S. Ding, M. Schroeder, J. Alvarado, K. Xu, Y. S. Meng, J. Liu, J.-G. Zhang, W. Xu, *Chem* **2018**, 4, 1877; b)T. Nakajima, K.-i. Dan, M. Koh, T. Ino, T. Shimizu, *J. Fluor. Chem.* **2001**, 111, 167; c)C. Zu, N. Azimi, Z. Zhang, A. Manthiram, *J. Mater. Chem. A* **2015**, 3, 14864.
[39] X. Wang, Y. Tan, G. Shen, S. Zhang, *J. Energy Chem.* **2020**, 41, 149.
[40] a)M. L. Gordin, F. Dai, S. Chen, T. Xu, J. Song, D. Tang, N. Azimi, Z. Zhang, D. Wang, *ACS Appl. Mater. Interfaces* **2014**, 6, 8006; b)S. Gu, R. Qian, J. Jin, Q. Wang, J. Guo, S. Zhang, S. Zhuo, Z. Wen, *Phys. Chem. Chem. Phys.* **2016**, 18, 29293; c)S. Drvarič Talian, S. Jeschke, A. Vizintin, K. Pirnat, I. Arčon, G. Aquilanti, P. Johansson, R. Dominko, *Chem. Mater.* **2017**, 29, 10037.
[41] C.-W. Lee, Q. Pang, S. Ha, L. Cheng, S.-D. Han, K. R. Zavadil, K. G. Gallagher, L. F. Nazar, M. Balasubramanian, *ACS Cent. Sci.* **2017**, 3, 605.
[42] R. Younesi, G. M. Veith, P. Johansson, K. Edström, T. Vegge, *Energy. Environ. Sci.* **2015**, 8, 1905.
[43] K. Xu, *Chem. Rev.* **2004**, 104, 4303.
[44] S. Zhang, *Front. Energy Res.* **2013**, 1.
[45] a)G. G. Eshetu, X. Judez, C. Li, M. Martinez-Ibañez, I. Gracia, O. Bondarchuk, J. Carrasco, L. M. Rodriguez-Martinez, H. Zhang, M. Armand, *J. Am. Chem. Soc.* **2018**, 140, 9921; b)H. Zhang, U. Oteo, X. Judez, G. G. Eshetu, M. Martinez-Ibañez, J. Carrasco, C. Li, M. Armand, *Joule* **2019**, 3, 1689.
[46] R. Cao, J. Chen, K. S. Han, W. Xu, D. Mei, P. Bhattacharya, M. H. Engelhard, K. T. Mueller, J. Liu, J.-G. Zhang, *Adv. Funct. Mater.* **2016**, 26, 3059.
[47] a)S. S. Zhang, *J. Electrochem. Soc.* **2012**, 159, A920; b)S. Xiong, K. Xie, Y. Diao, X. Hong, *Electrochim. Acta* **2012**, 83, 78.
[48] E. Peled, D. Golodnitsky, C. Menachem, D. Bar - Tow, *J. Electrochem. Soc.* **1998**, 145, 3482.
[49] Y. Tsao, M. Lee, E. C. Miller, G. Gao, J. Park, S. Chen, T. Katsumata, H. Tran, L.-W. Wang, M. F. Toney, Y. Cui, Z. Bao, *Joule* **2019**, 3, 872.
[50] M. Zhao, B.-Q. Li, X. Chen, J. Xie, H. Yuan, J.-Q. Huang, *Chem* **2020**, 6, 3297.

This article is protected by copyright. All rights reserved.

Author Manuscript

15214095, 2024, 29, Downloaded from https://advanced.onlinelibrary.wiley.com/doi/10.1002/adma.202401263 by Office Of Scientific And Technical Information, Wiley Online Library on [19/08/2025]. See the Terms and Conditions (https://onlinelibrary.wiley.com/terms-and-conditions) on Wiley Online Library for rules of use; OA articles are governed by the applicable Creative Commons License

[51] Y. Liu, Y. Elias, J. Meng, D. Aurbach, R. Zou, D. Xia, Q. Pang, *Joule* **2021**, 5, 2323.
[52] R. Soni, J. B. Robinson, P. R. Shearing, D. J. L. Brett, A. J. E. Rettie, T. S. Miller, *Energy Storage Mater.* **2022**, 51, 97.
[53] Z.-X. Chen, L.-P. Hou, C.-X. Bi, Q. Cheng, X.-Q. Zhang, B.-Q. Li, J.-Q. Huang, *Energy Storage Mater.* **2022**, 53, 315.
[54] Z. X. Chen, Q. Cheng, X. Y. Li, Z. Li, Y. W. Song, F. Sun, M. Zhao, X. Q. Zhang, B. Q. Li, J. Q. Huang, *J. Am. Chem. Soc.* **2023**, 145, 16449.
[55] Z.-W. Zhang, H.-J. Peng, M. Zhao, J.-Q. Huang, *Adv. Funct. Mater.* **2018**, 28, 1707536.
[56] a)S. S. Zhang, *Electrochim. Acta* **2013**, 97, 226; b)Y. Jung, S. Kim, *Electrochem. Commun.* **2007**, 9, 249.
[57] a)N. N. Rajput, V. Murugesan, Y. Shin, K. S. Han, K. C. Lau, J. Chen, J. Liu, L. A. Curtiss, K. T. Mueller, K. A. Persson, *Chem. Mater.* **2017**, 29, 3375; b)F. Wu, F. Chu, G. A. Ferrero, M. Sevilla, A. B. Fuertes, O. Borodin, Y. Yu, G. Yushin, *Nano. Lett.* **2020**, 20, 5391.
[58] K. Sun, N. Li, D. Su, H. Gan, *J. Electrochem. Soc.* **2019**, 166, A50.
[59] H. Ji, Z. Wang, Y. Sun, Y. Zhou, S. Li, J. Zhou, T. Qian, C. Yan, *Adv. Mater.* **2023**, 35, e2208590.
[60] L.-P. Hou, X.-Q. Zhang, B.-Q. Li, Q. Zhang, *Mater. Today* **2021**, 45, 62.
[61] a)Z. Li, H. Rao, R. Atwi, B. M. Sivakumar, B. Gwalani, S. Gray, K. S. Han, T. A. Everett, T. A. Ajantiwalay, V. Murugesan, N. N. Rajput, V. G. Pol, *Nat. Commun.* **2023**, 14, 868; b)K. Sun, Q. Wu, X. Tong, H. Gan, *ACS Appl. Energy Mater.* **2018**, 1, 2608.
[62] a)Y. Chen, Z. Yu, P. Rudnicki, H. Gong, Z. Huang, S. C. Kim, J.-C. Lai, X. Kong, J. Qin, Y. Cui, Z. Bao, *J. Am. Chem. Soc.* **2021**, 143, 18703; b)H. Zhang, Z. Zeng, F. Ma, Q. Wu, X. Wang, S. Cheng, J. Xie, *Angew. Chem. Int. Ed.* **2023**, 62, e202300771.
[63] Y. Zhang, V. Viswanathan, *J. Phys. Chem. Lett.* **2021**, 12, 5821.
[64] X. Gao, Z. Yu, J. Wang, X. Zheng, Y. Ye, H. Gong, X. Xiao, Y. Yang, Y. Chen, S. E. Bone, L. C. Greenburg, P. Zhang, H. Su, J. Affeld, Z. Bao, Y. Cui, *Proc. Natl. Acad. Sci.* **2023**, 120, e2301260120.
[65] K. Dokko, N. Tachikawa, K. Yamauchi, M. Tsuchiya, A. Yamazaki, E. Takashima, J.-W. Park, K. Ueno, S. Seki, N. Serizawa, M. Watanabe, *J. Electrochem. Soc.* **2013**, 160, A1304.
[66] Q. Pang, A. Shyamsunder, B. Narayanan, C. Y. Kwok, L. A. Curtiss, L. F. Nazar, *Nat. Energy* **2018**, 3, 783.
[67] Y. Liu, L. Xu, Y. Yu, M. He, H. Zhang, Y. Tang, F. Xiong, S. Gao, A. Li, J. Wang, S. Xu, D. Aurbach, R. Zou, Q. Pang, *Joule* **2023**, 7, 2074.
[68] M. Cuisinier, P. E. Cabelguen, B. D. Adams, A. Garsuch, M. Balasubramanian, L. F. Nazar, *Energy. Environ. Sci.* **2014**, 7, 2697.
[69] H. Shin, M. Baek, A. Gupta, K. Char, A. Manthiram, J. W. Choi, *Adv. Energy Mater.* **2020**, 10, 2001456.
[70] H.-J. Peng, J.-Q. Huang, X.-Y. Liu, X.-B. Cheng, W.-T. Xu, C.-Z. Zhao, F. Wei, Q. Zhang, *J. Am. Chem. Soc.* **2017**, 139, 8458.
[71] Q. He, Y. Gorlin, M. U. M. Patel, H. A. Gasteiger, Y.-C. Lu, *J. Electrochem. Soc.* **2018**, 165, A4027.
[72] M. Cuisinier, C. Hart, M. Balasubramanian, A. Garsuch, L. F. Nazar, *Adv. Energy Mater.* **2015**, 5, 1401801.
[73] Q. Zou, Y.-C. Lu, *J. Phys. Chem. Lett.* **2016**, 7, 1518.
[74] A. Gupta, A. Bhargav, A. Manthiram, *Adv. Energy Mater.* **2019**, 9, 1803096.
[75] Z. Li, Y. Zhou, Y. Wang, Y.-C. Lu, *Adv. Energy Mater.* **2019**, 9, 1802207.

This article is protected by copyright. All rights reserved.

Author Manuscript

15214095, 2024, 29, Downloaded from https://advanced.onlinelibrary.wiley.com/doi/10.1002/adma.202401263 by Office Of Scientific And Technical Information, Wiley Online Library on [19/08/2025]. See the Terms and Conditions (https://onlinelibrary.wiley.com/terms-and-conditions) on Wiley Online Library for rules of use; OA articles are governed by the applicable Creative Commons License

[76] K. H. Wujcik, D. R. Wang, A. Raghunathan, M. Drake, T. A. Pascal, D. Prendergast, N. P. Balsara, *J. Phys. Chem. C* **2016**, 120, 18403.
[77] a)B. Scharifker, G. Hills, *Electrochim. Acta* **1983**, 28, 879; b)A. Bewick, M. Fleischmann, H. R. Thirsk, *Trans. Faraday Soc.* **1962**, 58, 2200.
[78] G. Zhang, H.-J. Peng, C.-Z. Zhao, X. Chen, L.-D. Zhao, P. Li, J.-Q. Huang, Q. Zhang, *Angew. Chem. Int. Ed.* **2018**, 57, 16732.
[79] A. Elabd, J. Kim, D. Sethio, S. Kang, T. Kang, J. W. Choi, A. Coskun, *ACS Energy Lett.* **2022**, 7, 2459.
[80] B. Yang, H. Jiang, Y. Zhou, Z. Liang, T. Zhao, Y.-C. Lu, *ACS Appl. Mater. Interfaces* **2019**, 11, 25940.
[81] H. Chu, H. Noh, Y.-J. Kim, S. Yuk, J.-H. Lee, J. Lee, H. Kwack, Y. Kim, D.-K. Yang, H.-T. Kim, *Nat. Commun.* **2019**, 10, 188.
[82] R. Meng, X. He, S. J. H. Ong, C. Cui, S. Song, P. Paoprasert, Q. Pang, Z. J. Xu, X. Liang, *Angew. Chem. Int. Ed.* **2023**, 62, e202309046.
[83] A. Gupta, A. Bhargav, A. Manthiram, *ACS Energy Lett.* **2021**, 6, 224.
[84] J. Jung, H. Chu, I. Kim, D. H. Lee, G. Doo, H. Kwon, W. Jo, S. Kim, H. Cho, H.-T. Kim, *Adv. Sci.* **2023**, 10, 2301006.
[85] H. Chu, J. Jung, H. Noh, S. Yuk, J. Lee, J.-H. Lee, J. Baek, Y. Roh, H. Kwon, D. Choi, K. Sohn, Y. Kim, H.-T. Kim, *Adv. Energy Mater.* **2020**, 10, 2000493.
[86] Q. Zou, Z. Liang, G.-Y. Du, C.-Y. Liu, E. Y. Li, Y.-C. Lu, *J. Am. Chem. Soc.* **2018**, 140, 10740.
[87] H. Pan, K. S. Han, M. Vijayakumar, J. Xiao, R. Cao, J. Chen, J. Zhang, K. T. Mueller, Y. Shao, J. Liu, *ACS Appl. Mater. Interfaces* **2017**, 9, 4290.
[88] H. Pan, K. S. Han, M. H. Engelhard, R. Cao, J. Chen, J.-G. Zhang, K. T. Mueller, Y. Shao, J. Liu, *Adv. Funct. Mater.* **2018**, 28, 1707234.
[89] H. Dai, K. Xi, X. Liu, C. Lai, S. Zhang, *J. Am. Chem. Soc.* **2018**, 140, 17515.
[90] J.-Q. Huang, Q. Zhang, F. Wei, *Energy Storage Mater.* **2015**, 1, 127.
[91] Y. Luo, Z. Fang, S. Duan, H. Wu, H. Liu, Y. Zhao, K. Wang, Q. Li, S. Fan, Z. Zheng, W. Duan, Y. Zhang, J. Wang, *Angew. Chem. Int. Ed.* **2023**, 62, e202215802.
[92] Y. Chen, H. Zhang, W. Xu, X. Yang, Y. Yu, X. Li, H. Zhang, *Adv. Funct. Mater.* **2018**, 28, 1704987.
[93] T. Liu, S. Sun, J. Hao, W. Song, Q. Niu, X. Sun, Y. Wu, D. Song, J. Wu, *ACS Appl. Mater. Interfaces* **2019**, 11, 15607.
[94] J. Zheng, G. Ji, X. Fan, J. Chen, Q. Li, H. Wang, Y. Yang, K. C. DeMella, S. R. Raghavan, C. Wang, *Adv. Energy Mater.* **2019**, 9, 1803774.
[95] T. Liu, H. Li, J. Yue, J. Feng, M. Mao, X. Zhu, Y.-s. Hu, H. Li, X. Huang, L. Chen, L. Suo, *Angew. Chem. Int. Ed.* **2021**, 60, 17547.
[96] H. Cheng, S. Zhang, B. Zhang, Y. Lu, *Small* **2023**, 19, e2206375.
[97] C. V. Amanchukwu, X. Kong, J. Qin, Y. Cui, Z. Bao, *Adv. Energy Mater.* **2019**, 9, 1902116.
[98] C.-C. Su, M. He, R. Amine, Z. Chen, K. Amine, *Angew. Chem. Int. Ed.* **2018**, 57, 12033.
[99] a)X.-Q. Zhang, Q. Jin, Y.-L. Nan, L.-P. Hou, B.-Q. Li, X. Chen, Z.-H. Jin, X.-T. Zhang, J.-Q. Huang, Q. Zhang, *Angew. Chem. Int. Ed.* **2021**, 60, 15503; b)L.-P. Hou, X.-Q. Zhang, N. Yao, X. Chen, B.-Q. Li, P. Shi, C.-B. Jin, J.-Q. Huang, Q. Zhang, *Chem* **2022**, 8, 1083.
[100] Z. Li, L.-P. Hou, N. Yao, X.-Y. Li, Z.-X. Chen, X. Chen, X.-Q. Zhang, B.-Q. Li, Q. Zhang, *Angew. Chem. Int. Ed.* **2023**, 62, e202309968.
[101] H. Kojima, A. J. Bard, *J. Am. Chem. Soc.* **1975**, 97, 6317.

This article is protected by copyright. All rights reserved.

Author Manuscript

15214095, 2024, 29, Downloaded from https://advanced.onlinelibrary.wiley.com/doi/10.1002/adma.202401263 by Office Of Scientific And Technical Information, Wiley Online Library on [19/08/2025]. See the Terms and Conditions (https://onlinelibrary.wiley.com/terms-and-conditions) on Wiley Online Library for rules of use; OA articles are governed by the applicable Creative Commons License

[102] a)X.-B. Han, S. Ye, *ACS Catal.* **2020**, 10, 9790; b)L. C. H. Gerber, P. D. Frischmann, F. Y. Fan, S. E. Doris, X. Qu, A. M. Scheuermann, K. Persson, Y.-M. Chiang, B. A. Helms, *Nano. Lett.* **2016**, 16, 549.
[103] Z. Shen, Q. Gao, X. Zhu, Z. Guo, K. Guo, X. Song, Y. Zhao, *Energy Storage Mater.* **2023**, 57, 299.
[104] H. Ye, J. Sun, X. F. Lim, Y. Zhao, J. Y. Lee, *Energy Storage Mater.* **2021**, 38, 338.
[105] S. Meini, R. Elazari, A. Rosenman, A. Garsuch, D. Aurbach, *J. Phys. Chem. Lett.* **2014**, 5, 915.
[106] a)K. R. Kim, K.-S. Lee, C.-Y. Ahn, S.-H. Yu, Y.-E. Sung, *Sci. Rep.* **2016**, 6, 32433; b)M. Zhao, H.-J. Peng, J.-Y. Wei, J.-Q. Huang, B.-Q. Li, H. Yuan, Q. Zhang, *Small Methods* **2020**, 4, 1900344.
[107] W. Guo, W. Zhang, Y. Si, D. Wang, Y. Fu, A. Manthiram, *Nat. Commun.* **2021**, 12, 3031.
[108] R. Steudel, *Chem. Rev.* **2002**, 102, 3905.
[109] a)Z. Wang, H. Ji, L. Zhou, X. Shen, L. Gao, J. Liu, T. Yang, T. Qian, C. Yan, *ACS Nano* **2021**, 15, 13847; b)S. Chen, D. Wang, Y. Zhao, D. Wang, *Small Methods* **2018**, 2, 1800038.
[110] M. Zhao, X. Chen, X.-Y. Li, B.-Q. Li, J.-Q. Huang, *Adv. Mater.* **2021**, 33, 2007298.
[111] a)S. Chen, F. Dai, M. L. Gordin, Z. Yu, Y. Gao, J. Song, D. Wang, *Angew. Chem. Int. Ed.* **2016**, 55, 4231; b)S. Chen, Y. Gao, Z. Yu, M. L. Gordin, J. Song, D. Wang, *Nano Energy* **2017**, 31, 418.
[112] a)M. Wu, Y. Cui, A. Bhargav, Y. Losovyj, A. Siegel, M. Agarwal, Y. Ma, Y. Fu, *Angew. Chem. Int. Ed.* **2016**, 55, 10027; b)J. Liu, T. Qian, N. Xu, M. Wang, J. Zhou, X. Shen, C. Yan, *Energy Storage Mater.* **2020**, 24, 265.
[113] M. Wu, A. Bhargav, Y. Cui, A. Siegel, M. Agarwal, Y. Ma, Y. Fu, *ACS Energy Lett.* **2016**, 1, 1221.
[114] M. Zhao, X.-Y. Li, X. Chen, B.-Q. Li, S. Kaskel, Q. Zhang, J.-Q. Huang, *eScience* **2021**, 1, 44.
[115] W. Zhang, F. Ma, Q. Wu, Z. Zeng, W. Zhong, S. Cheng, X. Chen, J. Xie, *Energy Environ. Mater.* **2023**, 6, e12369.
[116] W. Guo, A. Bhargav, J. D. Ackerson, Y. Cui, Y. Ma, Y. Fu, *Chem. Commun.* **2018**, 54, 8873.
[117] a)J. Zhou, T. Qian, N. Xu, M. Wang, X. Ni, X. Liu, X. Shen, C. Yan, *Adv. Mater.* **2017**, 29, 1701294; b)G.-L. Xu, H. Sun, C. Luo, L. Estevez, M. Zhuang, H. Gao, R. Amine, H. Wang, X. Zhang, C.-J. Sun, Y. Liu, Y. Ren, S. M. Heald, C. Wang, Z. Chen, K. Amine, *Adv. Energy Mater.* **2019**, 9, 1802235.
[118] L. Peng, Z. Wei, C. Wan, J. Li, Z. Chen, D. Zhu, D. Baumann, H. Liu, C. S. Allen, X. Xu, A. I. Kirkland, I. Shakir, Z. Almutairi, S. Tolbert, B. Dunn, Y. Huang, P. Sautet, X. Duan, *Nat. Catal.* **2020**, 3, 762.
[119] G. Zhou, H. Tian, Y. Jin, X. Tao, B. Liu, R. Zhang, Z. W. Seh, D. Zhuo, Y. Liu, J. Sun, J. Zhao, C. Zu, D. S. Wu, Q. Zhang, Y. Cui, *Proc. Natl. Acad. Sci.* **2017**, 114, 840.
[120] P. Sang, Q. Chen, D.-Y. Wang, W. Guo, Y. Fu, *Chem. Rev.* **2023**, 123, 1262.
[121] J. Lian, W. Guo, Y. Fu, *J. Am. Chem. Soc.* **2021**, 143, 11063.
[122] W. Hua, Z. Yang, H. Nie, Z. Li, J. Yang, Z. Guo, C. Ruan, X. a. Chen, S. Huang, *ACS Nano* **2017**, 11, 2209.
[123] C. N. Cramer, K. F. Haselmann, J. V. Olsen, P. K. Nielsen, *Anal. Chem.* **2016**, 88, 1585.
[124] M. Liu, X. Chen, C. Chen, T. Ma, T. Huang, A. Yu, *J. Power Sources* **2019**, 424, 254.
[125] H.-L. Wu, M. Shin, Y.-M. Liu, K. A. See, A. A. Gewirth, *Nano Energy* **2017**, 32, 50.
[126] a)Z. Yuan, H.-J. Peng, T.-Z. Hou, J.-Q. Huang, C.-M. Chen, D.-W. Wang, X.-B. Cheng, F. Wei, Q. Zhang, *Nano. Lett.* **2016**, 16, 519; b)Y. Li, J. Wu, B. Zhang, W. Wang, G. Zhang, Z. W. Seh, N. Zhang, J. Sun, L. Huang, J. Jiang, J. Zhou, Y. Sun, *Energy Storage Mater.* **2020**, 30, 250; c)C. Ye, Y. Jiao, H. Jin, A. D. Slattery, K. Davey, H. Wang, S.-Z. Qiao, *Angew. Chem. Int. Ed.* **2018**, 57, 16703.
[127] Z. Shen, X. Jin, J. Tian, M. Li, Y. Yuan, S. Zhang, S. Fang, X. Fan, W. Xu, H. Lu, J. Lu, H. Zhang, *Nat. Catal.* **2022**, 5, 555.

This article is protected by copyright. All rights reserved.

Author Manuscript

15214095, 2024, 29, Downloaded from https://advanced.onlinelibrary.wiley.com/doi/10.1002/adma.202401263 by Office Of Scientific And Technical Information, Wiley Online Library on [19/08/2025]. See the Terms and Conditions (https://onlinelibrary.wiley.com/terms-and-conditions) on Wiley Online Library for rules of use; OA articles are governed by the applicable Creative Commons License

[128] a)Y. Song, W. Cai, L. Kong, J. Cai, Q. Zhang, J. Sun, *Adv. Energy Mater.* **2020**, 10, 1901075; b)D. Liu, C. Zhang, G. Zhou, W. Lv, G. Ling, L. Zhi, Q.-H. Yang, *Adv. Sci.* **2018**, 5, 1700270.
[129] X. Liang, C. Hart, Q. Pang, A. Garsuch, T. Weiss, L. F. Nazar, *Nat. Commun.* **2015**, 6, 5682.
[130] Y. Lin, Y. Zhou, S. Huang, M. Xiao, D. Han, J. Qin, S. Wang, Y. Meng, *Adv. Energy Mater.* **2022**, 12, 2201912.
[131] R. Jayan, M. S. Nahian, M. M. Islam, *ACS Appl. Energy Mater.* **2022**, 5, 9782.
[132] C. Luo, X. Liang, Y. Sun, W. Lv, Y. Sun, Z. Lu, W. Hua, H. Yang, R. Wang, C. Yan, J. Li, Y. Wan, Q.-H. Yang, *Energy Storage Mater.* **2020**, 33, 290.
[133] J. Jung, H. Cho, I. Kim, S. Kim, W. Jo, H.-T. Kim, *Energy Storage Mater.* **2023**, 63, 103040.

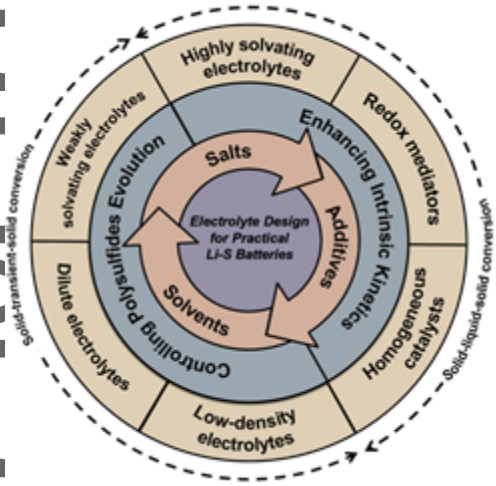

Implementing lean electrolyte is a required condition to achieve high specific energy of lithium-sulfur batteries at the cell level. This review analyzes the challenges induced by lean electrolyte condition focusing on the connection between polysulfide evolution pathways and fundamental solvation properties of the electrolytes. The working mechanisms and design principle of redox mediators and catalysts are also discussed.

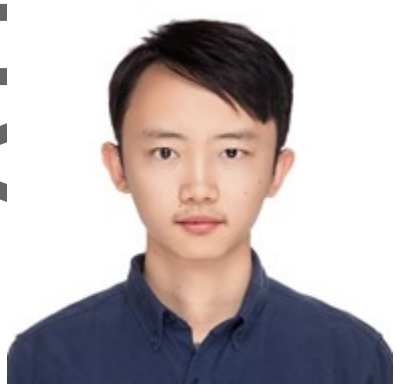

This article is protected by copyright. All rights reserved.

Author Manuscript

15214095, 2024, 29, Downloaded from https://advanced.onlinelibrary.wiley.com/doi/10.1002/adma.202401263 by Office Of Scientific And Technical Information, Wiley Online Library on [19/08/2025]. See the Terms and Conditions (https://onlinelibrary.wiley.com/terms-and-conditions) on Wiley Online Library for rules of use; OA articles are governed by the applicable Creative Commons License

Jianjun Chen earned his BS degree from Huazhong University of Science and Technology in 2019. He is currently a PhD candidate at the University of California. His research interest lies in electrolyte and interface designs for rechargeable batteries and the development of Lithium-sulfur batteries.

Yuqing Fu is a PhD candidate at the University of California, Riverside. She received her BS degree in chemistry from Huazhong University of Science and Technology in 2019. Her current research focuses on computational materials for energy storage, specifically electrolyte and electrode chemistry in lithium batteries and aluminum batteries.

Juchen Guo is a Professor of Chemical Engineering and Materials Science at University of California – Riverside. He earned his Bachelor degree from Zhejiang University in 1999 and his Ph.D. degree from University of Maryland in 2007. He performed postdoctoral studies at University of Maryland (2007 to 2011) and Cornell University (2011 to 2012). He joined the Department of Chemical and Environmental Engineering and the Materials Science and Engineering Program at UC Riverside in 2012. He was the recipient of 2014 Hellman Fellowship and 2018 NSF CAREER Award. His research interests are interfacial phenomena and material properties in electrochemical energy storage systems.

This article is protected by copyright. All rights reserved.

Author Manuscript

15214095, 2024, 29, Downloaded from https://advanced.onlinelibrary.wiley.com/doi/10.1002/adma.202401263 by Office Of Scientific And Technical Information, Wiley Online Library on [19/08/2025]. See the Terms and Conditions (https://onlinelibrary.wiley.com/terms-and-conditions) on Wiley Online Library for rules of use; OA articles are governed by the applicable Creative Commons License